11-17-2016

Gene Expression Profiling and the Role of HSF1 in Ovarian Cancer in 3D Spheroid Models

Trillitye Paullin
University of South Florida, trillpaullin@gmail.com

Gene Expression Profiling and the Role of HSF1 in Ovarian Cancer in 3D Spheroid Models

by

Trillitye Paullin

A dissertation submitted in partial fulfillment
of the requirements for the degree of
Doctor of Philosophy in Cell and Molecular Biology
Department of Cell Biology, Microbiology, and Molecular Biology
College of Arts and Sciences
University of South Florida

Major Professor: Sandy Westerheide, Ph.D.
Brant Burkhardt, Ph.D.
Meera Nanjundan, Ph.D.
Ken Wright, Ph.D.

Date of Approval:
November 18, 2016

Key words: HSF1, Spheroid model, Epithelial-Mesenchymal Transition

DEDICATION

I dedicate this dissertation to my husband and friend, Peter, for his immeasurable support and love through this journey. His devotion to my career and our family is what made this endeavor possible. I would also like to dedicate this to my mother, Nancy Hollis, who is an ovarian cancer survivor and the strongest person I know. Her belief in me as a daughter and a woman has catalyzed my success in so many ways. Finally, this work is dedicated to the Pat Tillman Foundation and the Tillman Scholars. This organization kept me focused and determined while inspiring me to be more each day.

ACKNOWLEDGMENTS

My most sincere appreciation goes to my mentor Dr. Sandy Westerheide, who made this work possible through her guidance and support. I would also like to extend a special thanks to Dr. Brant Burkhardt, Dr. Meera Nanjundan, and Dr. Ken Wright for their advice and feedback throughout this process. Finally, I would like to thank Dr. Heidi Super for hiring and mentoring me as an undergraduate. Her dedication to my development as a young scientist was pivotal and laid the foundation for the researcher that I am today.

TABLE OF CONTENTS

LIST OF TABLES

LIST OF FIGURES

ABSTRACT

Ovarian cancer is the most lethal gynecological cancer, with over 200,000 women diagnosed each year and over half of those cases leading to death. These poor statistics are related to a lack of early symptoms and inadequate screening techniques. This results in the cancer going undetected until later stages when the tumor has metastasized through a process that requires the epithelial to mesenchymal transition (EMT). In lieu of traditional monolayer cell culture, EMT and cancer progression in general is best characterized through the use of 3D spheroid models. In this study, we examine gene expression changes through microarray analysis in spheroid versus monolayer ovarian cancer cells treated with TGFβ to induce EMT. Transcripts that included Coiled-Coil Domain Containing 80 (CCDC80), Solute Carrier Family 6 (Neutral Amino Acid Transporter), Member 15 (SLC6A15), Semaphorin 3E (SEMA3E) and PIF1 5'-To-3' DNA Helicase (PIF1) were downregulated more than 10-fold in the 3D cells while Inhibitor Of DNA Binding 2, HLH Protein (ID2), Regulator Of Cell Cycle (RGCC), Protease, Serine 35 (PRSS35), and Aldo-Keto Reductase Family 1, Member C1 (AKR1C1) were increased more than 50-fold.

Interestingly, stress responses and epigenetic processes were significantly affected by 3D growth. The heat shock response and the oxidative stress response were also identified as transcriptome responses that showed significant changes upon 3D growth. Subnetwork enrichment analysis revealed that DNA integrity (e.g. DNA

damage, genetic instability, nucleotide excision repair, and the DNA damage checkpoint pathway) were altered in the 3D spheroid model. In addition, two epigenetic processes, DNA methylation and histone acetylation, were increased with 3D growth. These findings support the hypothesis that three dimensional ovarian cell culturing is physiologically different from its monolayer counterpart.

The proteotoxic stress-responsive transcription factor HSF1 is frequently overexpressed in a variety of cancers and is vital to cellular proliferation and invasion in some cancers. Upon analysis of various patient data sets, we find that HSF1 is frequently overexpressed in ovarian tumor samples. In order to determine the role of HSF1 in ovarian cancer, inducible HSF1 knockdown cell lines were created. Knockdown of HSF1 in SKOV3 and HEY ovarian cancer cell lines attenuates the epithelial-to-mesenchymal transition (EMT) in cells treated with TGFβ, as determined by western blot and quantitative RT-PCR analysis of multiple EMT markers.

To further explore the role of HSF1 in ovarian cancer EMT, we cultured multicellular spheroids in a non-adherent environment to simulate early avascular tumors. In the spheroid model, cells more readily undergo EMT; however, EMT inhibition by HSF1 knockdown becomes more pronounced in the spheroid model. These findings suggest that HSF1 is important in the ovarian cancer TGFβ response and in EMT.

CHAPTER ONE: INTRODUCTION

Ovarian Cancer

In the United States, an estimated 22,280 new cases of ovarian cancer will emerge and 14,240 deaths will occur in 2016, making ovarian cancer the fifth leading cause of cancer deaths in women [2]. Despite research efforts, ovarian cancer is still the most lethal gynecological malignancy [2]. This is due to several factors, including inadequate screening techniques, the absence of early stage symptoms, insufficient chemotherapy options, and the molecular heterogeneity found in ovarian tumors [4]. Ovarian cancer's high molecular heterogeneity is due to the large tumor volume, often several cubic centimeters, found in most patients who present with the disease [5]. Each cubic centimeter may be composed of up to a billion cells, indicating a high number of cell divisions which leads to high molecular and genetic heterogeneity. The number of cancer cells and how long they have been present are directly related to the patient's probability of chemotherapy resistance through the development of resistant clone cells [6].

Due to a lack of early symptoms, ovarian cancer is commonly referred to as a silent disease. Some patients may experience abdominal pain, swelling, gastrointestinal distress, abnormal vaginal bleeding, appetite changes, frequent

urination, and/or fatigue [7]. Commonly, patients will experience little to no symptoms until the cancer has metastasized and is affecting other organs. Current screening techniques include pelvic examination, ultrasound, computed tomography (CT) scanning, magnetic resonance imaging (MRI), and CA-125 blood testing [8]. The CA-125 serum tumor marker is elevated in 80% of epithelial ovarian cancers and is detected by a radioimmunoassay [9]. Unfortunately, only half of stage I patients have significantly elevated levels of this marker [10]. This, in addition to the fact that CA-125 levels are also elevated in many cancer-free women, makes it an inadequate screening technique [10].

Carcinogenesis is described as the process in which a sufficient number of somatic mutations occur within a single cell to cause molecular modifications which yield a malignant phenotype [11]. The first phase of this step-wise process is initiation, where DNA damage occurs. Second, the precancerous cells continue to proliferate and accumulate genetic alterations in the step known as promotion. Lastly, progression is considered the last phase in which these alterations lead to the transformation to malignant cells.

A number of factors contribute to a patient's likelihood of developing ovarian cancer. It has been proposed that incessant ovulation may lead to genetic damage which could cause ovarian cancer in some women [12]. For instance, the use of oral contraceptives (OC), child-bearing, breastfeeding, and a healthy weight all reduce a woman's risk of presenting with the disease [13]. Contradictory to the incessant ovulation theory is the finding that taking OCs for three years, only inhibiting ten percent of lifetime ovulation cycles, reduces the risk of ovarian cancer by as much as fifty

percent [14]. Likewise, a single pregnancy is linked to a thirty-five percent reduction [15]. Studies such as these indicate that ovarian biology, including ovarian cancer risk, may be greatly affected by the patient's hormonal balance. Receptors for estrogen, progestin, androgens, vitamin D, and retinoids are all present in the ovarian epithelium. During normal pregnancy, women express high levels of progestin which induces apoptosis and may be the underlying cause for the subsequent reduction in ovarian cancer risk [16]. In fact, Rodriguez *et al*. showed that primates treated with estrogen or progestin presented with a six-fold increase in ovarian epithelium cell apoptosis for progestin-only subjects [17]. Contraceptives containing progestin only do not dependably deter ovulation which again does not support the incessant ovulation theory [18]. Markedly, androgens, however, may have stimulatory effects leading to an increased risk of ovarian cancer [19]. These studies support the theory that ovarian cancer develops from the ovarian epithelium's response to the individual's hormone expression.

Genes also play a role in the risk equation. Hereditary genetic mutations are seen in about ten percent of ovarian cancer patients, wherein lifestyle choices may have little effect on the outcome [20]. Research has shown that two genes commonly associated with hereditary types of breast cancer, BRCA1 and BCRA2, are also linked to a greater chance of ovarian cancer [21, 22]. PTEN, a tumor-suppressor gene, is frequently mutated in endometrioid ovarian cancer, but PTEN mutation is not seen in other histological subtypes, indicating that the cancer develops through separate distinct pathways [23]. It has also been shown that the HER2 oncogene is overexpressed in nearly thirty percent of ovarian cancers that are linked to poor prognosis [24, 25].

Approximately 90% of ovarian cancers develop in the epithelium, while the remaining cases originate from germ or stromal cells. The major morphological subtypes of epithelial ovarian cancer include serous, clear cell, mucinous, and endometrioid [26]. Recent research has shown that accurate pathological typing is imperative to successful treatment, as each subtype independently responds to therapy and may indicate underlying genetic conditions [27-29]. These tumors are characterized as benign, malignant, or intermediate/borderline. Surface epithelial tumors can be further categorized into type I or type II based on their tumorigenesis pathways [27]. This categorization is based on broad tumor development mechanisms to be used in conjunction with the above histological subtypes. Type I tumors are typically described as low-grade neoplasms which arise from borderline tumors and type II tumors are high-grade neoplasms with *de novo* development [27].

Ovarian Cancer Treatment

Upon diagnosis, patients may undergo a series of treatment options to include surgery, chemotherapy, and in rare cases, radiation. Surgical procedures may aim to remove the uterus via a hysterectomy, the ovaries and fallopian tubes through a bilateral salpingo-oophorectomy, the omentum, and/or other affected tissues and organs [30].

Once surgery is complete, patients typically receive a combinational approach to chemotherapy utilizing a platinum-based medication such as carboplatin or cisplatin with a taxane such as paclitaxel or docetaxel. Increased survival rates have been

shown in women whose drugs are administered in an amalgamation of intravenous and intraperitoneal injections [31]. Platinum-based medications have a cytotoxic effect through several cellular events, the most important being DNA platination. DNA platination is a specific cross-linking event which occurs when the platinum compound reacts with the N(7) of guanine. Conversely, taxane chemotherapy agents utilized for ovarian cancer treatment induce cell cycle arrest, and consequentially apoptosis, by stabilizing microtubules through preventing depolymerization. However, both medications are accompanied by an array of side effects to include dose-limiting nephrotoxicity, ototoxicity, dizziness, blurred vision, nausea, painful urination, and vomiting.

Although most patients respond to platinum and taxane chemotherapeutic agents at first, the relapse rate is roughly 85% [32]. Ovarian cancer recurrence is seen when cancerous or precancerous cells remain after treatment and eventually proliferate into a tumor. Once relapse occurs, it is not unusual for patients to no longer respond to traditional chemotherapy, as a resistance is developed to the previously exposed medications. At this stage, supplementary treatment options include topotecan, hormones, additional surgery, and experimental agents [33]. Topotecan induces apoptosis by intercalating between the topoisomerase-I cleavage complex and DNA, thereby leading to an accumulation of double stand DNA breaks. Hormone therapy may also be utilized to reduce estrogen and increase progesterone levels, which has an inhibitory effect on cancer proliferation. Even with these alternate treatment routes, relapse rates are still staggering and most patients with advanced ovarian cancer succumb to their disease within five years of initial diagnosis [34].

Epithelial Mesenchymal Transition

The epithelial to mesenchymal transition (EMT) was first described by Greenburg in 1982 as a distinct process wherein “cuboidal” epithelial cells undergo changes to adopt an elongated mesenchymal phenotype (Fig. 1.1) [35]. EMT is most commonly observed during metazoan embryonic development when epithelial cells must migrate and dedifferentiate, such as during the formation of the mesoderm layer during gastrulation [36]. Processes such as gastrulation and neural crest formation are examples of primary developmental EMTs while secondary developmental EMT is implicated in organogenesis [37]. Equally as important in embryogenesis is the

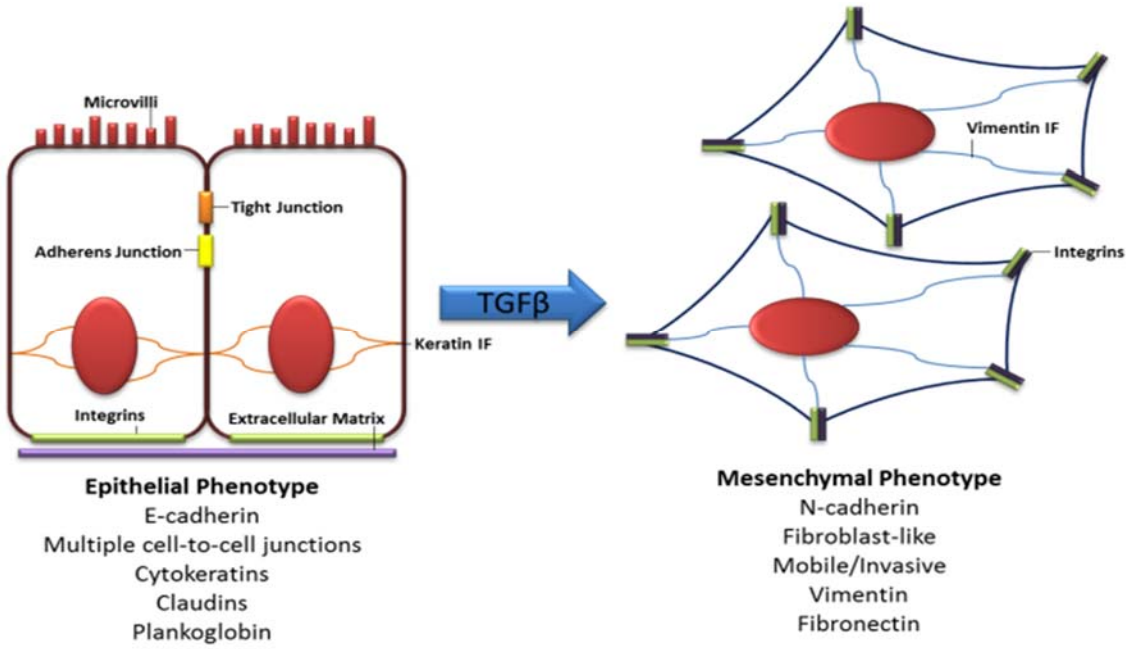

Figure 1.1: TGFβ Induction of Epithelial to Mesenchymal Transition.

Addition of TGFβ to epithelial cells promotes their transition to a mesenchymal phenotype through expression of mesenchymal proteins. This disrupts cell-cell and cell-extracellular matrix connections to allow the cells to disengage from the tumor and metastasize to other organs. In ovarian cancer patients, these separated cells can be found free floating within the peritoneal cavity, making organs such as the stomach, liver, and kidneys prime locations for secondary tumors. (Adapted from Palena *et al*., 2011). (Figure created by Trillitye Paullin).

mesenchymal to epithelial transition (MET) which is the reverse process of EMT [38]. This advancement in embryogenesis allowed for higher organism complexity from diploblastic to triploblastic embryos [35]. In addition to development, EMT is also vital for wound healing and tissue regeneration. During this processes, EMT is associated with inflammation and is induced by a repair response in order to reconstruct tissues [39].

EMT is tightly regulated by a number of genes. Specifically, downregulation of E-cadherin is considered a hallmark for this process and one of the most studied EMT markers [40]. The protein is responsible for epithelial cell-cell adhesion and downregulation can affect other proteins during EMT including cytokeratins, desmosomes, and cell polarity proteins. During EMT, expression of E-cadherin "switches" to N-cadherin, allowing for a more fibroblast-like morphology and increased cell motility [41]. This phenomenon can be triggered through cellular release of growth factors, such as TGFβ, PDGF, EGF, and FGF2 [42]. Specifically, TGFβ initiates a response through the binding of receptors with serine/threonine kinase activity, which subsequently phosphorylates Smad2 and Smad3 [43]. Activated Smad2 and Smad3 form a complex with Smad4 which is then translocated into the nucleus to activate transcription of target genes [44, 45]. These genes act as transcription factors which are responsible for regulating the EMT process (Fig. 1.2) [46].

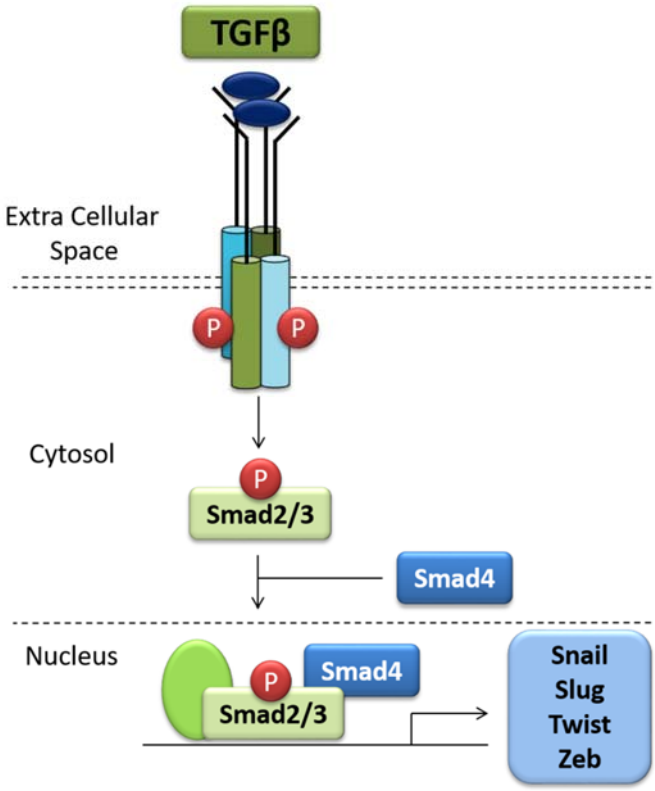

Figure 1.2: TGFβ Induces Transient EMT within Hours of Treatment through Phosphorylation of the TGFβ Receptor.

The binding of TGFβ ligand to TGFβ receptors results in phosphorylation of the receptor and a cascade of signaling events. First, Smad2/3 is activated through phosphorylation and forms a trimer with Smad4. This trimer then translocates to the nucleus to form a complex with co-transcription factors. Lastly, the complex activates or represses target gene transcription. Of these, the EMT markers Snail, Slug, Twist, and Zeb are all transcribed. (Adapted from Debangshu and Datta, 2012). (Figure created by Trillitye Paullin).

TGFβ is secreted by several cell types, including macrophages, B cells, and dendritic cells, and its activation can be regulated by the BMP1 protease family [47]. Its signaling is implicated in driving several developmental pathways and controlling cellular behavior [48]. As such, TGFβ plays dual roles of both anti- and pro-tumorigenesis depending on the cancer stage. In early-stage tumors, increased TGFβ expression levels are linked to favorable prognosis due to its ability to stimulate cell cycle arrest [49, 50]. However, it has been shown to enhance motility, invasion, EMT,

and stemness in advanced stage tumors [51]. This phenomenon has been coined the "TGFβ paradox" [52]. Similarly, TGFβ is vital to inhibiting cell proliferation in normal ovarian epithelial cells, however 40% of ovarian carcinomas are shown to contain mutated TGFβ which negates its cytostatic effects while preserving its ability to induce EMT [53]. In serous epithelial ovarian cancer, the 3q26.2 chromosomal region containing TGFβ co-repressors, ecotropic viral integration site-1 (EVI1) and SnoN/SKiL, is frequently amplified [54, 55]. In our studies, TGFβ was utilized to induce EMT in SKOV3 and HEY ovarian cancer cell lines.

Recently, scientists have focused on EMT processes that are activated under pathological situations as well, including tumor progression and metastasis [46, 56, 57]. In tumor progression, EMT allows the cells to detach from one another, invade the basement membrane, and migrate to other organs within the body [58]. Once the mesenchymal-like cell has migrated into a new organ, it can undergo MET and begin to form a secondary tumor [46]. In fact, many studies have shown a functional loss of E-cadherin as one of the most important steps in cancer progression [59, 60]. The most common E-cadherin alterations found in tumors include exon skipping and out-of-frame mutations and it is believed that the protein acts as a tumor suppressor for certain cancer types [61]. In many carcinomas, EMT-inducing transcription factors, such as Snail, Slug, Twist, and Zeb, appear to be induced or activated by signals stemming from the tumor-associated stroma [62, 63]. Such signals include growth factors such as TGFβ, EGF, PDGF, and HGF. Downstream, these transcription factors activate EMT through a series of signaling networks involving proteins such as MAPK, PI3K, Akt, Smads, ERK, and many others [64].

Monolayer versus Spheroid Cell Culture

HeLa was the first continuous human cancer cell line which was derived from a woman's cervical cancer and developed in 1952 [65]. Today, there are hundreds of cells lines originating from every histological type of cancer. A majority of cell lines used for experimental purposes are considered adherent or monolayer cultures because they are anchorage-dependent and grow on a solid substrate. While monolayer cultures are commonly used to study ovarian cancer and the EMT process, the spheroid culture model has been shown to be more physiologically relevant due to its significant similarity to *in vivo* solid tumors in regards to pH conditions, oxygen levels, extracellular matrix interaction, cell to cell interaction, and glucose levels [66-68]. This is especially the case when studying metastasis, angiogenesis, and drug sensitivity [69-71]. Using spheroid cultures is particularly important for this study, as ovarian cancer patients often present with ascites [72]. Ascites is the accumulation of fluid in the peritoneal cavity, in which ovarian cancer cells, lymphocytes, and mesothelial cells can be found [73]. This occurs when malignant cells detach from the primary tumor into the ascitic fluid. These free-floating cancer cells have sphere-forming capability and have been shown to hinder treatment due to their role in metastasis, progression, and resistance to chemotherapy treatment [74-77].

Biomedical science began utilizing spheroidal cell clusters as early as the 1940's as a means to study morphogenesis in embryonic and malignant cells [78-81]. Sutherland and associates later used this concept to determine therapy response in multicellular tumor spheroids [82, 83]. Research using 3D spheroids has led to new discoveries in the processes behind invasion, angiogenesis, metastasis, and cell cycle kinetics. Due to the relevance of spheroid cell cultures to actual *in vivo* solid tumors (Fig. 1.3), 3D culture should become a mandatory test system in therapeutic screening [84].

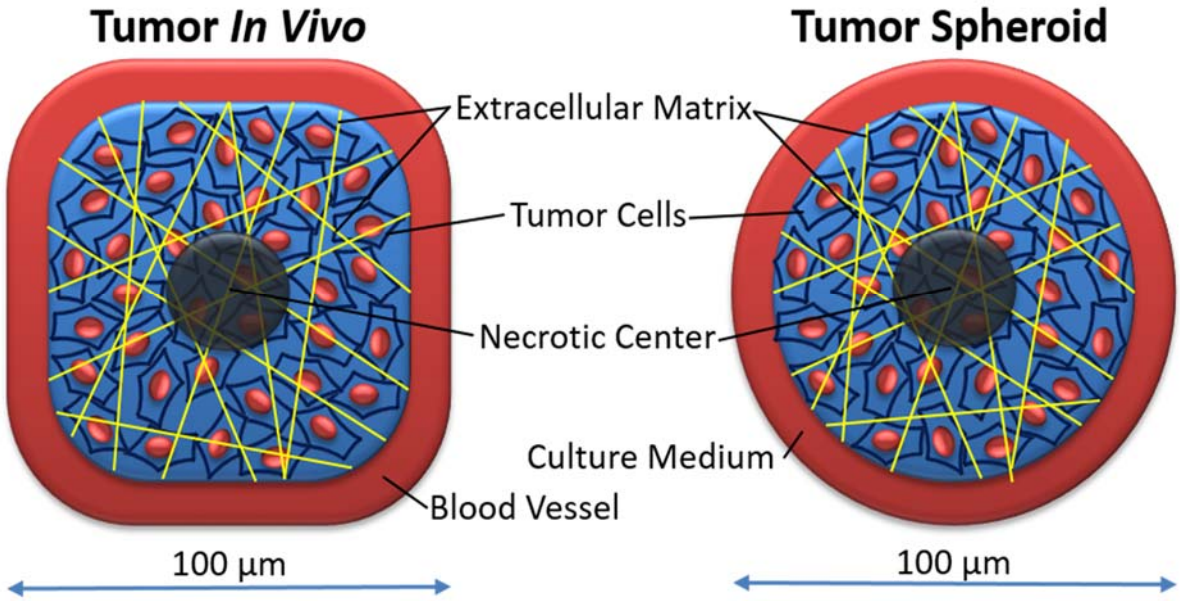

Figure 1.3: Spheroid Cell Culturing Closely Mimics Patient Tumors *In Vivo*.

Compared to monolayer cell culturing, which does not allow for areas of hypoxia, diverse cell proliferation rates, and varying nutrient and waste transport, tumor spheroids have been shown to be more physiologically relevant to tumors analyzed *in vivo [1]*, even though these tumors are capable of developing into nearly any shape. Some spheroid culturing methods also include tissue support matrices which mimic the ECM *in vivo*. This makes spheroids a better experimental model than monolayer cells. (Adapted from Phung *et al.*, 2011). (Figure created by Trillitye Paullin).

A wide variety of techniques are used to form spheroids from monolayer cell culture. The spinner flask culture was the first method described and is still commonly

used. In this method, fluid turbulence promotes cellular aggregation by preventing attachment to other surfaces [82]. Using the same basic concept, the rotary wall vessel reactor mimics microgravity by suspending cells between rotating cylindrical walls [85]. While these two approaches produce large quantities of spheroids, they also required special equipment and processing methods. Another technique consists of placing cells in non-adherent plates, however this usually results in less consistent spheroid size [86]. An alternative method involves a microfluidic device that is based on hydrodynamic trapping of cells in controlled geometries [87]. More recently, the hanging drop method, was established and provided more reliable spheroid size and arrangement [88]. Many new models for spheroid generation have been developed and patented based around these original techniques [89]. Today, three dimensional cell culture methods are grouped into three basic categories: cells cultured as multicellular aggregates, on plastic inserts containing a rich matrix such as a matrigel, or embedded in tissue support matrices meant to closely mimic the tumor microenvironment [89]. For its simplicity and reproducibility, we utilized the hanging drop method to study the effect of 3D spheroid cell culturing compared to monolayer in ovarian cancer cells.

Cancer Stem Cells

It has been postulated that a tumor may only arise through a small subclass of cells known as cancer stem cells (CSC) or tumor-initiating cells. CSC are characterized as tumorigenic, self-renewing, and pluripotent, meaning that they are capable of developing into a tumor comprised of heterogeneous cells. CSC are resistant to current conventional therapy options, allowing for their survival throughout treatment and leading to patient relapse after treatment is discontinued. Research has implicated

CSC targeting mechanisms, such as differentiation therapy, as a necessity to halt the reestablishment of the tumor. This treatment would involve introducing inhibitory RNA, thereby blocking pathways which maintain stemness and causing the cells to differentiate.

Research supports the existence of stem cell populations in ovarian cancer patients [90]. *In vitro* studies have shown that a higher population of cancer stem cells can be located within anchorage-independent growing spheres and that the formation of said spheres is associated with cell differentiation [91]. This is important for ovarian cancer because the disease disseminates into both peritoneum adherent nodules containing their own blood supply as well as non-adherent spheroids which can be found within the peritoneal cavity. Additional evidence relating cancer stem cells to ovarian cancer progression is its unique reaction to bevacizumab, an anti-angiogenic therapy through VEGF blockage which is vital to the interaction of stem cells to the vascular niche [92]. In Chapter Two, we show that pathways for cancer stemness are enhanced upon 3D spheroid culturing methods in HEY ovarian cancer cells.

The Heat Shock Response

The heat shock response (HSR) was discovered accidentally by Ferruccio Ritossa in the 1960s. At the time, Ritossa was studying puffing patterns observed in *Drosophila busckii* salivary gland chromosomes. The salivary glands are of particular interest due to the chromosomal puffing changes directly related to expression levels of the growth hormone, ecdysone [93]. After one of his lab mates changed the incubator temperature for the fruit fly, Ritossa witnessed a puffing pattern change, indicating new

RNA synthesis [94]. The first journal that he submitted these findings to rejected Ritossa's manuscript outright, claiming that it lacked biological significance. Eventually, his article would be published in *Experientia* in 1962 [95].

Initially, this discovery slowly sparked different experiments at the cytological level. It was discovered that the chromosomal response to temperature could be produced in minutes [96, 97] and was associated with newly synthesized RNA [95, 98]. In early research, it was discovered that this shift in chromosomal puffing patterns could be induced by stressors not related to temperature, such as inhibition of hydrogen transfer between NADH and Coenzyme Q_{10} [98] or by the increase of oxygen tension [99]. Since then, several other stress mechanisms have been linked to the HSR, to include oxygen-free radicals, aging, cancer, infection, and heavy metals [100]. Further studies in different *Drosophila* species and tissue types led scientists to believe that this response was not limited to *Drosophila busckii* salivary gland chromosomes [97, 101, 102]. In fact, the HSR has been shown to be a highly conserved, universal response which is found in every organism and nearly every cell and tissue type [103, 104].

Mechanics of the Heat Shock Response

The HSR is regulated by the phosphoprotein heat shock factor 1 (HSF1) is located on chromosome 8 and exists naturally as a monomer bound to heat shock protein 90 (HSP90). HSF1 and HSP90 dissociate upon stress, then homotrimerization of HSF1 allows it to bind to heat shock elements (HSEs) in the promoter regions of heat shock protein genes and stimulate transcription (Fig. 1.4) [105, 106]. HSF1 trimer binding to adjacent HSE sites is highly cooperative [107]. Posttranslational

modifications such as phosphorylation, deacetylation, and sumoylation are responsible for controlling HSF1 activation [108]. HSF1 can be acetylated by p300, causing it to attenuate off DNA, and can be deacetylated by the NAD+ dependent regulator SIRT1 [100]. Deletion of HSF1 in mammalian cells abolishes stress-induced HSPs expression, however it does not change their normal basal expression [109].

HSEs are denoted by a five base pair sequence of nGAAn, where n is any nucleotide, ordered in alternating orientation [110, 111]. The number of units within a HSE usually ranges from three to five, producing a sequence such as

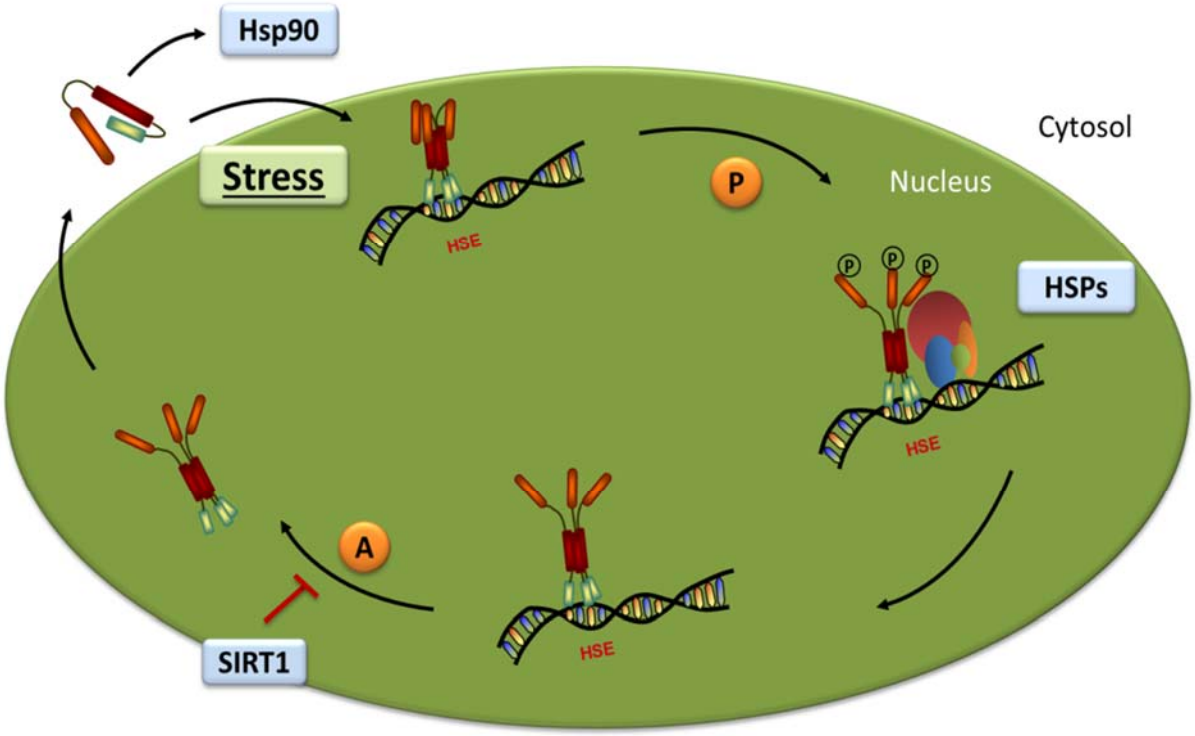

Figure 1.4: The Heat Shock Response through Activation of HSF1.

HSF1 is a phosphoprotein which exists as a monomer bound to Hsp90 under normal conditions. Upon stress HSF1 binds to HSEs of HSPs and promotes transcription. HSF1 is later attenuated off of the HSEs through negative feedback from Hsp70 and Hsp90 as well as acetylation. HSF1 is deacetylated by SIRT1, a NAD+ dependent protein deacetylase. (Adapted from Akerfelt *et al*., 2010). (Figure created by Trillitye Paullin).

TTCnnGAAnnTTC which is found approximately 1.5 helical turns upstream of the TATA box [112]. This sequence is bound by each of the three HSF1 trimer's DNA binding sites within seconds of stress exposure [113-115]. Upon heat shock, HSE chromatin regions become refractory to digestion, indicating protein binding [103].

Other Heat Shock Factors

The transcription factor HSF was originially discovered in 1984 through studying DNA-protein interactions in *Drosophila melanogaster* cells [116, 117]. While invertebrates only contained a single HSF, further research revealed expression of multiple HSFs in plants and vertebrates [118, 119]. The HSFs expressed in mammals, HSF1, HSF2, HSF3, and HSF4, HSF5, HSFX1, and HSFY1 exhibit both distinct and corresponding functions. HSF1, found in mammals, is the ortholog to the single HSF in *S. cerevisiae*, *C. elegans*, and *D. melanogaster* [120, 121]. The protein is vital to development and *Hsf1*$^{-/-}$ mice exhibit female infertility, growth retardation, elimination of the classical HSR, and prenatal lethality [109].

HSF2

In 1991, it was discovered that there were at least two separate HSF-related genes in humans, coined HSF1 and HSF2 [122, 123]. These two sequences have 40% idenity at the amino acid level, with the highest conservation found within the DNA binding domain and heptad repeats. However, unlike HSF1, HSF2 in not activated by celluar stress but instead by distinct signaling mechanisms related to the ubiquitin-proteasome pathway [124]. Hemin, an iron containing protoporphyrin, induces erythroid differentiation in K562 cells and activates HSF2 [125]. Through studies in

mouse embryogenesis and spermatogensis, HSF2 has been found to be vital for development and differentiation [126, 127]. Interestingly, while HSF2 deficiency is not embryonically lethal, Hsf2-/- mice present with brain abnormalities, and meitotic and gametogenesis defects in both males and females [128]. Recent research has shown that HSF2 is decreased in a wide range of cancer tumor types, including ovarian serous papillary eithelial cancer [129]. Furthermore, HSF2 suppresses prostate cancer tumor invasion and low expression levels have been linked to poor prostate cancer patient survival [129].

HSF3

Shortly after the discovery of HSF2, HSF3 was isolated and characterized from avian cells in 1993 [130]. The sequence for HSF3 is approximately 40% related to both HSF1 and HSF2, mainly found within the DNA binding domain and heptad repeats. Sequencing of the syntenic regions for HSF3 between chicken, mouse, and human revealed the mouse HSF3 gene, but only a human HSF3 psuedogene [131]. In avian cells, HSF1 and HSF3 are coactivated by stressors and are both required for induction of the HSR [132]. In fact, HSF3-null chicken B-lymphocyte cells significantly reduced HSP70 inducible expression and halted expression of HSP40, HSP90α, HSP90β, and HSP110 [133]. Independent of HS, HSF3 can be activated by the Myb oncogene via direct protein-protein interaction [134].

HSF4

Through screening of human and mouse cDNA libraries with a chicken HSF3 cDNA probe, HSF4 was isolated and characterized [135]. HSF4 is highly expressed in

the lens as a trimer due to its lack of a trimerization inhibitory domain, HR-C [135]. Deficiency in this gene causes cataracts in mice at early postnatal days [136]. HSF4 has been found to regulate nontraditional heat shock genes in murine lens cells independently of the HSR. Among the genes associated with HSF4 binding regions, approximately a third were induced upon HS [137]. In half of these genes, HSF4 was required as a chromatin remodeler to facilitate the binding of HSF1 to the promoter region [137].

HSF5, HSFY, and HSFX

HSF5 was discovered in 2001 as a potential HSF family member with a conserved region of the DNA binding domain, however it has yet to be fully characterized [138]. The HSFY gene is located within one of the three candidate regions for azoospermic factor (AZF) of the Y chromosome. Three HSFY transcripts were found to be differentially expressed in different tissue types, with transcripts 2 and 3 being testis-specific [139]. While the first transcript shares portion of the DNA binding domain with other HSF family members, the other two transcripts lack this conservation [139]. The expression of HSFY within the testis is highly dependent on its spermatogenic stage [140]. Reduced expression of HSFY within the testis may be associated with altered differentiation of spermatogenic cells in testes with deteriorated spermatogenesis [141]. There is little information about HSFX as it has yet to be fully characterized.

HSF1 Functional Domains

HSF1 is made up of several highly characterized domains. The DNA binding domain (DBD) is located on the amino-terminal region of the protein, and forms a globular structure with a flexible wing section [142, 143]. This wing allows for a protein-protein interface between the HSF1 monomers in order to promote the trimer binding to HSEs in the promoter regions of HSPs. This binding is highly cooperative between the subunits of the HSF1 trimer and from trimer to trimer, increasing the chances of a second trimer binding to an adjacent HSE by over 2000-fold [144].

Just after the DBD lies an oligomerization domain composed of hydrophobic heptad repeats (HR-A and HR-B) which are responsible for mediating HSF1 trimerization. This domain forms a coiled-coil, which is typical of a region containing several Leucine zippers. However, while most Leucine zippers facilitate the assembly of homodimers, the HSF1 heptad repeats form a triple-stranded configuration [119]. A third heptad repeat domain (HR-C) is located more closely to the carboxyl-terminus and is responsible for suppression of spontaneous HSF1 trimerization by folding back to interact with the HR-A and HR-B domains [119, 145].

Located between HR-A/B and HR-C, amino acids 221-310, is the regulatory domain (RD) which contains several serine residues that are phosphorylated upon stress. This domain is responsible for inhibition of the transactivation domains which make up the carboxy-terminal region of HSF1 [146]. The transactivation domains (AD-1 and AD-2) contain hydrophobic and acidic residues allowing the proteins to provide a prompt and sustained response to stress [146, 147]. AD-1 is made up of amino acids

371-430, is negatively charged, and forms an α-helix, while AD-2 is made up of the last 100 amino acids in the protein, is negatively charged, and is rich in proline and glycine [146, 148].

HSF1 Post-Translational Modification

HSF1 may undergo several different post-translational modifications which dictate the proteins overall function within a cell at any given time (Fig. 1.5). Activation of HSF1 is dependent on phosphorylation and several kinases have been shown to activate HSF1. Such kinases include casein kinase 2 (CK2) phosphorylation of Thr142 [149], calcium/calmodulin-dependent protein kinase II (CaMKII) phosphorylation of Ser230 [150], protein kinase A (PKA) phosphorylation of Ser320 [151], p38 mitogen-activated protein kinase (MAPK) phosphorylation of S326 [152], and polo-like kinase 1 (PLK1) phosphorylation of Ser419 [153]. Some HSF1 phosphorylation events, such as Ser121, Ser303, Ser307, and Ser363, have a negative impact on transcriptional activity [154, 155]. In addition to the sites described in Fig. 1.5, further phosphorylation sites have been located on serine residues 97, 230, 314, 319, and 363, however only S326 phosphorylation was shown to significantly activate HSF1 upon heat shock [3].

After HSF1 has been hyperphosphorylated, it undergoes sumoylation at lysine 298 by SUMO-1. Neighboring consensus sequences for phosphorylation and sumoylation together make up HSF1s phosphorylation-dependent sumolyation motif (PDSM). Phosphorylation-mediated sumoylation of this domain is stress sensitive and allows for the RD to restrict HSF1 activity. HSF1 sumoylation is persistent in cells exposed to mild heat stress while it is more transient in cells which experience a severe

heat stress [156].

HSF1 is subject to stress inducible acetylation which plays a role in the attenuation of HSF1 activity. The domains most affected by acetylation are responsible for protein subcellular location, oligomerization, and DNA recognition. Acetylation of this protein may be increased by sirtuin inhibition and likewise decreased by overexpression of sirtuin 1 (SIRT1), indicating that HSF1 is deacetylated by SIRT1 [100]. In fact, acetylation of K80 within the DBD deminishes the HSR by reducing DNA binding activity. HSF1 deacetylation by SIRT1 was shown to promote the HSR by

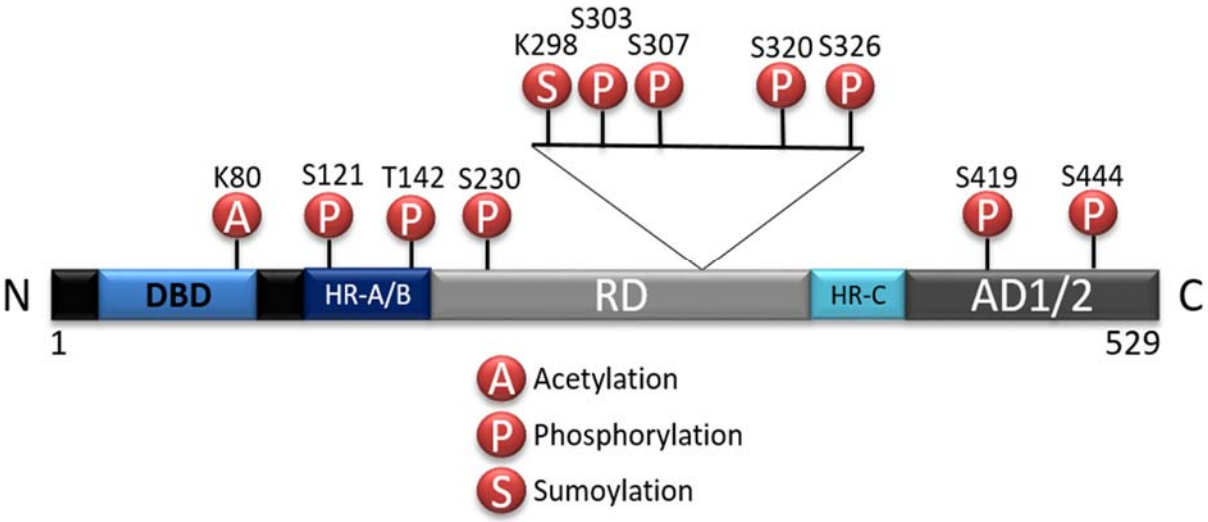

Figure 1.5: Well-Described HSF1 Post-Translational Modification Sites.

Acetylation of K80 is responsible for HSF1s loss of DNA affinity. S121, S230, S298, S303, S307, S320, S326, S419, and S444 are shown through mass spectrometry to be phosphorylated upon heat shock treatment [3]. Phosphorylation of T142 is also responsible for heat-induced transcriptional activity. Lastly, sumoylation at K298 by SUMO-1 inhibits HSF1 activity. (Adapted from Neef *et al*., 2011). (Figure created by Trillitye Paullin)

maintaining HSF1 in its DNA binding state [100]. This regulation of HSF1 via the longevity factor SIRT1 may indicate why a reduction of the HSR is seen with aging. Additional uncharacterized acetylation sites exist on lysine residues 116, 118, 126, 148, 157, 208, 224, 298, and 524 [100, 157].

Heat Shock Proteins

Once HSF1 is bound to HSEs, it promotes transcription of heat shock protein (HSP) genes, which are among the most highly conserved genes in existence. While their transcription is induced by a stressor such as heat, they are also essential for normal cellular functions at basal temperatures. HSPs are also responsible for reducing the accumulation of damaged and misfolded proteins commonly found in aging cells. A discrepancy in protein homeostasis is a hallmark of both normal aging and age-related neurodegenerative diseases [158-161]. Molecular chaperones, such as HSPs, prevent toxic protein aggregation by binding to non-native polypeptides and correctly folding such proteins or by degrading them through the ubiquitin-proteasome system [162]. There are six major classifications of HSPs based on their molecular mass: small HSP/HSPB, HSP40/DNAJ, HSP60/HSPD, HSP70/HSPA, HSP90/HSPC, and HSP110/HSPH.

HSP27/HSPB

One such sHSP is heat shock protein 27 (HSP27), also referred to as HSPB1. HSP27 contains a highly conserved α-crystallin domain, which is required for oligomerization, within its 205 amino acid protein complex. As a protein chaperone, HSP27 has been implicated in several cellular processes, to include growth, differentiation, survival, and tumorigenesis [163]. HSP27s serine residue phosphorylation can determine its biological function. Non-phosphorylated HSP27 acts as an actin capping protein on the plus end of actin filaments, thereby inhibiting actin

polymerization while phosphorylated HSP27 promotes polymerization [164]. HSP27 expression and HSP27 overexpression increased overall tumor size when colon adenocarcinoma cells were injected into syngeneic rats [165]. Phosphorylation inhibition of HSP27 causes reduced tumor cell migration and invasion in breast cancer cells [166] and phosphorylation of Ser78 on HSP27 correlates with Her2/neu expression [167].

HSP40/DNAJ

HSP40, or DNAJ, contains a J domain made up of 70 amino acid residues which are responsible for binding the HSP70 nucleotide-binding domain (NBD) and stimulating its ATPase activity through hydrolysis [168]. Known as co-chaperones, several members of the HSP40 family have been characterized as binding a diverse array of client proteins to be manipulated by HSP70. Through a multi-step process, hydrolysis of ATP to ADP causes a conformation change in the HSP70 substrate-binding domain (SBD), increasing HSP70 affinity for its aggregated target [169, 170]. After ADP is replaced for ATP via nucleotide exchange factors (NEFs), the polypeptide is released and can fold into its native conformation [171]. If the polypeptide remains misfolded, it can either reenter the cycle for refolding or be targeted for degradation by the ubiquitin-proteasome system [172].

HSP70/HSPA

HSP70 is one of the most highly induced proteins in response to cellular stress [173]. HSP70 is present in the cytosol and in membrane-bound organelles and has a number of client proteins. Misfolded client proteins are escorted by HSP40 to HSP70s'

substrate-binding domain as described above. Its chaperone function for a wide range of client proteins leads to HSP70s key influence on apoptosis [174], immunomodulation [175], and tumorigenicity [176]. HSP70 knockdown has been shown to enhance cancer cell death over normal cells because its down-regulation is cytotoxic to transformed cells [177].

HSP90/HSPC

HSP90 plays a role in cellular homeostasis by providing stability and correctly folding client proteins which have been denatured upon stress [112]. This chaperone exists as an ATPase which recruits the assistance of co-chaperones to refold denatured proteins [178]. Over 20 HSP90 co-chaperones have been discovered which work to inhibit or activate HSP90 by regulating its ATPase activity or recruiting client proteins [179, 180]. Identified client proteins are implicated in several physiological events, to include signal transduction [181], tumor progression [182], cell cycle machinery [183], apoptosis [184], telomere elongation [185], and cell invasion and metastasis [186]. Due to its role in several oncogenic pathways, inhibition of HSP90 is being studied for its potential anti-tumor affects [187, 188].

HSR Negative Feedback Mechanism

The HSR is thought to be regulated by a negative feedback loop mechanism where HSF1 is kept inactive by the presence of excess HSPs [189]. Upon stress, HSPs bind to client misfolded proteins and release HSF1 from chaperone complexes, allowing for HSF1 trimerization and induction of the HSR. Once HSP expression has been saturated, they will bind and inhibit HSF1 once more. This was shown through the

activation of HSF1 by injection of non-native denatured proteins into Xenopus oocytes [190].

HSF1 Target Genes

Target genes of HSF1 are implicated in a wide range of cellular functions including cell division, development, insulin signaling, energy production, cytoskeletal organization, and vesicular transport. The most investigated HSF1 target genes are HSPs, as discussed above, which may serve as molecular chaperones to refold and disaggregate damaged polypeptides. HSF1 activation of these genes is vital to cell survival upon a number of stressors.

In addition to molecular chaperones, HSF1 is associated with several genes implicated in other physiological responses. Through suppression of the NFKB pathway, HSF1 binds directly to the nuclear factor of interleukin 6 (NF-IL6) and represses transcription of IL-1 beta gene, which is an essential mediator of the inflammatory response [191]. HSF1 has been shown to regulate expression of several other non-HSP genes including heme oxygenase 1 (HO-1) [192], BCL2-associated athanogene 3 (BAG3) [193], clusterin (CLU) [194], thrombomodulin (THBD) [195], and plasminogen activator inhibitor-1 (PAI-1) [196].

HSF1 plays a critical role in oncogenesis which has been shown to be transcriptionally unique from that of the classical heat shock response. Utilizing ChIP-Seq analysis, it was determined that HSF1 strongly binds to several genes in cancer cells which are not bound upon heat shock to include chaperone containing TCP1 subunit 6A (CCT6A), CDC28 protein kinase regulatory subunit 2 (CKS2), CDC protein

kinase regulatory subunit 1B (CKS1B), eukaryotic translation initiation factor 4A2 (EIF4A2), lymphocyte antigen 6 complex locus K (LY6K), RNA binding motif protein 23 (RBM23), and suppression of tumorigenicity 13 (ST13) [197]. Conversely, heat shock protein family A (HSPA6/HSP70) and DnaJ heat shock family member C7 (DNAJC7/HSP40) genes were strongly bound by HSF1 upon heat shock but not in cancer cells [197]. While the exact mechanism for HSF1's district cancer role is not well defined, scientists have postulated that cancer activated pathways, such as EGFR/HER2 [198] and RAS/MAPK [199], may be implicated due to their ability to alter HSF1 activity [197]. Further analysis of this specialized transcription pathway could lead to new therapeutic targets in cancer treatment.

HSR and Aging

Several studies have implicated the HSR and HSPs in aging. Throughout the aging process, cellular death and degeneration occurs within vital organs. This degeneration causes an accumulation of damaged and dysfunctional proteins. However, an increase of misfolded proteins within the cell is also coupled with a diminishing of the HSR with age. Age-dependent decrease in the HSR can be found in the liver, neuronal tissues, and skeletal and cardiac muscle [200-202]. Specifically in neuronal tissues, this results in the formation of inclusion bodies, or aggregated proteins. Inclusion bodies have been linked to several neurodegenerative disorders, to include Alzheimer's and Parkinson's disease. Alzheimer's disease has been associated with amyloid-β peptide and tau aggregation while Parkinson's stems from α-synuclein inclusions. These connections implicate an age-dependent loss of protein quality control as a potential cause. In fact, downregulation of HSF1 results in a shortened

lifespan in *C. elegans* while overexpression lengthens it [203]. Additionally, shortened lifespan was found in *hsf1*$^{-/-}$ mice which were inoculated with prions compared to wild-type mice [204].

Several studies have been conducted which focus on exercise-induced stress response in skeletal muscles. In young organisms, non-damaging exercise results in a significant increase in HSPs, while this is not the case for old individuals [205]. Interestingly, DNA binding activity of HSF1 is not reduced in old organisms, suggesting that failure to induce the HSR occurring during or post-transcription [206].

HSR and Cancer

One of the basic hallmarks of cancer is that it must evade apoptosis in order to continue cell proliferation and create a tumor. Commonly, this is accomplished through the mutation or overexpression of one or more oncogenes or tumor suppressors. Recent studies have shown that many cancer types may utilize HSF1's potential chaperone function to stabilize such oncogenes within the cell, thereby allowing the cancer to progress [207]. Additionally, increased HSPs in tumor cells as compared to normal cells provide a cytoprotective response in advanced cancers with acidotic, hypoxic, and nutrient deprived microenvironments [208]. Likewise, HSP70 overexpression can cause reversible oncogenic transformation [209]. HSP70 may increase drug resistance in some cancer cells due to its ability to inhibit apoptosis both upstream and downstream of the mitochondria [210].

High HSP70 and HSF1 levels promote cell survival, migration, invasion, and angiogenesis [108, 211-214]. Increased expression of HSF1 has been shown in

prostate, breast, colon, bladder, and lung cancer [197, 215-217]. This influx in HSF1 and HSP70 levels has been connected to cancer metastasis, poor patient outcome, and chemotherapy and radiotherapy resistance. Interestingly, this effect can be seen in cancers derived from multiple oncogenes, including p53, RAS, NF1, and PDGF [207, 218-220]. HSF1 may also be used as a biomarker for poor patient prognosis and highly metastatic tumors in these cancer types [197, 221].

In mice, HSF1 is recruited to enhance cancer cell survival, causing tumor size to be greatly reduced in HSF1 knockout mice compared to wild type [207]. HSF1 knockdown in breast cancer cells inhibits spheroid formation, decreases cancer stem cell marker expression, and increased sensitivity to paclitaxel chemotherapy treatment [222]. Furthermore, HSF1 knockdown MEFs exhibited a significant suppression of focus formation induced by PDGF-B [207]. In our studies, Chapter Three shows that knockdown of HSF1 also reduced spheroid and focus formation in SKOV3 and HEY ovarian cancer cells. Through microarray analysis, spheroid formation resulted in differentially expressed genes involved in cancer stemness and tumorigenesis as seen in Chapter Two.

HSF1's ability to promote transcription of chaperones utilized for cancer progression makes it and subsequent chaperones strong potential targets for cancer therapy. New research has revealed that HSF1 expression is significantly higher in malignant ovarian cancer tumors than in benign tumors [223], however further studies have yet to be conducted showing its full effects within this deadly cancer. As shown in Chapter Three, our studies show that HSF1 plays a vital role in ovarian cancer

progression and that HSF1 knockdown reduces migration, invasion, and EMT in SKOV3 and HEY cell lines.

Specific Aims

The objective of this study is to investigate the difference between monolayer and spheroid culturing and determine what role HSF1 plays in ovarian cancer progression. **We hypothesize that ovarian cancer monolayer cells will significantly differ in gene expression profile from that of spheroidal cells, that HSF1 knockdown will inhibit ovarian cancer progression in both monolayer and spheroid model cells, that the effects of this knockdown will be more fully revealed in 3D culture, and that spheroids will prove more susceptible to the chemotherapy agents paclitaxel and cisplatin upon HSF1 knockdown or treatment with small molecule modulators of HSF1 and HSP90.** The following specific aims are intended to assess this hypothesis.

Specific Aim 1: Investigate the differences between monolayer and spheroid cell culturing in ovarian cancer (Chapter 2).

1.1: Determine gene expression profile changes in 3D spheroids versus 2D monolayers.

1.2: Validate microarray data through quantitative RT-PCR.

1.3: Evaluate pathways significantly affected by spheroid culturing.

Specific Aim 2: Determine HSF1's role in ovarian cancer proliferation and progression (Chapter 3).

2.1: Evaluate effects of HSF1 knockdown on ovarian cancer cell proliferation.

2.2: Test the colony formation ability, and the migration and invasion efficiency of ovarian cancer cells upon HSF1 knockdown.

2.3: Assess the consequence of HSF1 knockdown on EMT in 2D and 3D ovarian cell culture.

CHAPTER TWO: SPHEROID GROWTH IN OVARIAN CANCER ALTERS TRANSCRIPTOME RESPONSES FOR STRESS PATHWAYS AND EPIGENETIC RESPONSES

Authored by Trillitye Paullin, Chase Powell, Christopher Menzie, Robert Hill, Feng Cheng, Christopher J. Martyniuk, and Sandy D. Westerheide

Submitted to PLoS ONE. October 2016.

Experiments were designed, performed, and analyzed by T. Paullin or performed under the direction of T. Paullin. C. Menzie and T. Paullin performed qPCR analysis for Figure 2.4. Expression analysis and subsequent figures were created by C. Martyniuk and F. Cheng. Manuscript was written by T. Paullin and S. Westerheide.

Introduction

Despite recent improvements in surgery and chemotherapy, ovarian cancer is still the leading cause of death from gynecological malignancy [224]. Due to poor detection methods and a lack of symptoms, most patients are diagnosed at advanced stages, when the tumor has metastasized and spread [225]. Studies suggest that in order for metastasis to occur, the cancer cells must undergo phenotypic changes modulated by the epithelial-mesenchymal transition (EMT) [58].

EMT is a distinct process whereby epithelial cells undergo changes in favor of mesenchymal properties [35]. This process is most commonly observed during developmental stages when epithelial cells must migrate and dedifferentiate, such as in

the formation of the mesoderm during gastrulation [36]. A well-defined inducer of EMT is transforming growth factor-β (TGFβ) [226, 227]. The addition of TGFβ to epithelial cells induces transient EMT within hours of treatment through activation of the Smad pathway [228].

Although two dimensional (monolayer) tissue culture models are largely used to study the EMT process, evidence suggests that three dimensional (spheroid) culturing may be more physiologically relevant as it better emulates oxygen levels, pH conditions, glucose levels, extracellular matrix strength, and overall morphology of *in vivo* solid tumors [66-68, 229]. This is especially the case when focusing on metastasis, tissue invasion, angiogenesis, and drug sensitivity [69-71].

At least a third of ovarian cancer patients present with ascites [72]. Ascites is the accumulation of fluid in the peritoneal cavity which may contain ovarian cancer cells, lymphocytes, and mesothelial cells in the form of single cells and aggregates [73]. Further studies revealed that ascites spheroids may cause secondary tumors due to their ability to adhere to extracellular matrix proteins via interaction between multiple integrins and their ligands [230, 231]. Here, we conducted a comprehensive gene expression analysis for the process of culturing HEY ovarian cancer cells in 3D vs. 2D cultures during the TGFβ-induced EMT process. Using subnetwork enrichment analysis, we identified stress pathways, DNA integrity pathways, and epigenetic processes as those most affected by 3D vs. 2D growth.

Materials and Methods

Cell Culture and Treatments

The HEY human ovarian cancer cell line was authenticated by short tandem repeat (STR) DNA profiling (Genetica, Inc.) and was compared to ATCC and previously published profiles [232]. Cells were cultured in a humidified incubator containing 5% CO_2 at 37^oC in RPMI with 10% fetal bovine serum and 1% Pen-Strep-Glutamine. Spheroid formation was accomplished through the hanging drop method. Briefly, trypsinized HEY cells were resuspended at 1 x 10^6 cells/mL in supplemented RPMI. Multiple 25 µl droplets of the cell solution were then placed onto plate lids, inverted, and incubated for 72 hours to allow cells to aggregate into spheroids. To induce EMT, a final concentration of 10 ng/µl TGFβ was added to cells and incubated for 72 hours as monolayer cell culture or hanging drops during the creation of spheroids. Following incubation, monolayer cells and spheroids were photographed using an Evos® FL Cell Imaging microscope (ThermoFisher Scientific) and then collected in 1X PBS.

Quantitative RT-PCR

RNA was extracted from harvested cells using the RNeasy Mini Kit (Qiagen). RNA samples were then reversed transcribed with a High Capacity cDNA Reverse Transcription Kit (Applied Biosystems) per the manufacturer's instructions. Subsequent samples were then diluted to 50 ng/ µL and used as a template for quantitative PCR (qPCR). qPCR was accomplished with a Step One Plus Real-time PCR system (Applied Biosystems) and SYBR® Green Supermix with ROX (BioRad) according to the

manufacturer's protocol. Relative mRNA levels were quantified for *ahnak2*, *akr1c1*, *ccdc80*, *hspa1a*, *hsph1*, *prss35*, *rgs2*, and *rrad* using gene-specific primers (Table 2.1).

Affymetrix GeneAtlas Platform and 3'IVT Compatible U219 Probe Arrays

The oligonucleotide probe arrays used were the Affymetrix HG-U219 human array strips. These arrays consist of more than 530,000 probes detecting over 36,000 transcripts and variants-representing more than 20,000 genes.

Sample Processing and Validation

HEY Human ovarian carcinoma cells treated with TGF-β were cultured on a 2-dimensional substrate or 3-dimensional substrate as described above. Replicates of 4 separate experiments were performed on 4 different culturing days, cells isolated and stored in RNAlater Soln (Ambion) for no more than 7 days. Up to 100 µg of total RNA was isolated from all 8 samples using Qiagen's RNeasy Mini Kit according to the manufacturer's instructions. RNA integrity was verified with 1 µl of total RNA on RNA 6000 nanochips (Agilent) using The Agilent 2100 Bioanalyzer. All results for all 8 samples reported RNA Integrity Numbers (RIN) > 9. 100 ng of polyadenylated RNA was converted to cDNA and then amplified and labeled with biotin using Affymetrix 3'IVT Expression System according to the manufacturer's instructions. Hybridization with the biotin-labeled RNA, staining, and scanning of the chips followed the proscribed procedure outlined in the Affymetrix technical manual and has been previously described.

Data Analysis

Scanned output files were visually inspected for hybridization artifacts and then annotated and normalized using Affymetrix Expression Console v1.3.1. Additionally, all QC metrics reported no outlier samples. Signal intensity was scaled to an average intensity of 500 during comparison analysis. Annotated expression data were assigned an ANOVA P value for the likelihood that any perceived difference was due to chance. The P values for all probe sets were exported to a text file and all pairwise comparisons of Bi-weight average signals were then aligned in MS Excel. For the comprehensive analysis, $P < 0.05$ was identified as having a linear change (increased or decreased) for the comparison. This analysis reported ~3,329 genes that showed differential regulation greater or less than 2-fold. To increase stringency, only genes whose fold-change was greater than or less than four ($p < 0.05$) were considered to be differentially expressed, reducing the pool to 493 candidate genes.

Data were analyzed using different visualization techniques that included hierarchical clustering, principle component analysis (PCA), and Volcano plots. All analyses were conducted in JMP Genomics v7.0. Transcripts that showed $p<0.01$ were used in the two-way clustering using the Fast ward algorithm after each row was centered to a mean of zero (0) and variance scaled to one. Results from hierarchical cluster analyses were visualized using heat map dendrograms, and biological replicates are partitioned into groups based on similarity (i.e., individuals clustered together are most similar). PCA used spatially weighted averages and were conducted on normalized expression values, the same dataset used in the cluster analysis. Volcano

plots were generated in JMP Genomics 7.0 following an ANOVA to identify differentially expressed transcripts.

Pathway Studio Analysis

Pathway Studio 9.0 (Elsevier) and ResNet 10.0 were used for sub-network enrichment analysis (SNEA) of cell processes [233] . The option of "best p value, highest magnitude fold change" in Pathway Studio was used for duplicated probes. Transcripts were successfully mapped using GeneBank ID. SNEA was performed to identify gene networks that were significantly different. A Kolmogorov–Smirnov test with 1000 permutations was conducted to determine whether certain networks were preferentially regulated compared to the background reference probability distribution. Networks are constructed based on common regulators of expression and regulators of specific cell processes. The enrichment P-value for a gene seed was set at $P < 0.05$. Additional details on the use of SNEA can be found in Langlois and Martyniuk [234] .

Results and Discussion

HEY Cells Treated with TGFβ have Distinct Gene Expression Profiles when grown as 3D Spheroids vs. 2D Monolayers

To examine whether growth of HEY ovarian cancer cells as 3D spheroids vs. 2D monolayers could influence gene expression, we performed microarray analysis on biological quadruplets with cells grown under each condition. To create spheroids, the hanging drop method [235] was used as outlined (Fig. 2.1). We find that HEY cells treated with TGFβ have distinct gene expression profiles, depending on whether they are cultured under 2D vs. 3D conditions (Fig. 2.2). Hierarchical clustering reveals that

each of the two groups form into distinct clades based on gene expression (Fig. 2.2A). Additionally, principle component analysis shows that biological quadruplicates for HEY 2D and HEY 3D samples are more similar to themselves than to each other (Fig. 2.2B). Volcano plot analysis shows that there are numerous genes between the two groups that have a high fold change and that are also statistically significant (Fig. 2.3).

RT-qPCR was performed on eight different genes which were found to be up or downregulated by varying degrees upon 3D culturing to validate our microarray analysis (Fig. 2.4). The eight genes we chose to validate include two highly upregulated genes, the serine protease PRSS35 and the aldo-keto reductase AKR1C1, as well as the highly downregulated E-cadherin regulator CCDC80. Additionally, we chose some genes that were more moderately regulated, including the chaperones HSP110 and HSP70, the G-protein signaling inhibitor RGS2, the fibroblast growth factor secretion regulator AHNAK2 and the apoptotic inducer RRAD. Our results show that similar trends are observed via RT-qPCR for these genes as compared to our microarray results. Overall, our data show that HEY ovarian cancer cells, treated with TGFβ to induce EMT, show dramatic differences in gene expression profiles when grown as 3D spheroids vs. standard 2D culture.

Transcripts Affected by 3D Culturing may Enhance the Tumorigenicity of HEY Cells

Growth as 3D spheroids leads to both the upregulation and downregulation of gene expression (Table 2.2). The most highly upregulated gene under 3D growth conditions in HEY cells is AKR1C1 (Aldo-Keto Reductase Family 1, Member C1), part of a family of cytosolic NADP(H)-dependent oxidoreductases that is involved in

detoxification of xenobiotics, steroids, and polycyclic aromatic hydrocarbons [236]. Increased expression of AKR1C1 is associated with the development of cisplatin resistance in human ovarian carcinoma cells [237]. Previous work shows that ovarian cancer cells, grown in 3D, are more resistant to chemotherapy treatment [74]. It is therefore plausible that the increased expression of AKR1C1 upon ovarian cancer cell 3D growth may promote chemotherapy resistance. PRSS35 (Protease, Serine 35), another highly upregulated gene upon 3D growth, belongs to the trypsin class of serine proteases. This protease is highly expressed in the mouse ovary [238]. Proteases play an important role in proteolysis that is essential for tissue remodeling that occurs during EMT by breaking down the extracellular matrix. While metalloproteases play the largest role in this process, serine proteases also contribute [239]. We postulate that enhanced expression of PRSS35 under 3D growth conditions may promote ovarian EMT through the proteolytic digestion of cell attachments. A transcript that was highly downregulated upon 3D growth is CCDC80 (Coiled-Coil Domain Containing 80). Interestingly, CCDC80 null mice develop thyroid adenomas and ovarian carcinomas, and CCDC80 gene expression is decreased in human ovarian cancer samples as compared to normal ovarian samples [240]. The mechanism for the tumor suppressor properties of CCDC80 may be through its ability to induce E- cadherin expression [240]. E-cadherin provides crucial cell-cell adhesion to hold epithelial cells tightly together, and enhanced E-cadherin expression promotes the epithelial phenotype over the cancer-promoting mesenchymal phenotype [241]. Collectively, we propose that regulation of these and other genes upon 3D growth may enhance the tumorigenic properties of ovarian cancer cells.

Gene-Set Enrichment Analysis Reveals Novel Pathways that are enriched upon HEY Cell Growth as 3D Spheroids

Gene set enrichment analysis suggested that pathways downregulated by more than 15% include branched chain amino acid metabolism, folate biosynthesis, fatty acid oxidation, and the mevalonate pathway, while pathways upregulated in the 3D cells include those related to tumor necrosis factor receptor (TNFR) superfamily member 1A and 6. These pathways were increased more than 20% with 3D growth in HEY cells, and they have all been related to cancer growth. Branched chain amino acids, such as leucine, positively regulate the mammalian-target-of-rapamycin (mTOR) pathway [242]. The mTOR pathway is involved in regulating cellular functions involved in growth and proliferation, and upregulation of this pathway is commonly observed in human cancers [243]. Folate plays a role in nucleotide synthesis and methylation, making it essential to rapidly growing cancer cells [244]. Fatty acid oxidation is required for functional angiogenesis and is utilized by cancer cells to overcome metabolic stress to proliferate [245]. The mevalonate pathway is responsible for converting acetyl-coenzyme A into isoprenoids, which are required for cholesterol and steroid synthesis [246]. LDL-cholesterol accumulates in cancer tissues and is associated with migration, proliferation, and loss of adhesion from the primary tumor which are vital steps in the epithelial to mesenchymal transition [246]. Upregulation of TNFR family members allows signaling via the NF-κB transcription factor, which can promote tumorigenesis through the activation of the expression of genes involved in processes including cell proliferation, migration and anti-apoptosis [247].

Transcriptional Networks Involving Stress Pathways are Altered in HEY Cell Growth as 3D Spheroids

Unique sub-networks underlie the transition from 2D to 3D growth in HEY cells (Table 2.3, for a complete list of enriched cell networks see Appendix B). We note that a number of the identified sub-networks are related to the response to stress (Fig. 2.5, for a complete list of gene networks related to stress Appendix C). The finding that stress responses are activated upon 3D growth is not surprising, given that growth under these conditions is likely to cause nutrient limitation and hypoxia, among other cellular stresses.

Transcripts in the network that are related to the oxidative stress response include Peroxiredoxin 2 (PRDX2) (Fold change = +2.2), Catalase (CAT) (+1.3), Superoxide dismutase 1, soluble (SOD1) (+1.2), and Glutathione S-transferase omega 1 (GST01) (-1.3). In 1984, it was shown that transformation may result from the exposure of reactive oxygen species to mouse fibroblasts [248]. It has since then been hypothesized that the rise in cancer diagnosis for older individuals may be due to a lifetime of DNA damage by reactive species accumulated endogenously and exogenously [249]. Oxidative stress activates ERK/MEK and PI3K/AKT pathways and impacts signaling proteins important in cancer such as Ras, Raf, p53, PKC, c-Myc, and Nrf2 [250-252]. The changes detected in the oxidative stress pathway upon growth of HEY cells in 3D may thus promote tumorigenic properties of the cells.

Also changed in 3D cells are transcripts that are associated with the heat shock response. Some examples include heat shock protein 90kDa alpha (cytosolic), class A

member 1 (HSP90AA1) (+1.16), heat shock 27kDa protein 1(HSPB1)(+1.20), and heat shock transcription factor 1 (HSF1) (+1.28). Recent studies have suggested that many cancer types utilize activation of heat shock factor 1 (HSF1), the master regulator of the heat shock response, to stabilize oncogenes within the cell [207]. The heat shock response is a highly conserved response to specific environmental stressors such as heat shock, heavy metals, and oxidative stress [104]. HSF1 promotes the transcription of heat shock protein genes, many of which encode molecular chaperones. Increased chaperone expression provides a cytoprotective response in advanced cancers with acidotic, hypoxic, and nutrient-deprived microenvironments [208]. Elevated levels of one or more chaperones are commonly found in both solid cancer tumors and hematological malignancies [253-257]. In fact, overexpression of HSP27, HSP70, or HSP90 correlates with poor prognosis and may contribute to drug resistance in some cancer types [258-261]. Activation of the heat shock response in spheroids may promote cell survival, in the face of multiple cellular stresses, through enhanced expression of HSF1 target genes, including molecular chaperones. Further analysis of this spheroid model could offer valuable insight into how HSF1 and HSPs could be utilized as targets for chemotherapy in ovarian cancer patients.

Other examples of stress-related genes that show a high magnitude of response in terms of downregulation include the PIF1 5'-to-3' DNA helicase homolog (*S. cerevisiae*) (-13.0), epidermal growth factor receptor (-4.6), far upstream element (FUSE) binding protein (-4.4), and cysteine-rich, angiogenic inducer (-4.4). Increasing transcripts in the network included nuclear factor of kappa light polypeptide gene enhancer in B-cells inhibitor, alpha (+10.3), FBJ murine osteosarcoma viral oncogene

homolog (+14.7), prostaglandin-endoperoxide synthase 2 (prostaglandin G/H synthase and cyclooxygenase) (+29.5), and interleukin 8 (+49.8). Many of these aforementioned transcripts have been shown to play critical roles in the progression of cancer. For example, PIF1 is a DNA-dependent adenosine triphosphate (ATP)-metabolizing enzyme that is required for proper replication and repair during cell division. Studies show that this protein inhibits S-phase progression and reduces proliferation rates of RAS oncogene-transformed fibroblasts [262], and may therefore be a novel drug target for cancer therapy. Here, the downregulation of PIF1 mRNA may lead to increased proliferative activity during the transition from a non-cancerous cell to a cancerous cell. Our network analysis also identifies DNA duplex unwinding (down regulated -1.49) and S-M checkpoint (down-regulated -1.59) as processes significantly down-regulated in 3D spheroids, processes which may be related to changes in PIF1 expression. In terms of ovarian cancer, there are many studies implicating epidermal growth factor receptor (EGFR) as a key regulator of cell differentiation Specifically, EGF-induced EMT increases phosphorylation of Akt, ERK1/2, and S6 ribosomal protein, which alters ovarian cancer cell proliferation and differentiation [263]. Additionally, elevated EGFR expression in tumor stroma is linked to aggressive epithelial ovarian cancer in patients and relates to Ki-67 expression in tumor cells [264]. In terms of up-regulated transcripts, notable transcripts included FBJ murine osteosarcoma viral oncogene homolog, a member of the Fos family of transcription factors. In cancer, this gene is a proto-oncogene implicated in cell proliferation and transformation [265]. Lastly of interest in the network was IL8, a gene that showed a dramatic increase in expression of ~50-fold in 3D cells (Table 2.2). Polymorphisms in this gene have been shown to be

associated with a significantly higher risk of ovarian cancer [266, 267]. Studies also show that increases in IL8 is associated with increased tumor growth and metastases [268].

Various responses related to DNA integrity were altered, including the response to DNA damage, genetic instability, nucleotide excision repair, and the DNA damage checkpoint pathway. The hypoxic environment created within spheroids may lead to increased DNA damage. Spheroid culturing has shown to alter chromatin packaging which in turn improves DNA repair through what is known as the "contact" effect [269]. DNA damage via metabolic products and by-products, such as ROS, may decrease replication fidelity, resulting in increased mutagenesis. Mutations and chromosomal abnormalities can increase the risk of cancer through the activation of oncogenes or the inactivation of tumor suppressor genes. Complex DNA-damage response mechanisms have evolved in order to isolate and repair these mutations. One such mechanism is the nucleotide excision repair (NER) pathway. NER is able to eradicate a variety of DNA lesions due to its ability to circumvent recognition of the lesion itself and focus on a set of commonalities shared by many different lesions [40]. Our analysis showed a significant enrichment of the NER pathway when cells are cultured as 3D spheroids.

Sub-Network Enrichment Analysis Identifies that Genes Involved in Epigenetic Processes are enriched upon HEY Cell Growth as 3D Spheroids

Two epigenetic processes, DNA methylation and histone acetylation, are also enriched upon 3D growth. A number of genes are both up- and downregulated related to DNA methylation, and this process is affected by about 4-5% (Fig. 2.6). DNA methylation changes are seen in several cancer types and have been linked to changes

in gene expression in highly metastatic tumors [270]. The process of histone acetylation is also significantly affected in both positive and negative fashions (Fig. 2.7).

Conclusion

Spheroid formation more closely mimics that of an *in vivo* tumor due to the cells ability to form an extracellular matrix and cell adhesions. Here, using the HEY ovarian cancer cell line, we show that 3D spheroid growth utilizing the hanging drop method affects a number of cellular processes, including the multiple cellular stress pathways, DNA integrity pathways, and epigenetic pathways. As these pathways all could affect tumorigenesis and the response to chemotherapies, our studies suggest that using 3D culture instead of 2D monolayers may be more informative in studying the properties of ovarian cancer cell lines.

Table 2.1: List of Primers used in Quantitative RT-qPCR.

Gene Name	Sequence
AHNAK2	F: 5' - GAAAATCCCAGAGCCCCACA - 3' R: 5' - GTGCCCTCCTGAGTCCTAGA - 3'
AKR1C1	F: 5' - TGGCCATCCGAAGCAAGATT - 3' R: 5' - GAGGATCATCTCCAGCTGCC - 3'
CCDC80	F: 5' - CACGCAGAGTCCCAAGAAGT - 3' R: 5' - CAAAATTGCACGCCTGACCA - 3'
HSPA1A	F: 5' - GAGGGCCATGACGAAAGACA - 3' R: 5' - TCGCTGATCTTGCCCTTGAG - 3'
HSPH1	F: 5' - AGGATCTCCCAAGCCTGGAT - 3' R: 5' - TGGAGAAAGGAGCAGCATGG - 3'
PRSS35	F: 5' - GCTGAAGCGTGCTCACAAAA - 3' R: 5' - GTCGGACACACTGCAAAACC - 3'
RGS2	F: 5' -TCTACTCCTGGGAAGCCCAA - 3' R: 5' - GAGGACAGCTTTTGGGGTGA - 3'
RRAD	F: 5' - CCATGGGGGATGCCTATGTC - 3' R: 5' - CGGCTGTTACGAGCTACGAT - 3'

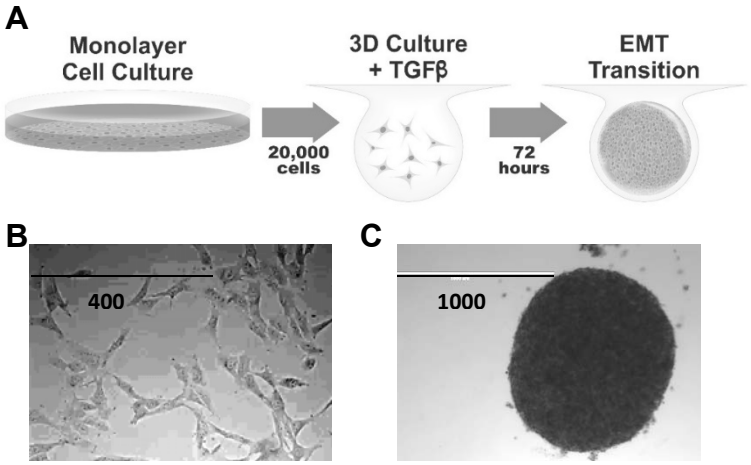

Figure 2.1: Establishment of 3D Mesenchymal Cell Populations from Confluent Monolayers.

A) HEY cells grown in a monolayer are released and then suspended in drops of culture media containing TGFβ (20,000 cells per drop) using the hanging drop method. After 72 hours, the resulting 3D spheroids are then assayed. B) Image of HEY cells grown in monolayer culture. C) Image of HEY cells grown as a 3D spheroid and treated with TGFβ.

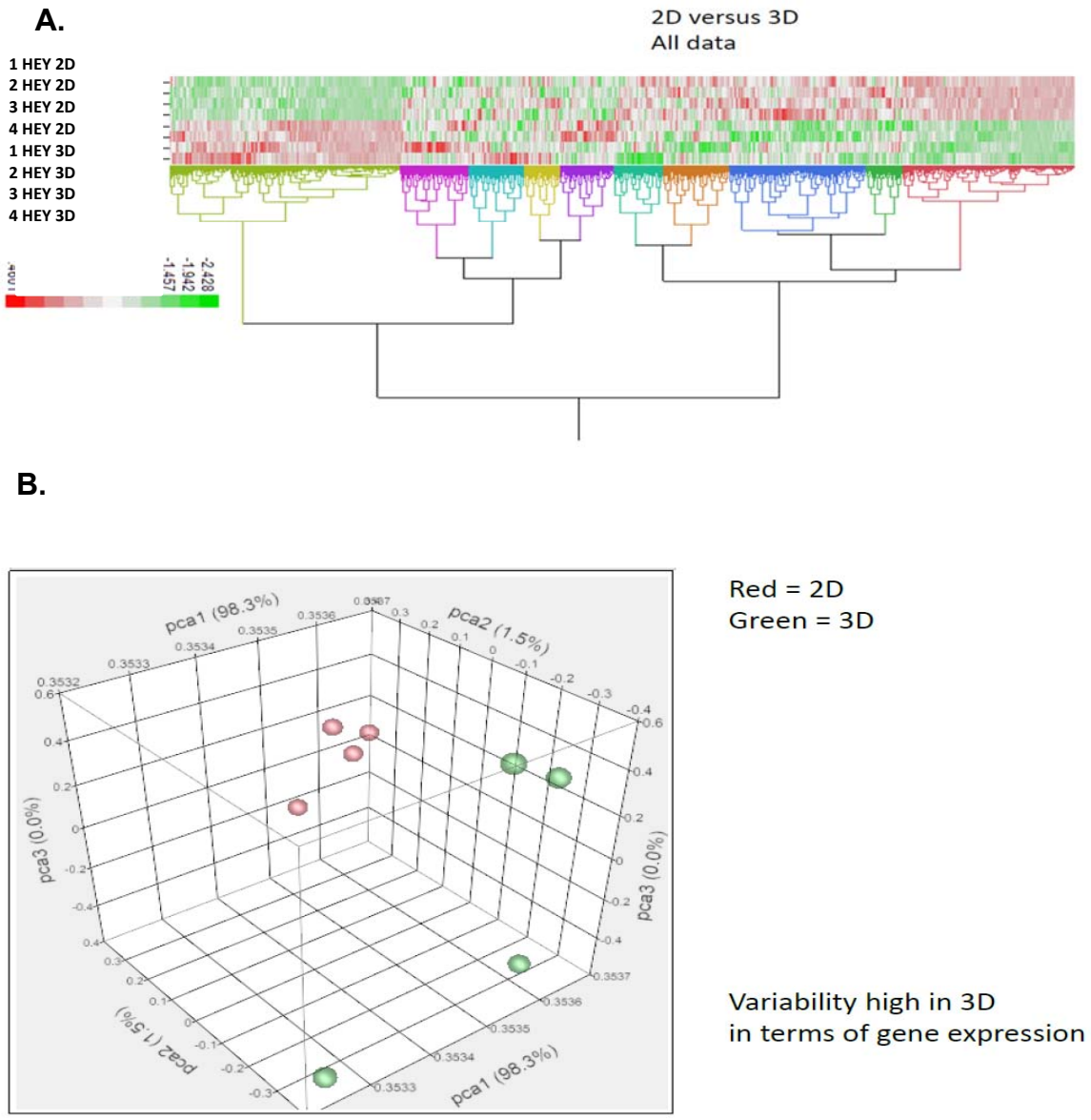

Figure 2.2: HEY Cells Treated with TGFβ have Distinct Gene Expression Profiles when grown as 3D Spheroids vs. 2D Monolayers.

A) Hierarchical clustering of expression profiles. Clustering revealed that each of the two groups form into distinct clades based on expression. B) Principle component analysis for expression profiles. Variability in transcriptome response separates strongly along the first PCA1. Red color is HEY 2D biological replicates and green color is HEY 3D biological replicates. Biological replicates for HEY2D are more closely related in expression compared to HEY 3D.

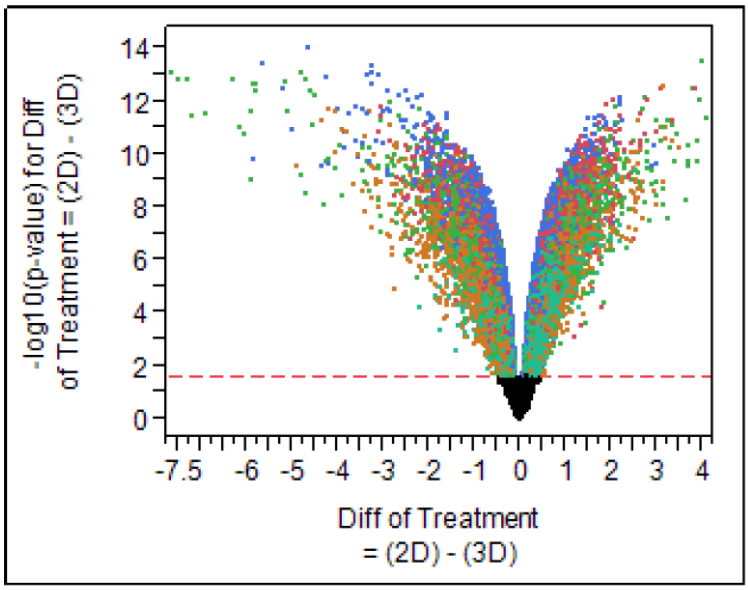

Volcano plot

Figure 2.3: Volcano Plot for Differentially Expressed Transcripts.

The Volcano plot shows the significantly expressed transcripts vs. fold change of the pairwise comparison made between the two groups. Negative log10 p value on y axis indicates the significance of each gene, and the fold change (log base 2) mean expression difference on x axis. The dashed line is the significance threshold for selecting the differentially expressed genes at FDR of 0.05.

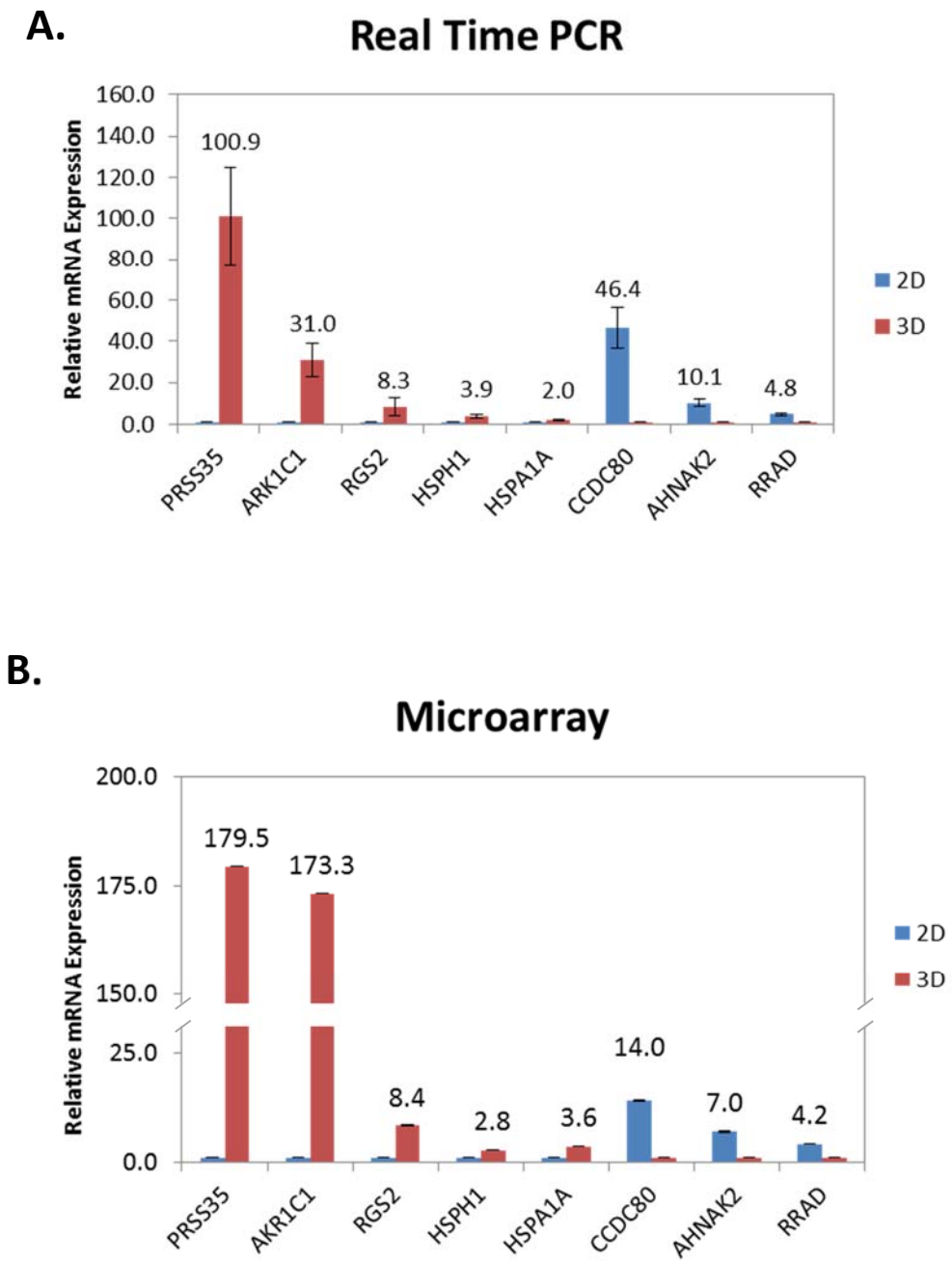

Figure 2.4: Real Time PCR Analysis Validates Microarray Results.

A) Real time PCR results for select genes that are moderately to highly affected by 3D vs. 2D growth. Biological and technical triplicates were utilized. B) Microarray results are plotted for the same genes.

Table 2.2: Top 20 Genes with most Significant Fold Changes

Direction of Change	*Gene*	*Role*	*Fold Change*	*p-value*
Down-regulated	CCDC80	Heparin binding and fibronectin binding	-17.39	2.87E-09
	SLC6A15	Amino acids transport	-14.75	2.3E-08
	SEMA3E	Axon guidance ligands	-14.67	9.33E-09
	TENM2	Protein homodimerization activity	-13.71	7.28E-10
	PLCB4	Catalyzes the formation of inositol 1,4,5-trisphosphate and diacylglycerol	-13.13	2.43E-08
	MIR17	Invovled in cancer and cell carcinomas	-13.09	2.91E-08
	PIF1	5' to 3' DNA helicase	-13.02	1.09E-08
	IL1RAP	Associates with interleukin to mediate NF kappaB signaling	-11.49	1.16E-08
	GPR126	G-protein orphan receptor	-10.83	6.66E-09
	FBN2	Component of connective tissue microfibrils	-10.45	2.36E-08
	MIR1304	mNA regulation	-9.92	1.22E-08
	TRMT13	Methyltransferase activity	-9.22	7.77E-09
	DLEU2	Associated with chronic lymphocytic leukemia	-9.09	4.32E-09
	TIGD1	Unknown	-8.98	6.51E-08
	TPM1	Involved in the contractile system of striated and smooth muscles	-8.91	9.32E-08
	KRTAP2	Formation of a rigid and resistant hair shaft	-8.78	4.61E-09
	RIMS2	ion channel binding and Rab GTPase binding	-8.77	6.88E-10
	ATP8B1	transport of phosphatidylserine and phosphatidylethanolamine	-8.60	7.27E-10
	AHNAK2	Cell differentiation	-8.56	8.9E-09
	AKAP12	Scaffold protein in signal transduction	-8.08	5.87E-09
Up-regulated	MRPS6	Protein synthesis in mitochondria	18.96	5.7E-10
	TNFSF15	Cytokine inducible by TNF and IL-1 alpha	20.18	2.85E-08
	RANBP3L	Binding protein	20.29	3.27E-09
	SLC1A3	Termination of excitatory neurotransmission in central nervous system	22.47	1.07E-09
	TMEM171	Unknown	24.17	7.76E-10
	F2RL1	Receptor for trypsin and trypsin-like enzymes coupled to G proteins	25.68	5.85E-10
	S100A4	Cell cycle progression and differentiation	28.15	5.7E-10
	PTGS2	prostaglandin biosynthesis	29.55	3.06E-08
	SOD2	Converts superoxide byproducts to H2O2	32.39	4.72E-09
	CXCR4	CXC chemokine receptor	35.08	6.24E-10
	IL8	Neutrophil chemotactic factor	55.81	7.76E-10
	SPOCK1	Protease inhibition	56.98	6.76E-10
	NADK2	Catalyzes the phosphorylation of NAD to yield NADP	57.98	2.16E-08
	GLS	Catalyzes the hydrolysis of glutamine to glutamate	59.61	6.06E-08
	ITGB8	Mediate cell-cell and cell-extracellular matrix interactions	60.23	2.1E-09
	ID2	Cellular growth, senescence, differentiation, apoptosis, angiogenesis	70.77	4.63E-09
	RGCC	Regulates cell cycle, induced by p53	78.93	5.85E-10
	PRSS35	Protease activity	179.46	5.85E-10
	AKR1C1	Conversion of aldehydes and ketones to their corresponding alcohols	198.09	5.7E-10

Transcripts are organized as those down-regulated and up-regulated between the two groups. The gene, as well as the role of the protein in the cell is provided in addition to the relative fold change and p-value. For a complete list of gene expression changes see Table S2.

Table 2.3: Top SNEA Pathways.

Theme	*Gene Set Seed*	*Total # of Neighbors*	*# of Measured Neighbors*	*Median change*	*p-value*
Autophagy	autophagy	418	402	1.08	5.9E-06
	autophagic cell death	78	75	1.15	0.00076
Cancer and Aging	senescence	651	596	1.05	7.79E-08
	cell aging	251	225	1.06	2.1E-07
	oncogenesis	523	486	1.05	1.36E-05
Cell Cycle	S phase	857	797	1.05	4.38E-09
	interphase	196	192	-1.05	1.13E-08
	G1/S transition	611	558	1.07	1.73E-06
	G2 phase	171	164	1.07	2.51E-05
	cell cycle checkpoint	161	150	1.06	4.1E-05
	exit from mitosis	62	59	1.06	0.000284
Chromosome Separation	spindle assembly	507	478	-1.06	1.14E-11
	centriole duplication	106	103	-1.10	6.98E-07
	mitotic spindle assembly	59	58	-1.18	2.98E-05
	microtubule/kinetochore interaction	19	19	-1.54	0.000872
DNA Damage and Repair	response to DNA damage	460	428	1.07	1.32E-12
	DNA repair	654	609	1.05	1.3E-10
	genome instability	292	272	1.06	4.09E-08
	genetic instability	113	111	1.08	3.76E-07
	nucleotide-excision repair	120	113	1.09	7.58E-06
	DNA damage checkpoint	126	122	1.06	6.2E-05
Protein Modification	protein degradation	470	449	1.06	7E-08
	ubiquitin-dependent protein degradation	193	186	1.16	1.23E-05
	protein ubiquitination	89	88	1.15	3.27E-05
	protein sumoylation	167	158	1.13	4.71E-05
Stress	response to oxidative stress	166	159	1.06	3.55E-05
	heat-shock response	65	59	1.14	0.000722
Transcription	poly(A)+ mRNA-nucleus export	84	77	-1.13	9.86E-05
	Polymerase II transcription	75	70	1.13	0.000393
	wall integrity	51	51	1.37	5.74E-06
	myoblast differentiation	212	196	1.08	1.85E-05
	nucleocytoplasmic transport	122	112	1.10	2E-05
	adherens junction assembly	52	50	1.12	2.79E-05
	skin development	69	67	1.10	0.000175
	blood vessel barrier	28	28	1.26	0.000545
	leiomyocyte adhesion	25	24	-1.14	0.000756

Only cell processes that showed >5% change in the pathway, as well a significant change at p>0.001 are shown. Provided are the total number of neighbors within a network, number of neighbors measured on the microarray, the median fold change of the network, and the p-value. All cell processes differentially expressed between cells are provided in Table S3. Major themes included those related to cell cycle DNA damage and repair, and stress.

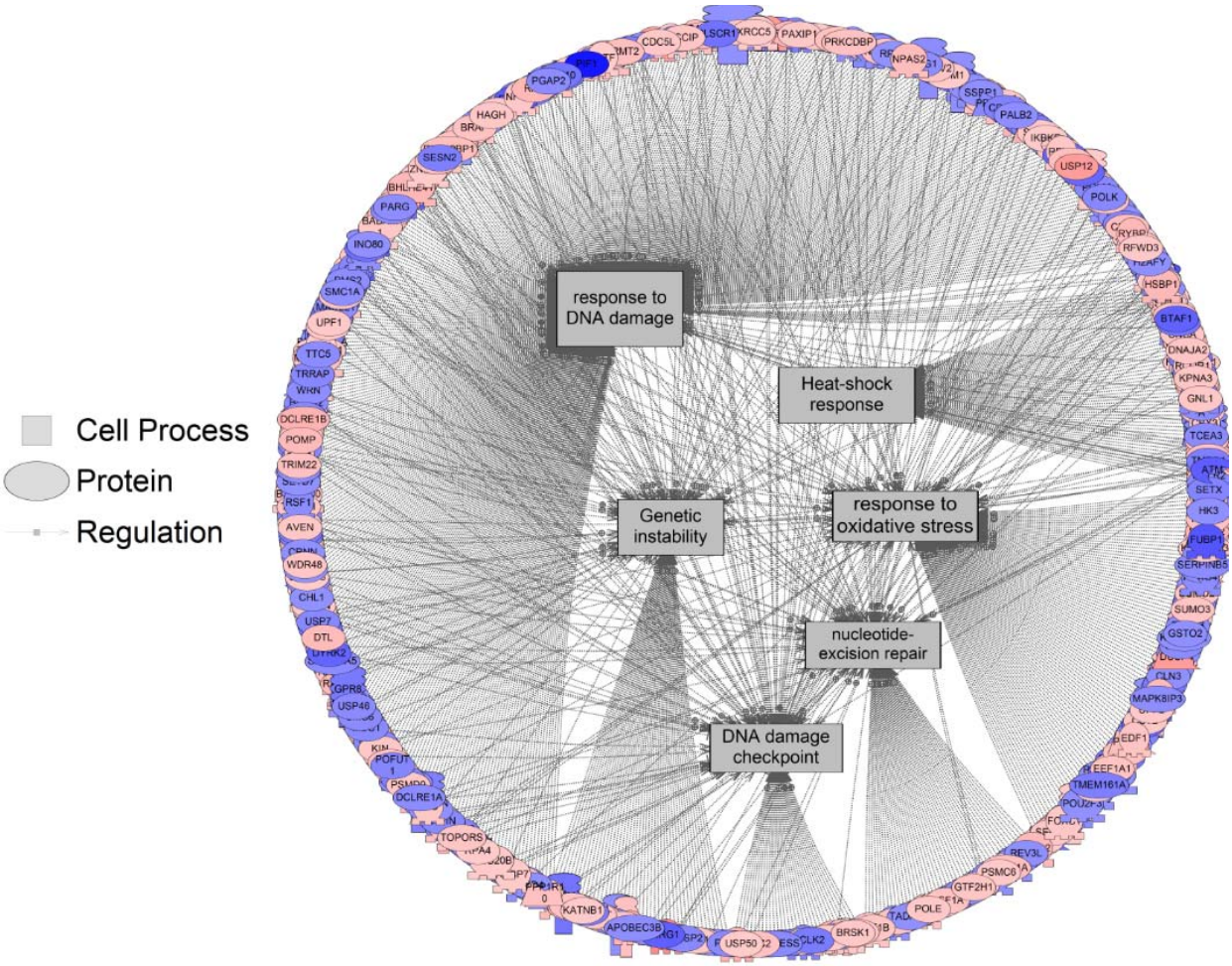

Figure 2.5: Gene Networks Related to Stress.

These cell processes were significantly enriched following sub-network enrichment analysis when comparing 3D vs. 2D growth. These processes were preferentially increased in the 3D group. Red indicates the gene is upregulated and blue indicates the gene is downregulated. All genes for pathways are listed in Supplemental Files.

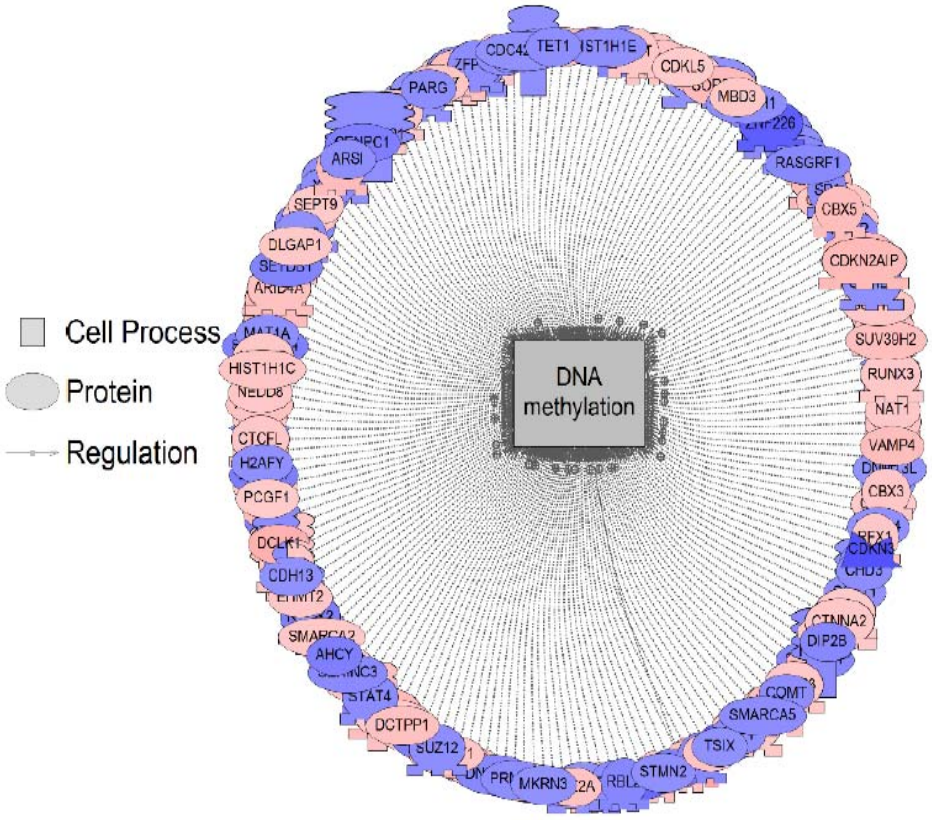

This process was significantly increased in the 3D group but about 4-5 %.
The red are increased genes and the blue are decreased genes.

Figure 2.6: DNA Methylation.

DNA methylation was significantly enriched following sub-network enrichment analysis when comparing 3D vs. 2D growth. DNA methylation was preferentially increased approximately 4% (197 genes measured, P = 0.006) in the 3D group at the level of the transcriptome based on the sub-network enrichment analysis. Red indicates the gene is up-regulated and blue indicates the gene is down-regulated. All genes for pathways are listed in Supplemental Files.

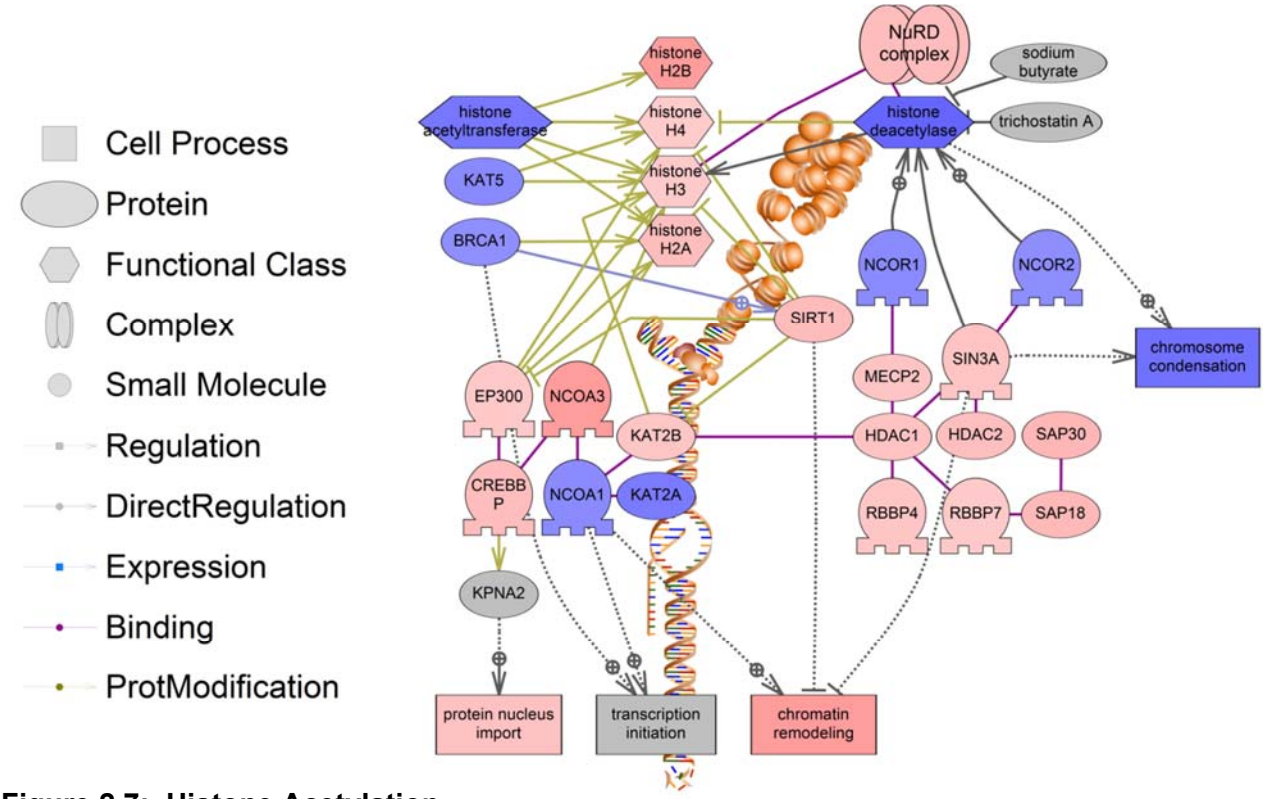

Figure 2.7: Histone Acetylation.

Pathway for histone acetylation. A number of histone modifying enzymes were increased in expression in the 3D group, and this may be reflective of chromatin remodeling during cancer progression. Red indicates the gene or process is up-regulated and blue indicates the gene or process is down-regulated. All genes for pathways are listed in Appendices.

CHAPTER THREE: THE HEAT SHOCK TRANSCRIPTION FACTOR HSF1 INDUCES OVARIAN CANCER EPITHELIAL-MESENCHYMAL TRANSITION IN A 3D SPHEROID GROWTH MODEL

Authored by Chase Powell*, Trillitye Paullin*, Candice Aoisa, Christopher Menzie, Ashley Ubaldini, and Sandy D. Westerheide *Co-first authors

Submitted to PLoS ONE. October 2016.

Experiments were designed, performed, and analyzed by C. Powell and T. Paullin or performed under the direction of C. Powell and T. Paullin. Manuscript was written by T. Paullin and S. Westerheide.

Introduction

Ovarian cancer is the number one gynecological malignancy cause of death [271]. This is partially due to a lack of physical symptoms during early cancer stages as well as shortcomings in screening techniques. In fact, a majority of newly diagnosed ovarian cancer cases present with stage III and IV disease [272]. Recent advances in surgery and chemotherapy treatment have led to improvement in short-term survival of ovarian cancer patients, however long-term survival remains bleak [225]. Conventional chemotherapy agents used to treat ovarian cancer include platinum and taxol-based drugs. While these agents are largely effective upon initial treatment, the patient commonly develops resistance to the drugs, yielding them inefficient should the patient relapse [273]. In addition, agents such as cisplatin can be toxic to the patient's organs,

such as the kidneys and gastrointestinal tract, indicating a need for more efficient, as well as safer, treatment options [274].

The heat shock response (HSR), driven by the heat shock transcription factor HSF1, is a cytoprotective response to proteotoxic stressors, including heat shock, that results in the induction of various genes including molecular chaperones essential for recovery from cellular damage [275]. Chaperones function to guide protein folding and protect cells against proteotoxic stress [276]. The HSR is regulated at the transcriptional level by the heat shock transcription factor 1 (HSF1) [275].

Multiple lines of evidence suggest that HSF1 is important in promoting tumorigenesis. For instance, studies in HSF1 null mice show they are refractory to chemically-induced tumors, and HSF1 -/- mouse embryonic fibroblasts resist oncogene-induced transformation [207]. In cancer, HSF1 controls many genes that may support the transformed phenotype, including genes involved in cell-cycle regulation, signaling, metabolism, adhesion and translation [197]. HSF1 is elevated in breast, colon, lung and hepatocellular cancers, and activated or elevated HSF1 often couples with poor cancer prognosis [197, 212].

The dissemination of primary tumors occurs through a multi-step process called the epithelial-to-mesenchymal transition (EMT). EMT consists of detachment of primary tumor cells, infiltration of local stroma, spread through cavities or vascular and lymphatic vessels, and adhesion followed by colonization at distant sites [277]. Sweeping changes are made in the cytoskeleton and extracellular matrix during EMT, and cells develop a spindle-like morphology. TGFβ inhibits proliferation in normal tissues, but this effect is lost in advanced cancer where it strongly promotes EMT [278]. The expression of a

number of transcription factors are induced by TGFβ and support the EMT process, including SNAI2/SLUG, SNAI1/SNAIL, TWIST1 and ZEB1 [277]. Once the mesenchymal-like cell has migrated into a new organ, it can then undergo the reverse mesenchymal-to-epithelial transition (MET) and begin to form a secondary tumor [46].

Here, we have established two ovarian cancer inducible HSF1 knockdown cell lines to study the effect of HSF1 on ovarian cancer. We show that HSF1 knockdown inhibits colony formation, wound healing, migration and the induction of FN1/fibronectin, a protein important in the EMT process. We also show that the induction of EMT markers by TGFβ is enhanced when cells are grown as 3D spheroid cultures vs. 2D monolayer cultures. Upon 3D culturing, there is a marked effect of HSF1 on the induction of transcription factors known to promote EMT. HSF1 knockdown also alters spheroid morphology. Thus, we conclude that HSF1 plays a striking role in regulating the EMT process under 3D growth conditions.

Materials and Methods

HSF1 Copy Number, Expression Determination, and Survival Analysis

Data comparing HSF1 copy number across multiple cancers with GISTIC analysis was obtained from The Cancer Genome Atlas (TCGA) via the cBio portal [279, 280]. HSF1 expression levels across multiple cancers were assessed from TCGA RNA seq V2 data via the cBio portal. Data for the comparison of ovarian cancer and normal ovarian tissue were obtained from GEO and the TCGA. The datasets analyzed were: GSE18520, consisting of 10 normal ovary and 53 ovarian cancer samples assayed on Affymetrix HG-U133 Plus 2.0 GeneChips, and TCGA data, consisting of 8 normal ovary

and 568 ovarian cancer samples assayed on Affymetrix HG-U133A GeneChips. Gene intensity was compared by one-sided unpaired T-test.

Cell Culture and Treatments

HEY, SKOV3 and T80 cells were authenticated using short tandem repeat (STR) DNA profiling (Genetica, Inc.) and comparing profiles to ATCC profiles and other previously published profiles [232]. Cells were cultured in RPMI 1640 medium supplemented with 10% fetal bovine serum (GIBCO) and 1% Pen-Strep-Glutamine (CellGro) in a humidified incubator at 37^{o}C with 5% CO_2. Heat shock treatment was performed by wrapping plates in parafilm and submerging them in a 42^{o}C circulating water bath for designated times. Cells were treated as indicated with 1 μg/ml doxycycline (Sigma-Aldrich) and 5 ng/mL TGFβ1 (Thermo Fisher).

Lentiviral Creation and Infection for Stable, Inducible shRNA-Mediated HSF1 Knockdown

To allow for inducible knockdown of HSF1, we utilized the doxycycline-inducible TRIPZ shRNAmir system (Thermo Scientific). Two shRNA sequences targeting HSF1 were obtained from the RNAi codex database [281]: CGCAGCTCCTTGAGAACATCAA (shHSF1A) and CCCACAGAGATACACAGATATA (shHSF1B). These two sequences were cloned into the pTRIPZ vector. For lentiviral packaging, a 2nd generation lentiviral system was used with the pCGP packaging and pVSVG envelope plasmids (Addgene). HEK293T cells, cultured in RPMI medium, were used as the packaging cell line. Transfection was achieved using Polyfect Transfection Reagent (Qiagen) according to the manufacturer's protocol using a 1:1:1 ratio of lentiviral vectors. 24 hours post-transfection, medium with transfection reagent was removed and replaced with fresh

RPMI. Medium containing viral stock from the HEK293T cells was harvested 48 hours post-transfection. A 0.45 micron PVDF filter was used to filter viral stock and infection of the HEY and SKOV3 cell lines was performed in a single round with the addition of 8 μg/mL of hexadimethrinebromide (Sigma-Aldrich). Selection of stable HEY and SKOV3 cells was achieved with 1 μg/ml and 0.5 μg/ml of puromycin (Thermo Fisher) for the HEY and SKOV3 cell lines, respectively. Infection was verified via immunoblotting analysis for knockdown of HSF1 after doxycycline-induced expression of the shRNAs.

Protein Isolation, SDS-PAGE, and Western Analysis

Cells were washed once and scraped in chilled PBS. After pelleting the cells, protein was extracted using the M-PER lysis buffer (Thermo Scientific) with a protease inhibitor cocktail (Halt™ Protease Inhibitors, Thermo Scientific). A Bio-Rad Protein Assay was then utilized to quantify protein concentrations. 20 μg of lysate was resolved on 8% to 12% sodium dodecyl sulphate polyacrylamide gel electrophoresis (SDS-PAGE) gels and transferred to Immun-Blot® 0.2μm PVDF Membrane with a Trans-Blot semi-dry transfer cell (Bio-Rad). Membranes were blocked in 2% w/v non-fat milk in TBS with 0.1% Tween (TBST milk). Blots were probed with primary and secondary antibodies before incubation in ECL Prime Western Blotting Detection System (Amersham™) and film exposure. Primary antibodies used were: HSF1 (Assay Designs), HSF1 P-S326 (Abcam) fibronectin (BD Biosciences), HSP90 (Cell Signaling), HSP70 (Cell Signaling) and Actin (Santa Cruz). HRP-conjugated secondary antibodies were from Millipore and Jackson ImmunoResearch.

Cell Viability Assay

Cells at a concentration of 2 x 10^5 cells/ml were seeded in a 96-well plate at 100 µl per well with eight replicates for each test condition. The cells were then incubated either with or without doxycycline treatment for 72 hours. After incubation, 10 µl of PrestoBlue Cell Viability Reagent (Invitrogen) was added to each well and incubated for 1 hour at 37°C. The reduction of the reagent was measured by fluorescence (excitation 570 nm, emission 600 nm) using a microplate reader (BioTek). Mean percent viability and standard error were then plotted.

Clonogenic Assay

Cells were seeded at 500 cells per well in 6-well plates and were treated with or without 1 µg/ml doxycycline to induce HSF1 knockdown. Treated wells were given an additional treatment with 1 µg/ml doxycycline on day 4 to maintain doxycycline levels. After 8 days, colonies were stained with 1% crystal violet (w/v) in methanol and rinsed 3X in deionized water. Stained colonies were subsequently photographed and counted.

Wound Healing Assay

Cells were plated at 3 x 10^5 cells per well in a 6-well plate, and then either treated with 1 µg/ml doxycycline 48 hours prior to the assay or left untreated. Once the cells reached confluency, a 2 µl pipet tip was used to scrape the cells in 2 vertical and 2 horizontal lines yielding 4 intersections per well. Cells were washed twice with PBS to remove debris and serum-free medium was added. Pictures were taken immediately and again 12 hours after the creation of the wound, using an EVOS inverted microscope (Advanced Microscopy Group). The experiment was performed in triplicate and wound

closure was determined using TScratch software [282]. Significant differences were calculated by ANOVA and Bonferroni post-hoc tests.

Cell Migration

For the transwell migration assay, cells were treated with or without 1 μg/ml doxycycline 48 hours prior to the assay to induce HSF1 knockdown, and cells were then serum-starved 24 hours before performing the assay. Cells were then resuspended in serum-free medium, and seeded at 2.5 x 10^4 cells per upper chamber. 400 μL of complete medium containing FBS was added as a chemoattractant to the lower chamber. After a 16-hour incubation, non-migrating cells on the upper surface of the filter were removed by scrubbing with a cotton swab. The remaining cells on the lower surface were fixed and stained with 1% (w/v) crystal violet in methanol. Migrated cells were counted from 10 random fields of view from each well and each condition was performed with triplicate samples. Statistical analysis done by paired t-test.

Spheroid Formation

The hanging drop method was utilized to form spheroids [283]. Briefly, cells released with trypsin were resuspended at 1 X 10^6 cells/mL in RPMI medium, supplemented as described above. Cell suspension droplets of 25 μl were placed on the plate lids, which were then inverted and put back on plates containing phosphate buffered saline (PBS) and incubated for 48 hours. Upon incubation, cells aggregated into spheroids. Prior to plating the cells, TGFβ1 was added to the suspension as indicated at a final concentration of 5 ng/mL. Following aggregation for 48 hours, spheroids were collected in 1X PBS. Pictures were obtained using an EVOS (Advanced Microscopy Group) inverted microscope.

Quantitative RT-PCR

Cells were harvested in cold 1X PBS and RNA extraction was completed utilizing the TRIzol reagent (Thermo Fisher) according to standard protocol. Reverse transcription reactions of the RNA were performed with the High Capacity cDNA Reverse Transcription Kit (Applied Biosystem), as per the manufacturer's protocol. The cDNA samples were then used as a template for qRT-PCR. Applied Biosystem's Step One Plus Real-time PCR machine was used with BioRad's iTaq™ Fast SYBR® Green Supermix with ROX according to the manufacturer's protocol. The primer sets used for each gene can be found in Table 3.1. GAPDH was used as the endogenous reference control. Statistical significance was measured by Student's t test.

Results

HSF1 is Overexpressed in Ovarian Cancer

We analyzed data from The Cancer Genome Atlas (TCGA) database to compare HSF1 levels across multiple cancer types. Interestingly, we find that HSF1 gene duplication is more common in ovarian cancer than in any other cancer type in this database by a large margin (Fig. 3.1A). Additionally, we find that HSF1 mRNA transcripts are elevated in ovarian cancer tumor tissue vs. normal epithelial tissue from matched patient samples (Fig. 3.1B). Other cancers with high HSF1 mRNA levels include liver cancer, head and neck cancer, and breast cancer (Fig. 3.1B). Two distinct data sets of matched ovarian tumor tissue vs. normal tissue show that HSF1 mRNA expression is significantly higher in tumor tissue (Fig. 3.1C-D). Given this data, we postulate that HSF1 may drive ovarian cancer progression. We thus sought to study the effect of HSF1 knockdown in ovarian cancer cell lines.

Establishment of SKOV3 and HEY Inducible HSF1 Knockdown Ovarian Cancer Cell lines

We chose two epithelial ovarian cancer cell lines for our studies, SKOV3 and HEY. These cell lines were authenticated by using short tandem repeat (STR) DNA profiling (Genetica, Inc.) and comparing the profiles to ATCC profiles and other previously published profiles [232]. We first wanted to test whether the cell lines we selected exhibited a normal response to heat, including the characteristic activation of HSF1 and induction of chaperones. We find that both SKOV3 and HEY cells exhibit multiple hallmarks of activation of the heat shock response (Fig. 3.2A). Upon treatment with a 42°C heat shock over a 6 hour timecourse, we observe stress-induced hyperphosphorylation of HSF1 followed by a return to the hypophosphorylated state. This result is characteristic of HSF1 activation by heat shock and can be readily detected by electrophoretic retardation on SDS-PAGE and Western blot analysis [284]. Interestingly, while SKOV3 cells contain a similar level of basal and activated HSF1 as compared to normal ovarian epithelial T80 cells, HEY cells express higher levels of HSF1, corresponding to the higher levels of HSF1 expression we identified in ovarian cancer patient databases. Upon heat shock, we also observed that both SKOV3 and HEY cells show HSF1 phosphorylation at serine 326, a marker of activated HSF1 [3]. Additionally, the chaperone HSP70 was induced by heat shock in both SKOV3 and HEY cells, and HSP90 was induced in HEY cells. Overall, we conclude that both SKOV3 and HEY cells express HSF1 and respond to heat shock, validating the choice of these two ovarian cancer cell lines for our studies.

We next wanted to generate HSF1 knockdown SKOV3 and HEY cell lines. Our initial attempts to create stable HSF1 knockdown in these cell lines were not successful, perhaps due to selective pressure for the cancer cells to re-express HSF1. We therefore employed a doxycycline-inducible shHSF1 system (pTRIPZ vector, Open Biosystems). To ensure that doxycycline treatment alone would not alter HSF1 levels or activity, we treated SKOV3 and HEY cells with both 0.5 and 2.0 μg/ml of doxycycline for 48 hours and found no changes in HSF1 levels or hyperphosphorylation status (Fig. 3.3). We also found no change in HSP90 levels (Fig. 3.4). We therefore concluded that a doxycycline-inducible system would be a viable option for HSF1 knockdown in our studies.

We used two shHSF1 sequences obtained from the RNAi codex database [281], shHSF1A (CGCAGCTCCTTGAGAACATCAA) and shHSF1B (CCCACAGAGATACACAGATATA), as well as a control sequence that is non-targeting, to create SKOV3.shControl, SKOV3.shHSF1A, SKOV3.shHSF1B, HEY.shControl, HEYshHSF1A and HEY.shHSF1B stable cell lines (Fig. 3.2B). The shHSF1A sequence knocks down HSF1 expression by about 75%, while shHSF1B knocks down HSF1 expression more completely. Knockdown of HSF1 resulted in only a marginal reduction of cell viability in the SKOV3 or HEY cell lines over a 72 hour doxycycline treatment timecourse (Fig. 3.2C). We thus have established an effective means of knocking down HSF1 to varying degrees in two different ovarian cancer cell lines.

HSF1 Knockdown Inhibits Colony Formation, Wound Healing, Cell Migration and Fibronectin Expression

We then assayed our HSF1 knockdown cell lines to determine whether HSF1 is important for ovarian cancer tumorigenicity. As a measure of the ability of HSF1 to allow cell survival and growth upon plating at a low cell density, clonogenic assays were performed (Fig. 3.4). SKOV3.shControl, SKOV3.shHSF1B, HEY.shControl and HEY.shHSF1B stable cells were treated with or without doxycycline to induce HSF1 knockdown and then plated at 250 cells per well in 6-well plates in triplicate. Colonies, stained after 8 days, show that HSF1 knockdown strongly inhibits colony formation in both HEY and SKOV3 cells.

To assess the ability of HSF1 to affect cellular motility, we used a wound healing assay as well as a cell migration assay. For the wound healing assay, cells were seeded in equal numbers into 6-well plates and grown to ~80% confluence prior to introducing scratches in straight lines through the monolayers. TScratch software was then used to automatically analyze wound healing rates (Fig. 3.5A). HSF1 knockdown in SKOV3 and HEY cells inhibits wound-healing ability by 25% and 28%, respectively. Next, cell migration assays were employed to assess the ability of cells to pass through a matrigel-coated transwell membrane (Fig. 3.5B). Cells were seeded in equal numbers into the insert of a transwell plate, with no cells in the lower chamber. The number of cells that passed through the membrane were then calculated and plotted after 48 hrs. HSF1 knockdown was found to inhibit cell migration by 29% in SKOV3 cells and 33% in HEY cells. These experiments in sum support a role for HSF1 in promoting cell motility in ovarian cancer.

We next wanted to test whether HSF1 knockdown can suppress the EMT process. Fibronectin, a mesenchymal marker, is upregulated during EMT and plays a crucial role in altering cell adhesion and migration processes, allowing for transition to the mesenchymal state [36]. We tested protein expression levels of fibronectin using Western blot analysis of SKOV3.shHSF1B and HEY.shHSF1B cells treated with and without doxycycline and with and without the EMT inducer TGFβ (Fig. 3.5C). As expected, TGFβ treatment induces fibronectin expression (Fig. 3.5C, compare lanes 1 with lanes 3). Interestingly, HSF1 knockdown in both SKOV3 and HEY cells reduces both the basal expression levels of fibronectin (Fig. 3.5C, compare lanes 1 and 2) as well as the TGFβ-induced levels of fibronectin (Fig. 3.5C, compare lanes 3 and 4). Therefore, HSF1 may promote the EMT process by enhancing TGFβ-induced fibronectin expression.

The Induction of Fibronectin by TGFβ is Enhanced in 3D Cultures as Compared to 2D Cultures

As ovarian cancer cells typically spread throughout the peritoneal cavity in the form of 3D spheroids, we cultured cells in 3D culture using the hanging drop method [235] in order to create a more biologically-relevant *in vitro* system for our studies. We first tested whether the induction of fibronectin by TGFβ is altered in 3D cultures as compared to 2D cultures. In both monolayer and spheroid SKOV3 cells, TGFβ increased fibronectin expression (Fig. 3.6). Surprisingly, this effect was enhanced in the SKOV3 spheroid model as compared to monolayer cells (Fig. 3.6, compare lanes 2 and 4). The HEY cells also showed enhanced fibronectin expression upon 3D growth,

although this effect was not enhanced by TGFβ. Therefore, we conclude that 3D culturing enhances fibronectin expression.

3D Culturing Reveals a Marked Effect of HSF1 on the Induction of EMT Transcription Factors

Various transcription factors, including snail, slug, twist, and zeb, help to coordinate the EMT process [277]. We tested whether 3D growth affected the expression of these genes (Fig. 4.6). We find that 3D growth enhances TGFβ induction of these transcription factors as shown by qRT-PCR (Fig. 3.7, compare lanes 2 and 4). We wondered whether HSF1 may regulate the expression of these EMT transcription factors. We thus tested our HSF1 knockdown cell lines, grown under both 2D and 3D conditions, to test for effects on the expression of *SNAIL, TWIST1, SLUG* and *ZEB1* mRNAs (Fig. 3.7). SKOV3.shControl, SKOV3.shHSF1B, HEY.shControl, and HEY.shHSF1B stable cell lines, grown both as 2D and 3D cultures, were treated with and without doxycycline treatment to induce HSF1 knockdown. We find that HSF1 knockdown in most cases slightly inhibits the expression of EMT transcription factors in SKOV3 and HEY cells grown in 2D (Fig. 3.7, compare lanes 2 with lanes 3). Interestingly, the effect of HSF1 knockdown on the expression of these genes is magnified for most of the genes upon growth in 3D conditions (Fig. 3.7, compare lanes 4 with lanes 5). Therefore, using a 3D ovarian cancer culturing system, we have uncovered a positive effect of HSF1 on the ability of TGFβ to induce EMT genes. We thus conclude that HSF1 promotes EMT in ovarian cancer 3D spheroids at least in part through regulating the levels of EMT-inducing transcription factors.

Discussion

As ovarian cancer is highly lethal and has few treatment options, identifying new therapeutic targets for this disease is highly important. Through mining patient data, we find that HSF1 DNA levels are most highly amplified in ovarian cancer as compared to other cancers, and also that ovarian cancer is one of the top cancer types with amplified HSF1 mRNA levels. A previous study of 37 malignant vs. benign ovarian tumors has shown that HSF1 expression is higher in the malignant tumors [223]. Our findings thus add to this data and suggest that HSF1 may be an important therapeutic target for ovarian cancer.

We have identified HSF1 as a critical player in promoting ovarian cancer tumorigenicity by multiple measures in both SKOV3 and HEY ovarian cancer cells. Via HSF1 knockdown and colony formation assays, we show that HSF1 promotes the ability of cells to grow under conditions of low cell density, a hallmark of cancer cells. Cell motility is another characteristic of cancer cells. Previous work has shown that cell motility is inhibited in immortalized mouse embryonic fibroblast cells derived from *hsf1* -/- mice [285]. In addition, HSF1 knockdown reduces the invasiveness of multiple types of tumor cells [212, 214, 286-288]. Consistent with these findings, we show that HSF1 knockdown inhibits wound healing and cell migration in SKOV3 and HEY ovarian cancer cell lines. Our results thus add further evidence that HSF1 enhances tumorigenicity in multiple types of cancer.

EMT is essential for cell migration and is a key rate-limiting step in metastasis. Previous studies have shown that HSF1 promotes EMT in breast cancer cells through a mechanism that requires HER2 [289, 290]. As ovarian cancer cells typically spread

throughout the peritoneal cavity in the form of 3D spheroids [74], culturing ovarian cancer cells as spheroids is likely to better mimic the *in vivo* growth conditions as compared to conventional 2D culturing conditions. Here, we show that HSF1 knockdown reduces the ability of TGFβ to induce EMT. Interestingly, we find that this effect is stronger upon growth in 3D spheroids. We also show that HSF1 is required for the compact morphological structure of spheroid growth.

Our data suggests that HSF1, either directly or indirectly, controls the expression of transcription factors that are important for the EMT process. Interestingly, upon promoter analysis, we find consensus heat shock element (HSE) sequences containing three inverted arrays of the sequence nGAAn [291] in the promoters of the EMT transcription factor genes *SNAIL, ZEB* and *TWIST1* (Table S2). Putative HSEs are also present in the *FN1* (*fibronectin*)*, VIM* (*vimentin*)*, and CDH2* (*N-cadherin*) promoters, additional genes that are associated with EMT (Table 3.2). Future experiments will be required to determine whether any of these genes are direct HSF1 targets. This is plausible given that HSF1 was recently found to bind to the *SLUG* promoter through an imperfect HSE motif [289].

In summary, we have identified HSF1 as a critical player in ovarian cancer progression, and have identified EMT as a process that is promoted by HSF1. The effects for HSF1 are more striking when cells are grown as 3D spheroids, which more closely mimic the *in vivo* growth conditions of ovarian cancer. Therefore, HSF1 deserves further research and development as a promising anticancer strategy for ovarian cancer.

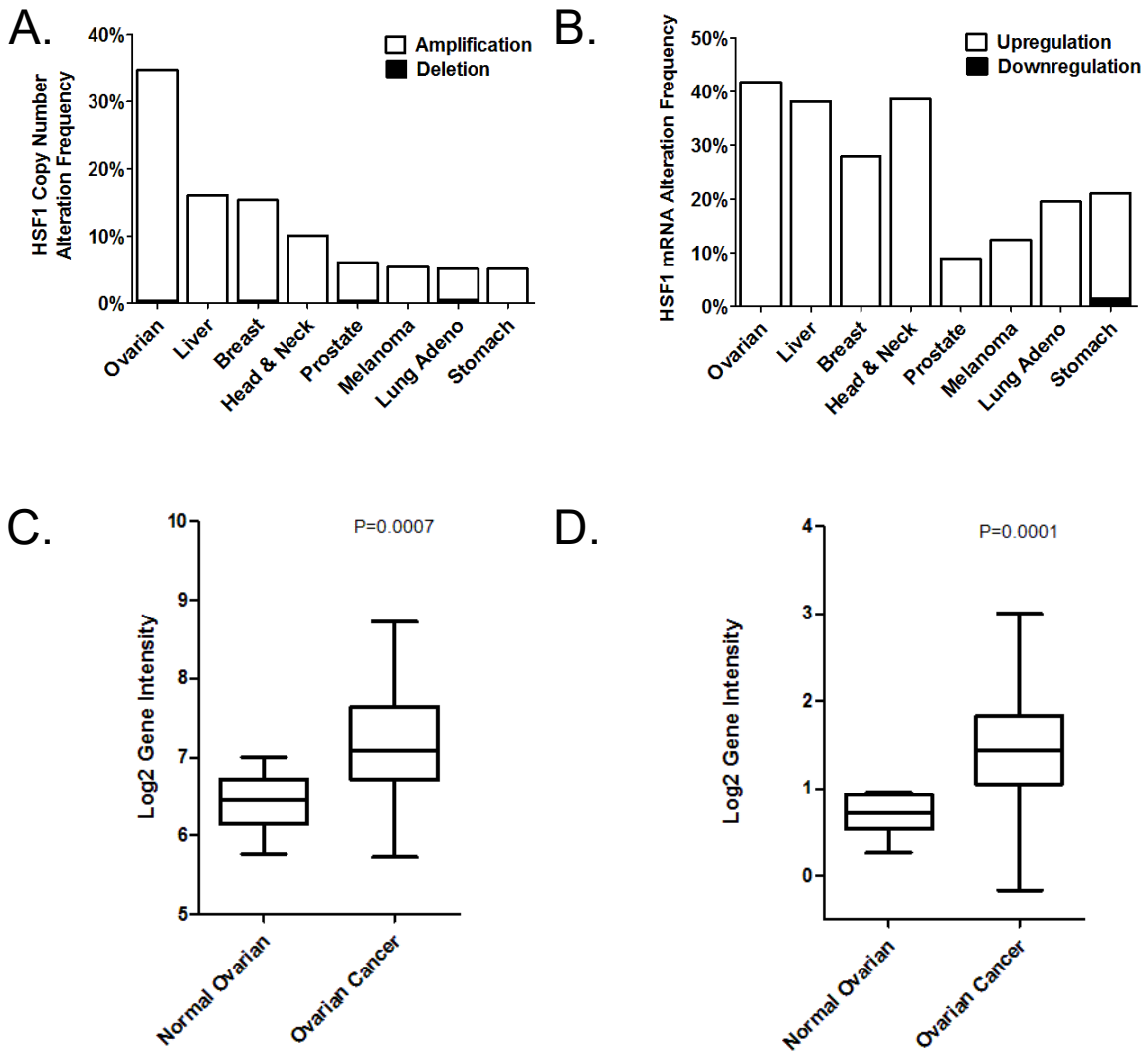

Figure 3.1. HSF1 Levels are Elevated in Ovarian Cancer Patient Samples.

A, HSF1 copy number is increased most frequently in ovarian cancer. HSF1 copy number was analyzed in a variety of cancers using TCGA data and GISTIC analysis with a threshold CNA change of +/-2. B, HSF1 transcripts are elevated in a variety of cancers. Samples from tumor tissue and matched normal tissue were compared in the TCGA database using RNA Seq V2 RSEM data with a z-score threshold of +/-2. C, HSF1 is increased at the mRNA level in an ovarian cancer data set GSE18520 consisting of 10 normal ovarian samples and 53 late stage, primary site, high grade ovarian cancer samples. D, HSF1 is increased at the mRNA level in a TCGA ovarian cancer data set consisting of 8 normal ovarian samples and 568 ovarian cancer samples.

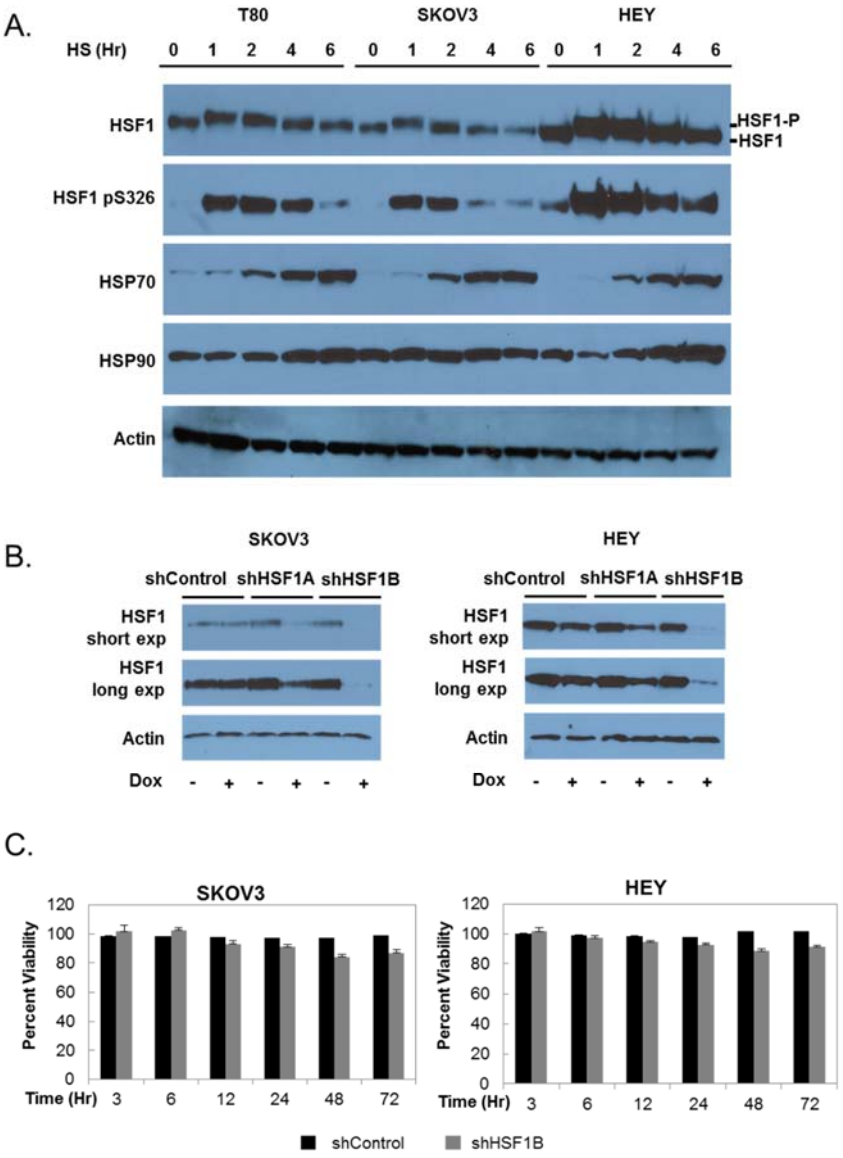

Figure 3.2. Validation of Inducible HSF1 Knockdown Ovarian Cancer Cell Lines.

A, The heat shock response in the epithelial ovarian carcinoma cell lines SKOV3 and HEY as compared to normal ovarian epithelial T80 cells. T80, SKOV3, and HEY cells were treated with a 42^{o}C heat shock for the indicated times and harvested immediately after. Cell lysates were subjected to Western blot analysis using antibodies recognizing HSF1, HSF1 phosphorylated at S326, HSP90, HSP70, and actin as a loading control. B, The pTRIPZ system was used to create the doxycycline-inducible HSF1 knockdown cell lines SKOV3.shHSF1A, SKOV3.shHSF1B, HEY.shHSF1A and HEY.shHSF1B. After treatment with 1 µg/ml doxycycline for 48 hours, cell lysates were subjected to Western blot analysis using antibodies recognizing HSF1 and actin as a loading control. Both short and long exposures are shown for the HSF1 blot. C, HSF1 knockdown does not cause a large decrease in cell viability. The viability of the SKOV3.shHSF1B and HEY.shHSF1B cell lines as compared to shControl cells was assessed after treatment with 1 µg/ml doxycycline for the indicated times using the PrestoBlue cell viability assay. Mean percent viability (n=8) and standard error is shown.

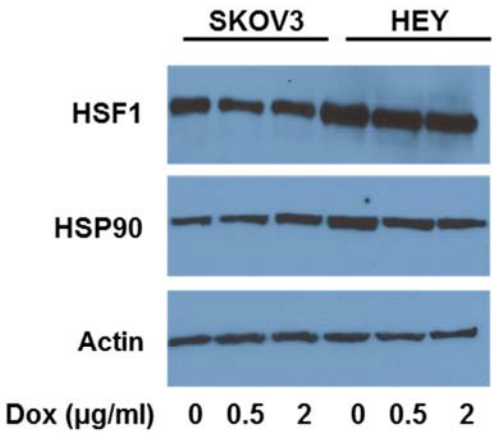

Figure 3.3. Doxycycline treatment alone does not alter HSF1 levels or induce HSP90 expression in ovarian cancer cell lines.

SKOV3 and HEY cells were treated with 0-2 µg/ml doxycycline, as indicated, for 48 hours. Cell lysates were subjected to Western blot analysis using antibodies recognizing HSF1, HSP90, and actin as a loading control.

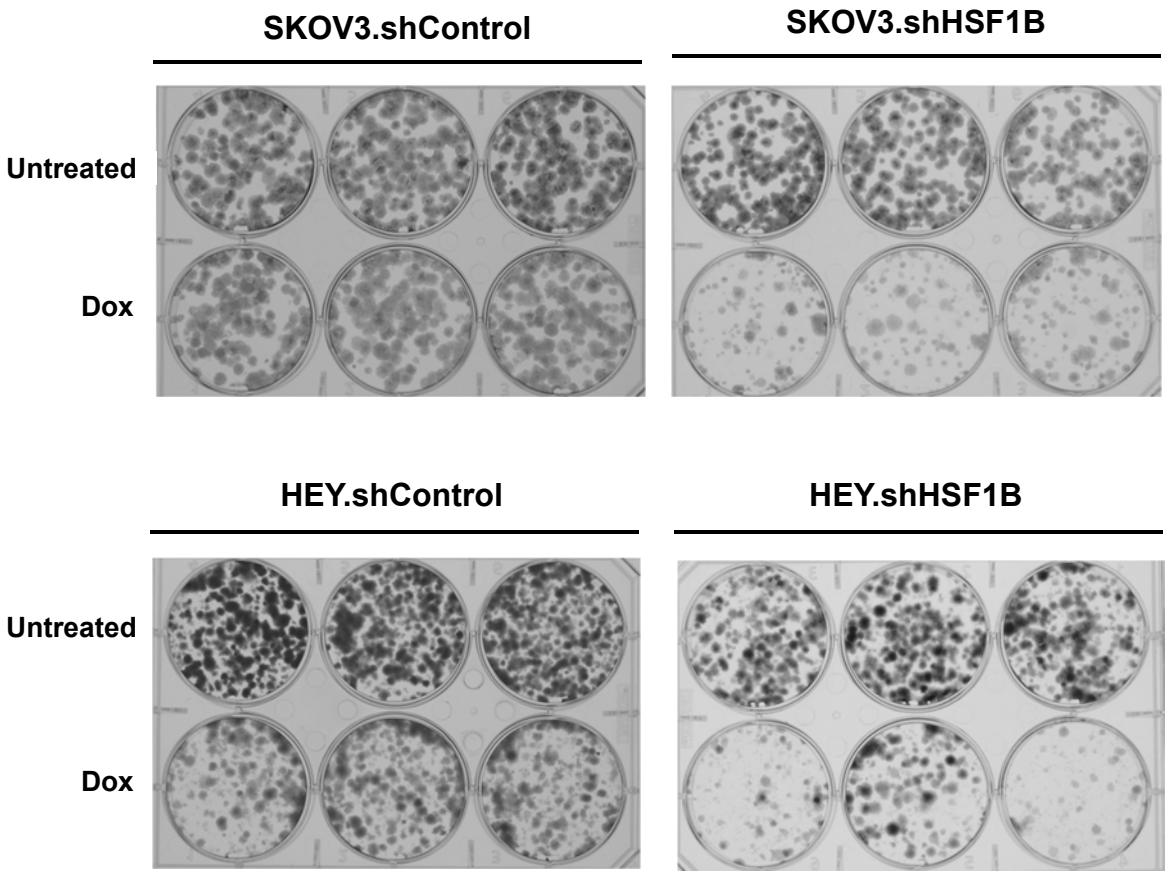

Figure 3.4. HSF1 Knockdown Reduces Colony Formation.

SKOV3.shHSF1B, HEY.shHSF1B and control cell lines were plated 250 cells per well in 6-well plates in triplicate. Cell were treated with or without 1 μg/ml doxycycline (Dox) to induce HSF1 knockdown and were given an additional dose after 4 days. Cells were stained with crystal violet after 8 days to visualize colonies.

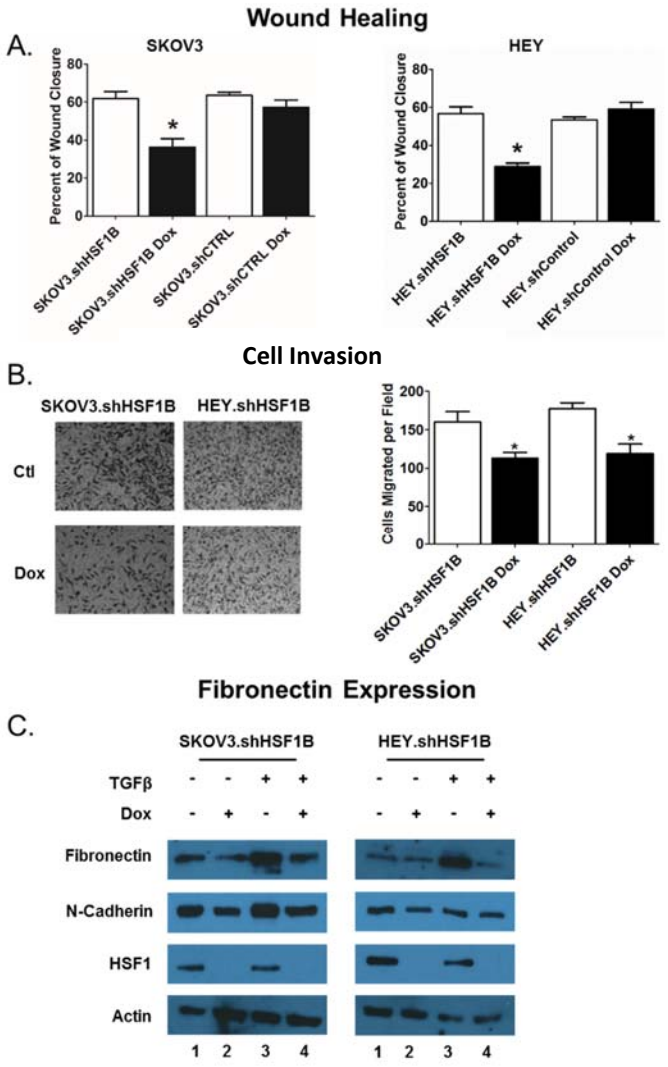

Figure 3.5. HSF1 Knockdown Inhibits Wound Healing, Migration, and Induction of Fibronectin.

A, HSF1 knockdown reduces wound closure. Cells treated with or without 1 μg/ml doxycycline were grown in 6-well plates to confluency. Cells were scraped to create wounds, the cells were washed and serum-free media was added. The intersections of perpendicular scratches were photographed immediately and 12 hours after and analyzed using Tscratch software. Asterisk denotes significant difference from all other samples calculated by ANOVA ($P < 0.05$). B, HSF1 knockdown reduces migration. After treatment with or without 1 μg/ml doxycycline and 12 hours of serum starvation, cells were added to a Boyden chamber at 2.5×10^4 cells per chamber. Serum was used as the chemoattractant in the lower chamber. After 16 hours, nonmigrating cells were scrubbed and cells which had migrated stained. The experiment was done in triplicate and analysis done by paired t-test. Asterisk marks significant difference ($P < 0.05$). C, HSF1 KD reduces TGFβ-induced expression of fibronectin. SKOV3.shHSF1B and HEY.shHSF1B were treated with 1ug/ml doxycycline, 10 ng/μl TGFβ, or both, and cell lysates were harvested for immunoblotting. Cell lysates were subjected to Western blot analysis using antibodies recognizing fibronectin, HSF1, and actin as a loading control.

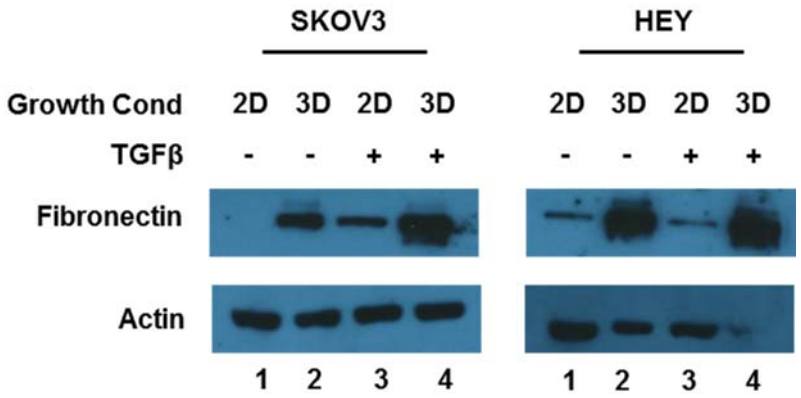

Figure 3.6. Fibronectin Expression is induced by 3D Growth.

SKOV3 and HEY cells were cultured under 2D or 3D conditions, with or without TGFβ, as indicated. Cell lysates were subjected to Western blot analysis using antibodies recognizing fibronectin, and actin as a loading control.

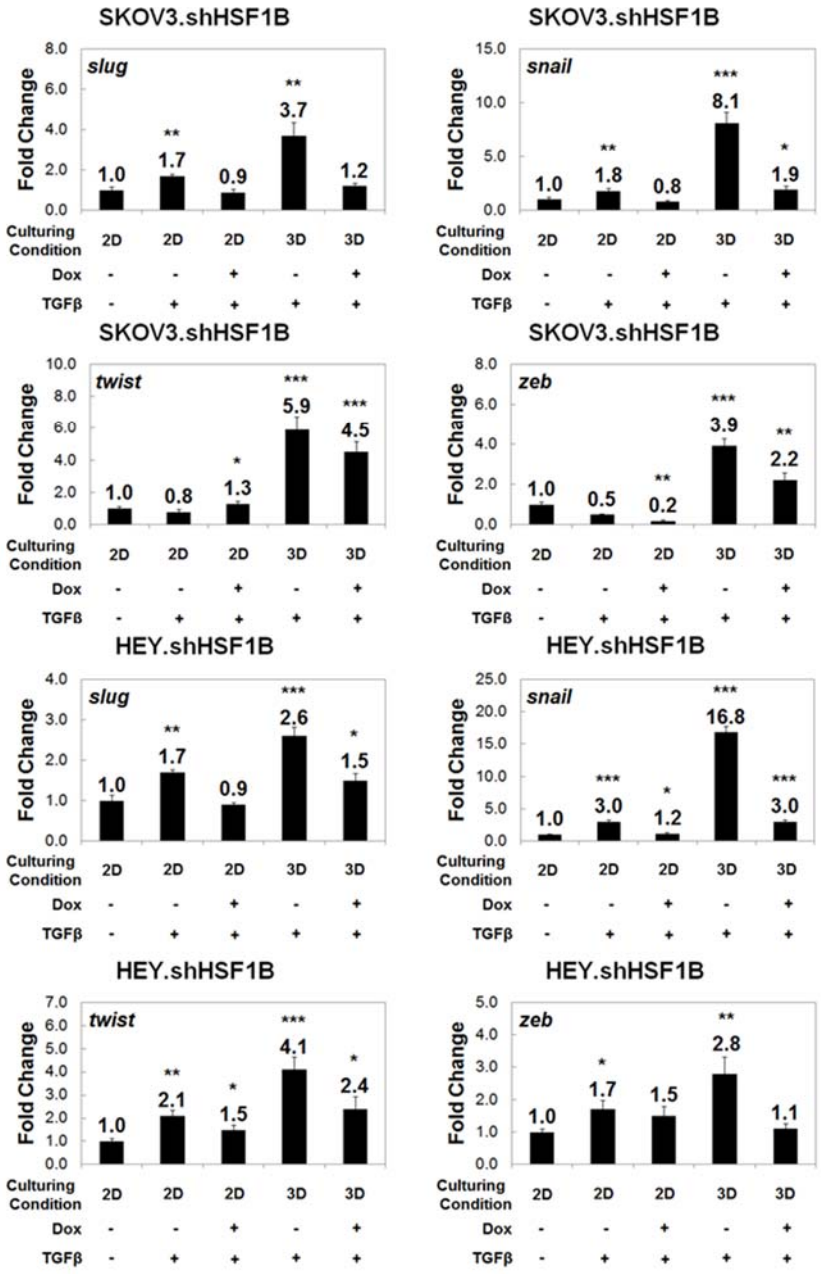

Figure 3.7. TGFβ Induction of EMT Master-Switch Transcription Factors are Reduced upon HSF1 Knockdown, and the effect is enhanced upon 3D Culturing.

Quantitative real-time polymerase chain reaction (qRT-PCR) of selected genes shows that the EMT master-switch transcription factors *SNAI1/SNAIL, TWIST1, ZEB1, and SNAI2/SLUG* are upregulated when HSF1 inducible knockdown SKOV3.shHSF1B and HEY.shHSF1B cells are cultured as 3D spheroids. This effect is significantly reduced upon knockdown of HSF1 via doxycycline treatment. Gene expression was normalized to the housekeeping gene *GAPDH*, and fold change was calculated relative to monolayer non-treated conditions. Statistical significance was measured by Student's t test as compared to untreated monolayer cell culture (*p<0.05; **p<0.01 ; ***p<0.001). Experiment performed with biological and technical triplicates.

Table 3.1. List of Primers used in Quantitative RT-qPCR.

Gene Name	Common Name	Sequence
GAPDH	*GAPDH*	F: 5′ - CCACTCCTCCACTTTGAC - 3′ R: 5′ - ACCCTGTTGCTGTAGCCA - 3′
SNAI1	*SNAIL*	F: 5′ - TCCCAGATGAGCATTGGCAG - 3′ R: 5′ - CGCGCTCTTTCCTCGTCAG - 3′
SNAI2	*SLUG*	F: 5′ - TTCGGACCCACACATTACCT - 3′ R: 5′ - GCAGTGAGGGCAAGAAAAAG - 3′
TWIST1	*TWIST*	F: 5′ - GGAGTCCGCAGTCTTACGAG - 3′ R: 5′ - TCTGGAGGACCTGGTAGAGG - 3′
ZEB1	*ZEB*	F: 5′ - CAATACCGTCATCCTCAGCA - 3′ R: 5′ - CCAATCCCAGGAGGAAAAAC - 3'

Table 3.2. Locations of HSEs in EMT Genes.

Gene Name	Common Name	Location from CDS	Sequence
FN1	*fibronectin*	-3254	TTCTGCAACTTTCA
VIM	*vimentin*	-3754	TTCCAGAAGGTTAA
SNAI1	*SNAIL*	-3201	TTCTAGAAGCTTCA
		-3207	TTCTAGAATTTTGG
CDH2	*N-cadherin*	-4429	TTCTGGGAAGTTCC
		-2183	TTCCGGAACCTTTT
		-2177	TTCCGGAAAATTTA
		-2544	TTCCTGGATTTTCT
ZEB1	*ZEB*	-289	TTCACTAACTTTCC
TWIST1	*TWIST*	-1301	TTCGAGCACCTTCC
Consensus			TTCnnGAAnnTTCn

CHAPTER FOUR: DISCUSSION AND FUTURE DIRECTIONS

Overview of Major Findings

We have shown that gene expression profiles significantly change upon three dimensional spheroid culturing when compared to two dimensional monolayers. Using the HEY ovarian cancer cell line, we show that 3D growth affects DNA integrity pathways, stem cell differentiation, epigenetic pathways, and stress pathways. Namely, transcripts that included Coiled-Coil Domain Containing 80 (CCDC80), Solute Carrier Family 6 (Neutral Amino Acid Transporter), Member 15 (SLC6A15), Semaphorin 3E (SEMA3E) and PIF1 5'-To-3' DNA Helicase (PIF1) were downregulated more than 10-fold in the 3D cells while Inhibitor Of DNA Binding 2, HLH Protein (ID2), Regulator Of Cell Cycle (RGCC), Protease, Serine 35 (PRSS35), and Aldo-Keto Reductase Family 1, Member C1 (AKR1C1) were increased more than 50-fold.

Several of the above genes have been implicated in increasing tumorigenicity, including upregulation of AKRC1C and PRSS35, in addition to a reduction in CCDC80 expression. More specifically, AKR1C1 expression has been linked to cisplatin resistance in ovarian cancer cells [237]. PRSS35, a serine protease, may be responsible for proteolytic digestion of cell attachment and thereby promote EMT in ovarian cancer. Lastly, CCDC80 has been shown to be reduced in human ovarian cancer samples compared to normal tissue. This is likely due to its role in inducing E –

cadherin [240], which is responsible for promoting an epithelial phenotype by enhancing cell-cell adhesion [241].

Novel pathways which were affected upon spheroid culturing included branched chain amino acid metabolism, folate biosynthesis, mevalonate pathway, and fatty acid oxidation. Branched chain amino acids, such as leucine, positively regulate the mammalian-target-of-rapamycin (mTOR) pathway [242]. FRAP/mTOR inhibition has been shown to reduce cancer cell growth in PTEN null cells [292]. Mutations in PTEN, a known tumor suppressor which regulates signaling through the PI3-kinase/Akt-signaling pathway, are seen in several cancer cell types. Consequently, recent ovarian cancer clinical trials have focused on molecular agents which target the P13K/Akt/mTOR pathway. Another possible target is folate and its membrane-bound folate receptors (FRs). Folate plays a role in nucleotide synthesis and methylation, making it essential to cancer cells for DNA replication. Analysis of 104 human ovarian carcinomas revealed 83% overexpressed alpha-folate receptor protein at moderate to high levels compared to 0% in non-neoplastic ovaries [293]. Therefore, antifolate and FR agents such as thymidylate synthase inhibitors, antifolate receptor antibodies, and folate-chemotherapy conjugates may have anti-tumor affects in ovarian cancer [294]. Conversely, the mevalonate pathway converts acetyl-coenzyme A into isoprenoids, which are vital for cholesterol synthesis. Low-density lipoprotein (LDL) cholesterol has been shown to collect in cancer tissues and increased levels have been linked to proliferation and migration [246].

Related specifically to stress pathways, networks involved in oxidative stress, DNA damage response, and heat shock response were all altered upon three

dimensional spheroid culturing methods. This is not shocking since it is known that spheroid growth conditions may cause hypoxia and a reduction in nutrient and waste transport. Gene expression changes related to oxidative stress included: Peroxiredoxin 2 (PRDX2), Catalase (CAT), Superoxide dismutase 1, soluble (SOD1), and Glutathione S-transferase omega 1 (GST01). Oxidative stress promotes tumorigenic properties by impacting important signaling cascades such as Ras, Raf, p53, PKC, and Nrf2 [250-252]. This oxidation process guards cancer cells from ROS through the synthesis of ATP and NADPH [245]. Related to oxidation, fatty acid oxidation is essential for angiogenesis and enables cancer tumors to overcome metabolic stress [245]. This makes fatty acid oxidation yet another potential target for cancer treatment.

DNA integrity responses, such as DNA damage, nucleotide excision repair (NER), and genetic instability were also altered upon three dimensional spheroid culturing. Microenvironment differences in the spheroid environment leads to hypoxia and ROS which causes DNA damage and therefore mutagenesis. To identify and repair this damage, mechanisms such as NER is utilized, which was enriched in our analysis.

Our gene expression studies show significant changes in transcripts which are related to the HSR, to include: heat shock protein 90kDa alpha (cytosolic), class A member 1 (HSP90AA1), heat shock 27kDa protein 1 (HSPB1), and heat shock transcription factor 1 (HSF1). Research has suggested that tumor progression for some cancer types may heavily rely on HSF1, the master regulator of the HSR. In our TCGA analysis, we revealed that HSF1 gene duplication is more common in ovarian cancer than any other cancer type and that HSF1 mRNA transcripts are significantly elevated in

ovarian cancer tumor tissue compared to that of normal epithelial tissue derived from the same patient.

Further analysis utilizing SKOV3 and HEY ovarian cancer cell lines shown that HSF1 plays an essential role in promoting ovarian cancer tumorigenicity. HSF1 knockdown SKOV3 and HEY ovarian cancer cells were created utilizing a doxycycline-inducible shHSF1 system. We ensured that doxycycline treatment alone would not alter HSF1 levels, HSF1 hyperphosphorylation status, or HSP90 levels.

Subsequent HSF1 knockdown diminishes cell invasiveness, mobility, and the cells ability to grow without contact inhibition. First, a matrigel-coated transwell membrane was utilized to determine that HSF1 knockdown inhibits cell migration in both SKOV3 and HEY. Second, a wound healing assay showed that reduction in HSF1 correlates to the inhibition of cell mobility in order to effectively close implemented scratches in monolayer cells. Lastly, focus assays proved that HSF1 knockdown significantly reduces focus formation in HEY and SKOV3 ovarian cancer cells. Knockdown of HSF1 also caused a reduction in Fibronectin, a mesenchymal marker which is vital for the EMT process. Further analysis revealed that HSF1 knockdown alters the expression of EMT transcription factor genes, *SNAIL*, *ZEB*, *TWIST1*, and *SLUG.*

Utilizing the hanging drop method, we determined that three dimensional culturing enhances TGFβs ability to induce EMT. Interestingly, this reduction in the ability TGFβ to induce EMT in response to decreased HSF1 expression is significantly stronger in three-dimensional spheroids. Therefore, we determined that HSF1

promotes EMT in ovarian cancer spheroids through regulating EMT-inducing transcription factor expression. In all, HSF1 is critical for ovarian cancer progression and should be further studied for possible antitumor treatments.

Spheroids as a Therapeutic Model

Approximately 35% of ovarian cancer patients present with metastasized single and aggregated ovarian cancer cells suspended within voluminous exudative fluid in the peritoneal cavity, known as ascites [73]. This phenomenon has been linked to drug insensitivity, amplified cancer progression, and reduced survival [74, 75, 295]. The aggregated cells free floating within the ascetic fluid very closely mimic those created utilizing spheroid cell culturing models. Therefore, spheroid culturing may be utilized to fully characterize and determine the best possible chemotherapeutic techniques.

Future Studies for Ovarian Cancer Spheroids

Upon discovering a plethora of differentially expressed genes between monolayer and spheroid cultured ovarian cancer cells, we suggest further exploration of spheroid treatment in regard to the HSR. We hypothesize that novel HSF1-regulated genes which are vital for EMT and ovarian cancer progression will be discovered. To accomplish this, the focus should be on identifying HSF1 dependent genes that are affected by ovarian cancer spheroid growth. First, target mRNAs that are regulated by 3D growth should be determined by mRNA-sequencing techniques with and without doxycycline treatment for HSF1 knockdown. High-throughput sequencing would determine genes which are induced in EMT in an HSF1 dependent fashion. Next, it would be interesting to identify target miRNAs that are regulated by spheroid growth.

miRNAs have been shown to be vital regulators in cancer progression and metastasis and therefore are essential to understanding the mechanism behind HSF1's role in ovarian cancer progression. Lastly, ChIP-seq would identify direct HSF1 targets. This would allow for the identification of HSF1 binding sites in gene promoters and other regulatory sequences.

Further expanding on our knowledge of HSF1's role in EMT, we propose analyzing protein expression changes upon HSF1 knockdown during spheroid culturing and identifying critical pathways in EMT and metastasis. This could be accomplished by utilizing mass spectrometry to evaluate protein expression changes in spheroid cells upon HSF1 knockdown. Analysis of global changes at the protein level is determined through stable isotope labeling by amino acids in cell culture (SILAC). Then, results would be evaluated via Pathway Studio™ to determine critical pathways and targets. From there, it would be interesting to determine the role of critical HSF1 targets on EMT through knockdown or overexpression of identified genes.

Implications for HSF1's Role in Ovarian Cancer Progression

Several cancer cell types exploit HSF1's survival properties in order to avoid apoptosis and to proliferate. Elevated HSF1 expression has been shown in prostate, breast, colon, and lung cancer, and is a biomarker for poor prognosis and tumor progression [197, 215-217]. Increased expression of HSPs has been similarly linked to a wide range of tumor histotypes and is linked to chemotherapy resistance and poor prognosis. For instance, HSP90's chaperone properties maintain the active conformation of overexpressed or mutated signaling proteins which are vital for

development and cell renewal within cancer tumors [296, 297]. Therapeutics which target HSP90 cause morphological differentiation and apoptosis through G1 cell cycle arrest [297]. Similarly, HSP70 correlates with metastasis and poor prognosis while inhibition through anti-sense HSP70 cDNA causes proliferation inhibition and promotes apoptosis [298, 299].

Therapeutically Targeting the HSR

Modulators of HSF1 and HSPs have been implicated in treatment of these various diseases. For instance, HSP90 is an attractive target for cancer treatment and several inhibitors of HSP90 are currently being studied in clinical trials [300, 301]. The first HSP90 inhibitor was not discovered until 1994 when Whitesell *et al.* described the natural product known as geldanamycin (GA) and its ability to bind HSP90's adenosine triphosphate pocket, causing degradation of client proteins such as the oncogene v-Src [302]. HSP90 aids in the stability of client oncoproteins, which promotes cancer cell progression [303]. HSP90 inhibitors cause ubiquitination and subsequent degradation of these oncoproteins by binding to HSP90's adenosine triphosphate pocket, rendering it functionally inactive, and preventing client stabilization [187]. Compared to normal cells, many cancer cells have elevated levels of the active HSP90 complex and are selectively sensitive to inhibition of HSP90 [304, 305]. Today, there are several synthetic, second-generation HSP90 inhibitors being studied for potential clinical use in a wide range of human diseases. These inhibitors, such as ganetespib seen in Figure 4.1, are less toxic than their natural first-generation counterparts [306]. Currently there are no agents targeting HSP90 which have been approved for clinical use, however substantial progress has been made in the past decade towards this goal.

Ganetespib (formally known as STA-9090) is a small molecule inhibitor of HSP90 which has superior anti-tumor effects and a superior safety profile as compared to first generation HSP90 inhibitors [306]. Ganetespib is a resorcinol-containing triazole compound developed by Synta Pharmaceuticals (Fig. 4.1). Thus far, the compound has been studied in clinical trials involving non-small cell lung cancer, acute myeloid leukemia, gastrointestinal stromal cancer, and metastatic breast cancer with mixed results [307-311]. In ovarian cancer, ganetespib significantly inhibited tumor progression and growth of orthotopic xenografts and spontaneous ovarian tumors in mice. Additionally, paclitaxel enhanced this effect [312].

Celastrol, an active compound derived from the Tripterygium wilfordii Hook F plant (TWHF) was first characterized by Westerheide *et al*. as an inducer of the HSR (Fig. 4.1) [313]. More specifically, it induces HSPs in multiple cell lines by inhibiting HSP90, allowing for HSF1 activation which in turn increases HSP expression [314]. Using this response, celastrol has been shown to improve neurodegenerative diseases such as ALS and Parkinson's [315, 316]. This compound is also capable of anti-tumor effects both *in vitro* and *in vivo* across multiple histological origins

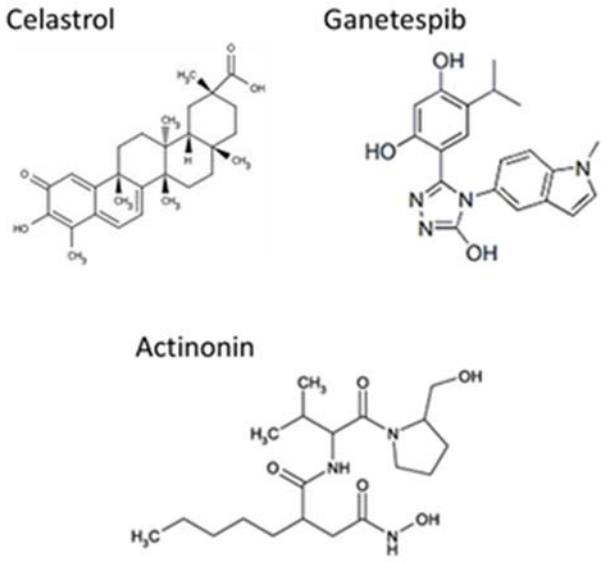

Figure 4.1: Small molecule modulators of the HSR and HSP90.

Both celastrol and ganetespib have been shown to regulate the HSR by inhibiting HSP90, allowing for HSF1 activation. Actinonin is a novel compound which reduces celastrol's HSR effects while increasing its anti-tumor properties.

[317, 318], likely due to it arresting cell cycle progression and inducing apoptosis as seen with other HSP90 inhibitors [319]. However, like other HSP90 inhibitors, celastrol's ability to induce the HSR is an unwanted effect when applying it to cancer treatment, since enhancing HSP levels increases tumor cell survival. Recently, the addition of the peptide deformylase inhibitor, actinonin, to celastrol-treated cancer cells showed a synergistic effect by reducing the HSR while enhancing proliferation inhibition [320]. Actinonin also has anti-tumor activity *in vitro* and *in vivo* for a number of cancer subtypes, however the exact mechanism has not been fully characterized [321].

Future in vitro Studies for Targeting the HSR in Ovarian Cancer

To build on our current studies, *in vitro* assays examining HSF1's mechanistic role in EMT as well as assays examining potential synergistic effects of HSF1 and HSP90 small molecule modulators with standard chemotherapy agents could be conducted. We propose using ovarian cancer monolayer and spheroid model cells to determine the mechanism for HSF1 regulation of EMT transcription factor genes and subsequent EMT-associated genes. To do so, one would first evaluate possible HSF1 binding in the promoter region of transcription factor genes *SNAIL*, *ZEB*, *TWIST1*, and *SLUG* in addition to EMT associated genes *FN1*, *VIM*, and *CDH2*. This could be accomplished through promoter studies using luciferase reporter plasmids to determine if HSF1 can regulate these promoters. Another possible option to shed light on this particular mechanism could be through HSF1 overexpression. Overexpression assays could further validate the findings with HSF1 knockdown in ovarian cancer cell lines by studying EMT gene and protein expression level changes. HSF1 overexpression should induce opposite effects from HSF1 knockdown on proliferation, invasion, and

EMT promotion. Yet another important factor is whether EMT gene or protein expression levels vary throughout a heat shock time course. This may shed some light on whether HSF1's role in EMT is independent or dependent of its classical HSR mechanism. We propose a study of mRNA and protein expression levels upon multiple heat shock time courses to fully understand the mechanism behind the HSR and ovarian cancer progression.

Due to limited ovarian cancer treatment options, compounded by the fact that relapsed patents are no longer susceptible to the drugs previously administered, it is vital to study ways to enhance treatment alternatives. We hypothesize that ovarian cancer cells will prove to be more susceptible to the chemotherapy agents paclitaxel and cisplatin upon treatment with small molecule modulators of HSF1 and HSP90 using the three dimensional EMT model. Determining the effects of the chemotherapy agents cisplatin and paclitaxel on ovarian cancer spheroid growth would accomplish this. Then followed by assessing the effects of ovarian cancer spheroid treatment with HSP90 and HSF1 small molecule modulators on apoptosis, cell proliferation, cell migration, and critical EMT and HSR genes. Once this has been established, it would be worthwhile to identify possible synergistic effects of combination treatments of chemotherapy drugs and HSP90 and HSF1 modulators in three dimensional spheroids.

While both celastrol and ganetespib have been shown to have anti-tumor affects, they also induce the HSR, which induces tumorigenicity. Reduction of HSR induction could be accomplished with the addition of the antibacterial agent actinonin. Interestingly, the addition of actinonin to celastrol-treated cancer cells showed a synergetic effect by reducing HSR induction while promoting proliferation inhibition

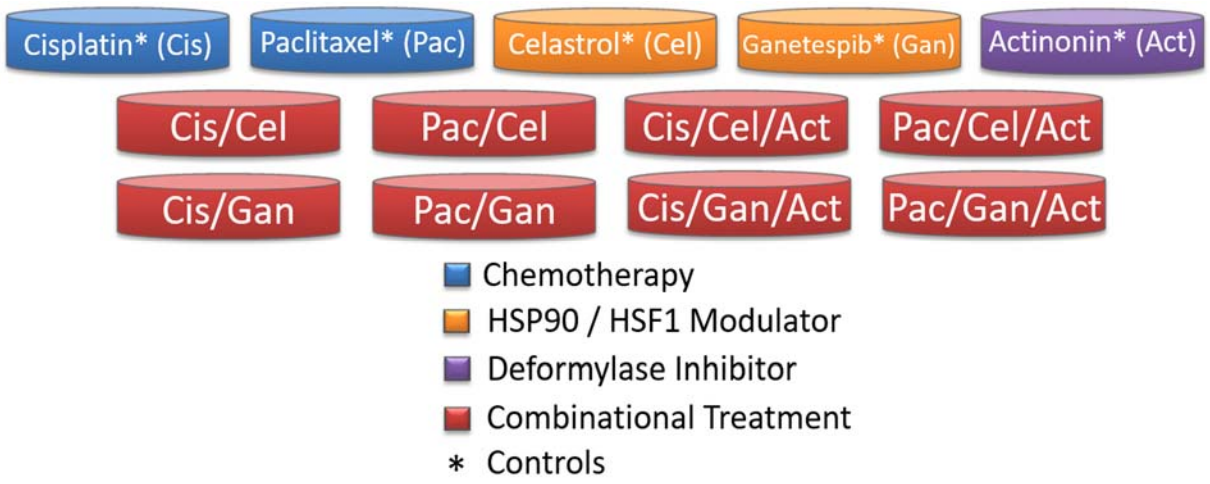

Figure 4.2: Proposed Combinational Treatment assay in 3D Spheroids.

Utilizing single treatments as controls, this experiment would analyze the effect of combining HSP90 and HSF1 small molecular modulators celastrol and ganetespib with standard chemotherapy agents, cisplatin and paclitaxel. Then, possible further synergistic effects are tested with the addition of actinonin, which may reduce induction of the HSR. Each sample type would be assessed for effects on viability, cell proliferation, cell migration, and critical EMT and HSR genes.

[320]. Figure 4.2 displays possible treatments which could be assayed to determine any possible synergistic combinations. After treatment, the spheroids could be tested for the effects on viability, cell proliferation, cell migration, and expression of EMT and HSR genes.

Another proposed alternative method for inhibiting HSP90 without inducing the cytoprotective effects of the HSR are newly developed C-terminal HSP90 modulators [322]. These compounds inhibit specific co-chaperone binding to the methionine-glutamic acid-glutamic acid-valine-aspartic acid (MEEVD) region of HSP90 while reducing HSP27, HSP40, and HSP70 expression levels in pancreatic, colon, and cervical cancer cells [323, 324]. Previously, C-terminal targeting agents such has Novobiocin and KU174 have been shown to reduce HSP90 activity without HSR induction, however these compounds may not be suitable for pre-clinical trials due to potency and solubility factors [325, 326]. Recently, Armstrong *et al*. described the novel

HSP90 inhibitor SM258's ability to significantly reduce proliferation in ex vivo cultured human prostate tumors without inducing the HSR [327]. As an alternative approach, we propose comparing SM258's activity in ovarian cancer spheroids to the proposed combinational treatment above. The lack of information regarding this compound's toxicity and potential off-target affects is a limiting factor in this experimentation.

Although initial response to traditional chemotherapy agents is over 80%, a majority of women ultimately relapse and develop drug-resistant ovarian cancer. Therefore, there is a strong need for second-line chemotherapeutic options. We propose to evaluate the response to HSP90 and HSF1 modulators in chemotherapy-resistant ovarian cancer cell lines. First, one could create cisplatin or paclitaxel resistant SKOV-3 and HEY ovarian cancer cells lines through a series of chemotherapy treatments. Next, one could determine the effect of resistance on the cells' ability to form spheroids and test the effect of resistance on the cells' ability to respond to HS and what changes this has on HSP mRNA and protein expression. This could then lead to evaluating the possibility of re-sensitizing resistant cells utilizing HSP90 and HSF1 modulators in combination with chemotherapy agents. Experiments should be performed at least in biological duplicate with technical triplicates. Student t test can be used for comparisons between two groups and one-way ANOVA analysis can be used for comparisons among three or more groups. $P< 0.050$ would be considered significant. Through these experiments, we can expand our understanding of HSF1's role in ovarian cancer and how it may be utilized as a novel therapeutic target.

Future in vivo Studies for Targeting the HSR in Ovarian Cancer

To further expand our knowledge of HSF1's role in ovarian cancer progression within a whole organism, it would be interesting to assess these affects using a mouse model. First, CMV-driven luciferase stable cell lines SKOV3.shHSF1B/Luc and HEY.shHSF1B/Luc could be established and grown as three dimensional spheroids. These spheroid cells could be injected directly into the intraperitoneal cavity of immunosuppressed humanized mice that have been treated with doxycycline (0.5 mg/mL) to knockdown HSF1 or left untreated (Fig. 4.3). Humanized mouse models have a high engraftment success rate while facilitating human-like hematology and immunology [328]. During metastasis, ovarian cancer cells commonly disassociate with the primary tumor and float within the peritoneal cavity before attaching to another organ and producing a secondary tumor. Luciferase expression throughout the mouse could then be assessed

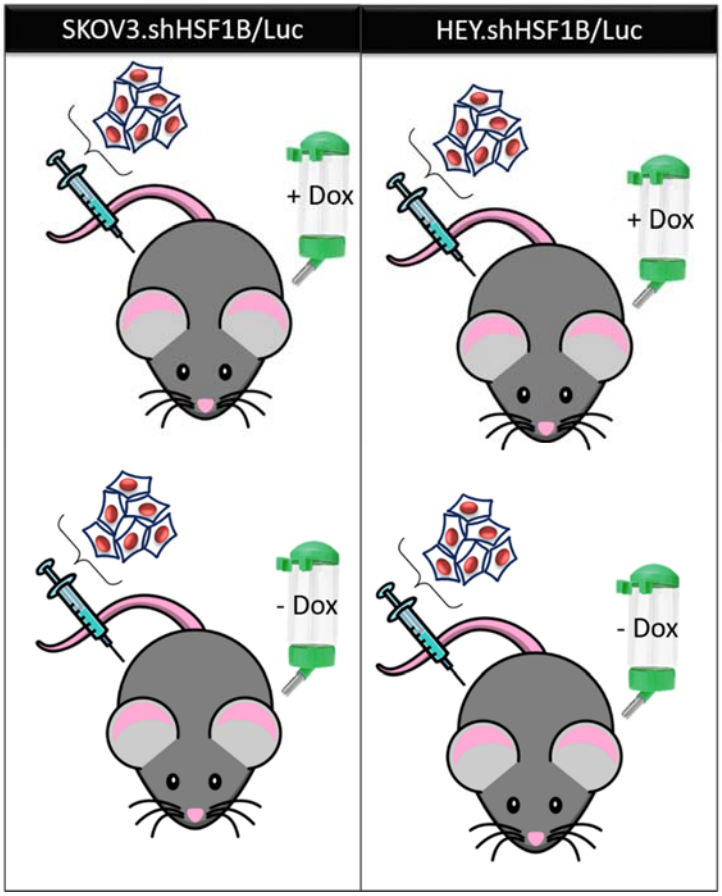

Figure 4.3: Proposed experimental outline to investigate HSF1's role in ovarian cancer progression and metastasis. In this study, shHSF1 luciferase stable ovarian cancer cell lines would be established and injected into the peritoneal cavity of immunosuppressed mice. Tumor growth and metastasis would be subsequently examined through bioluminescence imagining and then further tissue analysis would be performed after sacrificing the mice.

utilizing an IVIS imaging system which would indicate tumor size and metastasis. Metastasis is likely to occur within organs which reside in the peritoneal cavity, such as the liver, colon, stomach, and kidney, and therefore should be the focus of this study. The mice could then be sacrificed and various tissues analyzed for expression changes in HSF1, HSP70, and previously discussed EMT markers. We hypothesize that HSF1 knockdown will cause a reduction in tumor growth and metastasis *in vivo*. While HSF1 knockdown has been shown to reduce tumor size in other cancer tumor types [207], this experiment would determine what affects it may have for ovarian cancer in a whole organism.

Patient-Derived Xenograft (PDX) ovarian cancer models are also available for *in vivo* studies [329]. These xenograft tumors can be implanted into immunosuppressed mice and retain the genetic and phenotypic characteristics found in human ovarian cancer [329-331]. Ovarian cancer PDX models show a strong similarity to patient solid tumors in cancer proliferation, metastasis, and ascites formation [332]. We propose utilizing this model in conjunction with HSF1 and HSP90 small molecule modulators, as described in the above, to further elucidate the effects of HSF1 and HSP90 inhibition on ovarian cancer progression. However, this method can be limited by time and cost, which may not make it a feasible option. Distinguishable tumor growth can take up to eight months in PDX models and the cost to maintain and test these models can be restrictive [333].

Final Thoughts

These proposed studies investigating the *in vivo* and *in vitro* responses to manipulating HSF1 expression will provide a more thorough understanding of HSF1's role in ovarian cancer progression and EMT. This may offer a detailed mechanistic outline of how ovarian cancer relies on HSF1 to proliferate and progress. Specific insight on this role could lead to breakthroughs in current treatment options. Additionally, we hypothesize that combining HSR modulators with standard chemotherapy agents may lead to a synergistic effect on inhibiting ovarian cancer cell progression in the spheroid model by reducing proliferation, metastasis, and cell viability. It is yet unknown which combination will result in the most efficient anti-tumor properties, but we anticipate this approach to be closely related to the actual *in vivo* response that would be seen in ovarian cancer patients. Furthermore, we believe that expanding this research through the use of a whole organism model will solidify our *in vitro* findings of HSF1's vital role in ovarian cancers progression and metastasis.

REFERENCES

1. Phung, Y.T., et al., *Rapid generation of in vitro multicellular spheroids for the study of monoclonal antibody therapy.* J Cancer, 2011. **2**: p. 507-14.
2. Siegel, R.L., K.D. Miller, and A. Jemal, *Cancer statistics, 2016.* CA Cancer J Clin, 2016. **66**(1): p. 7-30.
3. Guettouche, T., et al., *Analysis of phosphorylation of human heat shock factor 1 in cells experiencing a stress.* BMC Biochem, 2005. **6**: p. 4.
4. Bast, R.C., Jr., B. Hennessy, and G.B. Mills, *The biology of ovarian cancer: new opportunities for translation.* Nat Rev Cancer, 2009. **9**(6): p. 415-28.
5. Kurman, R.J. and M. Shih Ie, *The origin and pathogenesis of epithelial ovarian cancer: a proposed unifying theory.* Am J Surg Pathol, 2010. **34**(3): p. 433-43.
6. Goldie, J.H. and A.J. Coldman, *A mathematic model for relating the drug sensitivity of tumors to their spontaneous mutation rate.* Cancer Treat Rep, 1979. **63**(11-12): p. 1727-33.
7. Olson, S.H., et al., *Symptoms of ovarian cancer.* Obstet Gynecol, 2001. **98**(2): p. 212-7.
8. Rosenthal, A. and I. Jacobs, *Ovarian cancer screening.* Semin Oncol, 1998. **25**(3): p. 315-25.
9. *NIH consensus conference. Ovarian cancer. Screening, treatment, and follow-up. NIH Consensus Development Panel on Ovarian Cancer.* JAMA, 1995. **273**(6): p. 491-7.
10. Einhorn, N., et al., *Prospective evaluation of serum CA 125 levels for early detection of ovarian cancer.* Obstet Gynecol, 1992. **80**(1): p. 14-8.
11. Tsao, A.S., E.S. Kim, and W.K. Hong, *Chemoprevention of cancer.* CA Cancer J Clin, 2004. **54**(3): p. 150-80.
12. Fathalla, M.F., *Incessant ovulation--a factor in ovarian neoplasia?* Lancet, 1971. **2**(7716): p. 163.
13. Booth, M., V. Beral, and P. Smith, *Risk factors for ovarian cancer: a case-control study.* Br J Cancer, 1989. **60**(4): p. 592-8.
14. Whittemore, A.S., R. Harris, and J. Itnyre, *Characteristics relating to ovarian cancer risk: collaborative analysis of 12 US case-control studies. II. Invasive epithelial ovarian cancers in white women. Collaborative Ovarian Cancer Group.* Am J Epidemiol, 1992. **136**(10): p. 1184-203.
15. Whiteman, D.C., et al., *Multiple births and risk of epithelial ovarian cancer.* J Natl Cancer Inst, 2000. **92**(14): p. 1172-7.
16. Risch, H.A., *Hormonal etiology of epithelial ovarian cancer, with a hypothesis concerning the role of androgens and progesterone.* J Natl Cancer Inst, 1998. **90**(23): p. 1774-86.
17. Rodriguez, G.C., et al., *Effect of progestin on the ovarian epithelium of macaques: cancer prevention through apoptosis?* J Soc Gynecol Investig, 1998. **5**(5): p. 271-6.
18. Collaborative Group on Epidemiological Studies of Ovarian, C., et al., *Ovarian cancer and oral contraceptives: collaborative reanalysis of data from 45 epidemiological studies including 23,257 women with ovarian cancer and 87,303 controls.* Lancet, 2008. **371**(9609): p. 303-14.
19. Ludwig, A.H., et al., *Androgen, progesterone, and FSH receptor polymorphisms in ovarian cancer risk and outcome.* Endocr Relat Cancer, 2009. **16**(3): p. 1005-16.
20. Easton, D.F., et al., *Genetic linkage analysis in familial breast and ovarian cancer: results from 214 families. The Breast Cancer Linkage Consortium.* Am J Hum Genet, 1993. **52**(4): p. 678-701.

21. Miki, Y., et al., *A strong candidate for the breast and ovarian cancer susceptibility gene BRCA1.* Science, 1994. **266**(5182): p. 66-71.
22. Thompson, D., D.F. Easton, and C. Breast Cancer Linkage, *Cancer Incidence in BRCA1 mutation carriers.* J Natl Cancer Inst, 2002. **94**(18): p. 1358-65.
23. Obata, K., et al., *Frequent PTEN/MMAC mutations in endometrioid but not serous or mucinous epithelial ovarian tumors.* Cancer Res, 1998. **58**(10): p. 2095-7.
24. Berchuck, A., et al., *Overexpression of HER-2/neu is associated with poor survival in advanced epithelial ovarian cancer.* Cancer Res, 1990. **50**(13): p. 4087-91.
25. Slamon, D.J., et al., *Studies of the HER-2/neu proto-oncogene in human breast and ovarian cancer.* Science, 1989. **244**(4905): p. 707-12.
26. Soslow, R.A., *Histologic subtypes of ovarian carcinoma: an overview.* Int J Gynecol Pathol, 2008. **27**(2): p. 161-74.
27. Shih Ie, M. and R.J. Kurman, *Ovarian tumorigenesis: a proposed model based on morphological and molecular genetic analysis.* Am J Pathol, 2004. **164**(5): p. 1511-8.
28. McCluggage, W.G., *Morphological subtypes of ovarian carcinoma: a review with emphasis on new developments and pathogenesis.* Pathology, 2011. **43**(5): p. 420-32.
29. Nomura, H., et al., *Lymph node metastasis in grossly apparent stages I and II epithelial ovarian cancer.* Int J Gynecol Cancer, 2010. **20**(3): p. 341-5.
30. Jelovac, D. and D.K. Armstrong, *Recent progress in the diagnosis and treatment of ovarian cancer.* CA Cancer J Clin, 2011. **61**(3): p. 183-203.
31. Ansaloni, L., et al., *Pharmacokinetics of concomitant cisplatin and paclitaxel administered by hyperthermic intraperitoneal chemotherapy to patients with peritoneal carcinomatosis from epithelial ovarian cancer.* Br J Cancer, 2015. **112**(2): p. 306-12.
32. Armstrong, D., *Update on treatment options for newly diagnosed ovarian cancer.* Clin Adv Hematol Oncol, 2010. **8**(10): p. 675-8.
33. Markmon, M., *Second-line chemotherapy of epithelial ovarian cancer.* Expert Rev Anticancer Ther, 2003. **3**(1): p. 31-6.
34. Moss, C. and S.B. Kaye, *Ovarian cancer: progress and continuing controversies in management.* Eur J Cancer, 2002. **38**(13): p. 1701-7.
35. Greenburg, G. and E.D. Hay, *Epithelia suspended in collagen gels can lose polarity and express characteristics of migrating mesenchymal cells.* J Cell Biol, 1982. **95**(1): p. 333-9.
36. Hay, E.D., *An overview of epithelio-mesenchymal transformation.* Acta Anat (Basel), 1995. **154**(1): p. 8-20.
37. Shook, D. and R. Keller, *Mechanisms, mechanics and function of epithelial-mesenchymal transitions in early development.* Mech Dev, 2003. **120**(11): p. 1351-83.
38. Hugo, H., et al., *Epithelial--mesenchymal and mesenchymal--epithelial transitions in carcinoma progression.* J Cell Physiol, 2007. **213**(2): p. 374-83.
39. Kalluri, R. and R.A. Weinberg, *The basics of epithelial-mesenchymal transition.* J Clin Invest, 2009. **119**(6): p. 1420-8.
40. Huber, M.A., N. Kraut, and H. Beug, *Molecular requirements for epithelial-mesenchymal transition during tumor progression.* Curr Opin Cell Biol, 2005. **17**(5): p. 548-58.
41. Nakagawa, S. and M. Takeichi, *Neural crest cell-cell adhesion controlled by sequential and subpopulation-specific expression of novel cadherins.* Development, 1995. **121**(5): p. 1321-32.
42. Strutz, F., et al., *Role of basic fibroblast growth factor-2 in epithelial-mesenchymal transformation.* Kidney Int, 2002. **61**(5): p. 1714-28.
43. Heldin, C.H., K. Miyazono, and P. ten Dijke, *TGF-beta signalling from cell membrane to nucleus through SMAD proteins.* Nature, 1997. **390**(6659): p. 465-71.

44. Wu, R.Y., et al., *Heteromeric and homomeric interactions correlate with signaling activity and functional cooperativity of Smad3 and Smad4/DPC4.* Mol Cell Biol, 1997. **17**(5): p. 2521-8.
45. Nakao, A., et al., *TGF-beta receptor-mediated signalling through Smad2, Smad3 and Smad4.* EMBO J, 1997. **16**(17): p. 5353-62.
46. Thiery, J.P., *Epithelial-mesenchymal transitions in tumour progression.* Nat Rev Cancer, 2002. **2**(6): p. 442-54.
47. Ge, G. and D.S. Greenspan, *BMP1 controls TGFbeta1 activation via cleavage of latent TGFbeta-binding protein.* J Cell Biol, 2006. **175**(1): p. 111-20.
48. Massague, J., *TGFbeta signalling in context.* Nat Rev Mol Cell Biol, 2012. **13**(10): p. 616-30.
49. Padua, D. and J. Massague, *Roles of TGFbeta in metastasis.* Cell Res, 2009. **19**(1): p. 89-102.
50. Jakowlew, S.B., *Transforming growth factor-beta in cancer and metastasis.* Cancer Metastasis Rev, 2006. **25**(3): p. 435-57.
51. Tian, M., J.R. Neil, and W.P. Schiemann, *Transforming growth factor-beta and the hallmarks of cancer.* Cell Signal, 2011. **23**(6): p. 951-62.
52. Wendt, M.K., M. Tian, and W.P. Schiemann, *Deconstructing the mechanisms and consequences of TGF-beta-induced EMT during cancer progression.* Cell Tissue Res, 2012. **347**(1): p. 85-101.
53. Helleman, J., et al., *Integrated genomics of chemotherapy resistant ovarian cancer: a role for extracellular matrix, TGFbeta and regulating microRNAs.* Int J Biochem Cell Biol, 2010. **42**(1): p. 25-30.
54. Nanjundan, M., et al., *Overexpression of SnoN/SkiL, amplified at the 3q26.2 locus, in ovarian cancers: a role in ovarian pathogenesis.* Mol Oncol, 2008. **2**(2): p. 164-81.
55. Nanjundan, M., et al., *Amplification of MDS1/EVI1 and EVI1, located in the 3q26.2 amplicon, is associated with favorable patient prognosis in ovarian cancer.* Cancer Res, 2007. **67**(7): p. 3074-84.
56. Petersen, O.W., et al., *Epithelial to mesenchymal transition in human breast cancer can provide a nonmalignant stroma.* American Journal of Pathology, 2003. **162**(2): p. 391-402.
57. Kalluri, R. and E.G. Neilson, *Epithelial-mesenchymal transition and its implications for fibrosis.* Journal of Clinical Investigation, 2003. **112**(12): p. 1776-1784.
58. Guarino, M., B. Rubino, and G. Ballabio, *The role of epithelial-mesenchymal transition in cancer pathology.* Pathology, 2007. **39**(3): p. 305-18.
59. Birchmeier, W. and J. Behrens, *Cadherin expression in carcinomas: role in the formation of cell junctions and the prevention of invasiveness.* Biochim Biophys Acta, 1994. **1198**(1): p. 11-26.
60. Takeichi, M., *Cadherins in cancer: implications for invasion and metastasis.* Curr Opin Cell Biol, 1993. **5**(5): p. 806-11.
61. Berx, G., et al., *Mutations of the human E-cadherin (CDH1) gene.* Hum Mutat, 1998. **12**(4): p. 226-37.
62. Kokudo, T., et al., *Snail is required for TGFbeta-induced endothelial-mesenchymal transition of embryonic stem cell-derived endothelial cells.* J Cell Sci, 2008. **121**(Pt 20): p. 3317-24.
63. Medici, D., E.D. Hay, and B.R. Olsen, *Snail and Slug promote epithelial-mesenchymal transition through beta-catenin-T-cell factor-4-dependent expression of transforming growth factor-beta3.* Mol Biol Cell, 2008. **19**(11): p. 4875-87.
64. Tse, J.C. and R. Kalluri, *Mechanisms of metastasis: epithelial-to-mesenchymal transition and contribution of tumor microenvironment.* J Cell Biochem, 2007. **101**(4): p. 816-29.
65. Gey, G.O., W.D. Coffman, and M.T. Kubicek, *Tissue culture studies of the proliferative capacity of cervical carcinoma and normal epithelium.* Cancer Research, 1952. **12**: p. 264-265.
66. Pampaloni, F., E.G. Reynaud, and E.H.K. Stelzer, *The third dimension bridges the gap between cell culture and live tissue.* Nature Reviews Molecular Cell Biology, 2007. **8**(10): p. 839-845.

67. Lee, G.Y., et al., *Three-dimensional culture models of normal and malignant breast epithelial cells.* Nature Methods, 2007. **4**(4): p. 359-365.
68. Ghajar, C.M. and M.J. Bissell, *Tumor Engineering: The Other Face of Tissue Engineering.* Tissue Engineering Part A, 2010. **16**(7): p. 2153-2156.
69. Santini, M.T., G. Rainaldi, and P.L. Indovina, *Apoptosis, cell adhesion and the extracellular matrix in the three-dimensional growth of multicellular tumor spheroids.* Crit Rev Oncol Hematol, 2000. **36**(2-3): p. 75-87.
70. Weaver, V.M., et al., *beta 4 integrin-dependent formation of polarized three-dimensional architecture confers resistance to apoptosis in normal and malignant mammary epithelium.* Cancer Cell, 2002. **2**(3): p. 205-216.
71. Padron, J.M. and G.J. Peters, *Cytotoxicity of sphingoid marine compound analogs in mono- and multilayered solid tumor cell cultures.* Investigational New Drugs, 2006. **24**(3): p. 195-202.
72. Auersperg, N., T. Ota, and G.W.E. Mitchell, *Early events in ovarian epithelial carcinogenesis: progress and problems in experimental approaches.* International Journal of Gynecological Cancer, 2002. **12**(6): p. 691-703.
73. Cvetkovic, D., *Early events in ovarian oncogenesis.* Reprod Biol Endocrinol, 2003. **1**: p. 68.
74. Shield, K., et al., *Multicellular spheroids in ovarian cancer metastases: Biology and pathology.* Gynecol Oncol, 2009. **113**(1): p. 143-8.
75. Burleson, K.M., et al., *Disaggregation and invasion of ovarian carcinoma ascites spheroids.* Journal of Translational Medicine, 2006. **4**.
76. L'Esperance, S., et al., *Global gene expression analysis of early response to chemotherapy treatment in ovarian cancer spheroids.* Bmc Genomics, 2008. **9**.
77. Zietarska, M., et al., *Molecular description of a 3D in vitro model for the study of epithelial ovarian cancer (EOC).* Mol Carcinog, 2007. **46**(10): p. 872-85.
78. Holtfreter, J., *Neural Induction in Explants Which Have Passed through a Sublethal Cytolysis.* Journal of Experimental Zoology, 1947. **106**(2): p. 197-222.
79. Holtfreter, J., *A study of the mechanics of gastrulation Part II.* Journal of Experimental Zoology, 1944. **95**(2): p. 171-212.
80. Moscona, A., *Rotation-Mediated Histogenetic Aggregation of Dissociated Cells - a Quantifiable Approach to Cell Interactions in Vitro.* Experimental Cell Research, 1961. **22**: p. 455-&.
81. Moscona, A., *Cell Suspensions from Organ Rudiments of Chick Embryos.* Experimental Cell Research, 1952. **3**(3): p. 535-539.
82. Sutherland, R.M., et al., *A multi-component radiation survival curve using an in vitro tumour model.* Int J Radiat Biol Relat Stud Phys Chem Med, 1970. **18**(5): p. 491-5.
83. Sutherland, R.M., J.A. McCredie, and W.R. Inch, *Growth of multicell spheroids in tissue culture as a model of nodular carcinomas.* J Natl Cancer Inst, 1971. **46**(1): p. 113-20.
84. Mueller-Klieser, W., *Tumor biology and experimental therapeutics.* Critical Reviews in Oncology Hematology, 2000. **36**(2-3): p. 123-139.
85. Lin, R.Z. and H.Y. Chang, *Recent advances in three-dimensional multicellular spheroid culture for biomedical research.* Biotechnol J, 2008. **3**(9-10): p. 1172-84.
86. Friedrich, J., et al., *Spheroid-based drug screen: considerations and practical approach.* Nat Protoc, 2009. **4**(3): p. 309-24.
87. Wu, L.Y., D. Di Carlo, and L.P. Lee, *Microfluidic self-assembly of tumor spheroids for anticancer drug discovery.* Biomed Microdevices, 2008. **10**(2): p. 197-202.
88. Timmins, N.E. and L.K. Nielsen, *Generation of multicellular tumor spheroids by the hanging-drop method.* Methods Mol Med, 2007. **140**: p. 141-51.
89. Kimlin, L.C., G. Casagrande, and V.M. Virador, *In vitro three-dimensional (3D) models in cancer research: an update.* Mol Carcinog, 2013. **52**(3): p. 167-82.

90. Bapat, S.A., et al., *Stem and progenitor-like cells contribute to the aggressive behavior of human epithelial ovarian cancer.* Cancer Res, 2005. **65**(8): p. 3025-9.
91. Fillmore, C.M. and C. Kuperwasser, *Human breast cancer cell lines contain stem-like cells that self-renew, give rise to phenotypically diverse progeny and survive chemotherapy.* Breast Cancer Res, 2008. **10**(2): p. R25.
92. Yang, Z.J. and R.J. Wechsler-Reya, *Hit 'em where they live: targeting the cancer stem cell niche.* Cancer Cell, 2007. **11**(1): p. 3-5.
93. Ashburner, M. and G. Richards, *Sequential gene activation by ecdysone in polytene chromosomes of Drosophila melanogaster. III. Consequences of ecdysone withdrawal.* Dev Biol, 1976. **54**(2): p. 241-55.
94. Ritossa, F., *Discovery of the heat shock response.* Cell Stress Chaperones, 1996. **1**(2): p. 97-8.
95. Ritossa, F., *New Puffing Pattern Induced by Temperature Shock and Dnp in Drosophila.* Experientia, 1962. **18**(12): p. 571.
96. Berendes, H.D., *Factors involved in the expression of gene activity in polytene chromosomes.* Chromosoma, 1968. **24**(4): p. 418-37.
97. Ashburner, M., *Patterns of puffing activity in the salivary gland chromosomes of Drosophila. V. Responses to environmental treatments.* Chromosoma, 1970. **31**(3): p. 356-76.
98. Leenders, H.J. and H.D. Berendes, *The effect of changes in the respiratory metabolism upon genome activity in Drosophila. I. The induction of gene activity.* Chromosoma, 1972. **37**(4): p. 433-44.
99. Kroeger, H. and M. Lezzi, *Regulation of gene action in insect development.* Annu Rev Entomol, 1966. **11**: p. 1-22.
100. Westerheide, S.D., et al., *Stress-Inducible Regulation of Heat Shock Factor 1 by the Deacetylase SIRT1.* Science, 2009. **323**(5917): p. 1063-1066.
101. Ritossa, F.M., *Behaviour of Rna and DNA Synthesis at the Puff Level in Salivary Gland Chromosomes of Drosophila.* Exp Cell Res, 1964. **36**: p. 515-23.
102. Berendes, H.D., *The induction of changes in chromosomal activity in different polytene types of cell in Drosophila hydei.* Dev Biol, 1965. **11**(3): p. 371-84.
103. Lindquist, S., *The heat-shock response.* Annu Rev Biochem, 1986. **55**: p. 1151-91.
104. Westerheide, S.D. and R.I. Morimoto, *Heat shock response modulators as therapeutic tools for diseases of protein conformation.* J Biol Chem, 2005. **280**(39): p. 33097-100.
105. Anckar, J. and L. Sistonen, *Regulation of HSF1 function in the heat stress response: implications in aging and disease.* Annu Rev Biochem, 2011. **80**: p. 1089-115.
106. Pelham, H.R. and M. Bienz, *A synthetic heat-shock promoter element confers heat-inducibility on the herpes simplex virus thymidine kinase gene.* EMBO J, 1982. **1**(11): p. 1473-7.
107. Shuey, D.J. and C.S. Parker, *Binding of Drosophila heat-shock gene transcription factor to the hsp 70 promoter. Evidence for symmetric and dynamic interactions.* J Biol Chem, 1986. **261**(17): p. 7934-40.
108. Ciocca, D.R., A.P. Arrigo, and S.K. Calderwood, *Heat shock proteins and heat shock factor 1 in carcinogenesis and tumor development: an update.* Arch Toxicol, 2013. **87**(1): p. 19-48.
109. Xiao, X., et al., *HSF1 is required for extra-embryonic development, postnatal growth and protection during inflammatory responses in mice.* EMBO J, 1999. **18**(21): p. 5943-52.
110. Xiao, H. and J.T. Lis, *Germline transformation used to define key features of heat-shock response elements.* Science, 1988. **239**(4844): p. 1139-42.
111. Amin, J., J. Ananthan, and R. Voellmy, *Key features of heat shock regulatory elements.* Mol Cell Biol, 1988. **8**(9): p. 3761-9.
112. Lindquist, S. and E.A. Craig, *The heat-shock proteins.* Annu Rev Genet, 1988. **22**: p. 631-77.

113. Pelham, H.R., *A regulatory upstream promoter element in the Drosophila hsp 70 heat-shock gene.* Cell, 1982. **30**(2): p. 517-28.
114. Perisic, O., H. Xiao, and J.T. Lis, *Stable binding of Drosophila heat shock factor to head-to-head and tail-to-tail repeats of a conserved 5 bp recognition unit.* Cell, 1989. **59**(5): p. 797-806.
115. Xiao, H. and J.T. Lis, *Closely related DNA sequences specify distinct patterns of developmental expression in Drosophila melanogaster.* Mol Cell Biol, 1990. **10**(6): p. 3272-6.
116. Wu, C., *Activating protein factor binds in vitro to upstream control sequences in heat shock gene chromatin.* Nature, 1984. **311**(5981): p. 81-4.
117. Parker, C.S. and J. Topol, *A Drosophila RNA polymerase II transcription factor binds to the regulatory site of an hsp 70 gene.* Cell, 1984. **37**(1): p. 273-83.
118. Nover, L., et al., *Arabidopsis and the heat stress transcription factor world: how many heat stress transcription factors do we need?* Cell Stress Chaperones, 2001. **6**(3): p. 177-89.
119. Wu, C., *Heat shock transcription factors: structure and regulation.* Annu Rev Cell Dev Biol, 1995. **11**: p. 441-69.
120. Clos, J., et al., *Molecular cloning and expression of a hexameric Drosophila heat shock factor subject to negative regulation.* Cell, 1990. **63**(5): p. 1085-97.
121. Sorger, P.K. and H.R. Pelham, *Yeast heat shock factor is an essential DNA-binding protein that exhibits temperature-dependent phosphorylation.* Cell, 1988. **54**(6): p. 855-64.
122. Schuetz, T.J., et al., *Isolation of a cDNA for HSF2: evidence for two heat shock factor genes in humans.* Proc Natl Acad Sci U S A, 1991. **88**(16): p. 6911-5.
123. Rabindran, S.K., et al., *Molecular cloning and expression of a human heat shock factor, HSF1.* Proc Natl Acad Sci U S A, 1991. **88**(16): p. 6906-10.
124. Mathew, A., S.K. Mathur, and R.I. Morimoto, *Heat shock response and protein degradation: regulation of HSF2 by the ubiquitin-proteasome pathway.* Mol Cell Biol, 1998. **18**(9): p. 5091-8.
125. Sistonen, L., et al., *Activation of heat shock factor 2 during hemin-induced differentiation of human erythroleukemia cells.* Mol Cell Biol, 1992. **12**(9): p. 4104-11.
126. Rallu, M., et al., *Function and regulation of heat shock factor 2 during mouse embryogenesis.* Proc Natl Acad Sci U S A, 1997. **94**(6): p. 2392-7.
127. Mezger, V., et al., *Heat shock factor 2-like activity in mouse blastocysts.* Dev Biol, 1994. **166**(2): p. 819-22.
128. Kallio, M., et al., *Brain abnormalities, defective meiotic chromosome synapsis and female subfertility in HSF2 null mice.* EMBO J, 2002. **21**(11): p. 2591-601.
129. Bjork, J.K., et al., *Heat-shock factor 2 is a suppressor of prostate cancer invasion.* Oncogene, 2016. **35**(14): p. 1770-84.
130. Nakai, A. and R.I. Morimoto, *Characterization of a novel chicken heat shock transcription factor, heat shock factor 3, suggests a new regulatory pathway.* Mol Cell Biol, 1993. **13**(4): p. 1983-97.
131. Fujimoto, M., et al., *A novel mouse HSF3 has the potential to activate nonclassical heat-shock genes during heat shock.* Mol Biol Cell, 2010. **21**(1): p. 106-16.
132. Tanabe, M., et al., *Different thresholds in the responses of two heat shock transcription factors, HSF1 and HSF3.* J Biol Chem, 1997. **272**(24): p. 15389-95.
133. Tanabe, M., et al., *Disruption of the HSF3 gene results in the severe reduction of heat shock gene expression and loss of thermotolerance.* EMBO J, 1998. **17**(6): p. 1750-8.
134. Kanei-Ishii, C., et al., *Activation of heat shock transcription factor 3 by c-Myb in the absence of cellular stress.* Science, 1997. **277**(5323): p. 246-8.
135. Nakai, A., et al., *HSF4, a new member of the human heat shock factor family which lacks properties of a transcriptional activator.* Mol Cell Biol, 1997. **17**(1): p. 469-81.
136. Min, J.N., et al., *Unique contribution of heat shock transcription factor 4 in ocular lens development and fiber cell differentiation.* Genesis, 2004. **40**(4): p. 205-17.

137. Fujimoto, M., et al., *Analysis of HSF4 binding regions reveals its necessity for gene regulation during development and heat shock response in mouse lenses.* J Biol Chem, 2008. **283**(44): p. 29961-70.
138. Ahn, S.G., et al., *The loop domain of heat shock transcription factor 1 dictates DNA-binding specificity and responses to heat stress.* Genes Dev, 2001. **15**(16): p. 2134-45.
139. Tessari, A., et al., *Characterization of HSFY, a novel AZFb gene on the Y chromosome with a possible role in human spermatogenesis.* Mol Hum Reprod, 2004. **10**(4): p. 253-8.
140. Shinka, T., et al., *Molecular characterization of heat shock-like factor encoded on the human Y chromosome, and implications for male infertility.* Biol Reprod, 2004. **71**(1): p. 297-306.
141. Sato, Y., et al., *Altered expression pattern of heat shock transcription factor, Y chromosome (HSFY) may be related to altered differentiation of spermatogenic cells in testes with deteriorated spermatogenesis.* Fertil Steril, 2006. **86**(3): p. 612-8.
142. Damberger, F.F., et al., *Solution structure of the DNA-binding domain of the heat shock transcription factor determined by multidimensional heteronuclear magnetic resonance spectroscopy.* Protein Sci, 1994. **3**(10): p. 1806-21.
143. Harrison, C.J., A.A. Bohm, and H.C. Nelson, *Crystal structure of the DNA binding domain of the heat shock transcription factor.* Science, 1994. **263**(5144): p. 224-7.
144. Xiao, H., O. Perisic, and J.T. Lis, *Cooperative binding of Drosophila heat shock factor to arrays of a conserved 5 bp unit.* Cell, 1991. **64**(3): p. 585-93.
145. Chen, Y., et al., *Identification of the C-terminal activator domain in yeast heat shock factor: independent control of transient and sustained transcriptional activity.* EMBO J, 1993. **12**(13): p. 5007-18.
146. Green, M., et al., *A heat shock-responsive domain of human HSF1 that regulates transcription activation domain function.* Mol Cell Biol, 1995. **15**(6): p. 3354-62.
147. Newton, E.M., et al., *The regulatory domain of human heat shock factor 1 is sufficient to sense heat stress.* Mol Cell Biol, 1996. **16**(3): p. 839-46.
148. Lis, J. and C. Wu, *Protein traffic on the heat shock promoter: parking, stalling, and trucking along.* Cell, 1993. **74**(1): p. 1-4.
149. Soncin, F., et al., *Transcriptional activity and DNA binding of heat shock factor-1 involve phosphorylation on threonine 142 by CK2.* Biochem Biophys Res Commun, 2003. **303**(2): p. 700-6.
150. Holmberg, C.I., et al., *Phosphorylation of serine 230 promotes inducible transcriptional activity of heat shock factor 1.* EMBO J, 2001. **20**(14): p. 3800-10.
151. Zhang, Y., et al., *Protein kinase A regulates molecular chaperone transcription and protein aggregation.* PLoS One, 2011. **6**(12): p. e28950.
152. Naidu, S., et al., *Heat Shock Factor 1 is a Substrate for p38 Mitogen-Activated Protein Kinases.* Mol cell biol, 2016.
153. Kim, S.A., et al., *Polo-like kinase 1 phosphorylates heat shock transcription factor 1 and mediates its nuclear translocation during heat stress.* J Biol Chem, 2005. **280**(13): p. 12653-7.
154. Wang, X., et al., *Phosphorylation of HSF1 by MAPK-activated protein kinase 2 on serine 121, inhibits transcriptional activity and promotes HSP90 binding.* J Biol Chem, 2006. **281**(2): p. 782-91.
155. Chu, B., et al., *Transcriptional activity of heat shock factor 1 at 37 degrees C is repressed through phosphorylation on two distinct serine residues by glycogen synthase kinase 3 and protein kinases Calpha and Czeta.* J Biol Chem, 1998. **273**(29): p. 18640-6.
156. Hietakangas, V., et al., *PDSM, a motif for phosphorylation-dependent SUMO modification.* Proc Natl Acad Sci U S A, 2006. **103**(1): p. 45-50.

157. Raychaudhuri, S., et al., *Interplay of acetyltransferase EP300 and the proteasome system in regulating heat shock transcription factor 1.* Cell, 2014. **156**(5): p. 975-85.
158. Dobson, C.M., *Protein folding and misfolding.* Nature, 2003. **426**(6968): p. 884-90.
159. Vacher, C., L. Garcia-Oroz, and D.C. Rubinsztein, *Overexpression of yeast hsp104 reduces polyglutamine aggregation and prolongs survival of a transgenic mouse model of Huntington's disease.* Hum Mol Genet, 2005. **14**(22): p. 3425-33.
160. Arslan, M.A., P. Csermely, and C. Soti, *Protein homeostasis and molecular chaperones in aging.* Biogerontology, 2006. **7**(5-6): p. 383-9.
161. Morimoto, R.I., *Proteotoxic stress and inducible chaperone networks in neurodegenerative disease and aging.* Genes Dev, 2008. **22**(11): p. 1427-38.
162. Urushitani, M., et al., *CHIP promotes proteasomal degradation of familial ALS-linked mutant SOD1 by ubiquitinating Hsp/Hsc70.* J Neurochem, 2004. **90**(1): p. 231-44.
163. Kostenko, S. and U. Moens, *Heat shock protein 27 phosphorylation: kinases, phosphatases, functions and pathology.* Cell Mol Life Sci, 2009. **66**(20): p. 3289-307.
164. Wettstein, G., et al., *Small heat shock proteins and the cytoskeleton: an essential interplay for cell integrity?* Int J Biochem Cell Biol, 2012. **44**(10): p. 1680-6.
165. Garrido, C., et al., *Heat shock protein 27 enhances the tumorigenicity of immunogenic rat colon carcinoma cell clones.* Cancer Res, 1998. **58**(23): p. 5495-9.
166. Kostenko, S., M. Johannessen, and U. Moens, *PKA-induced F-actin rearrangement requires phosphorylation of Hsp27 by the MAPKAP kinase MK5.* Cell Signal, 2009. **21**(5): p. 712-8.
167. Zhang, D., L.L. Wong, and E.S. Koay, *Phosphorylation of Ser78 of Hsp27 correlated with HER-2/neu status and lymph node positivity in breast cancer.* Mol Cancer, 2007. **6**: p. 52.
168. Tsai, J. and M.G. Douglas, *A conserved HPD sequence of the J-domain is necessary for YDJ1 stimulation of Hsp70 ATPase activity at a site distinct from substrate binding.* J Biol Chem, 1996. **271**(16): p. 9347-54.
169. Bukau, B. and A.L. Horwich, *The Hsp70 and Hsp60 chaperone machines.* Cell, 1998. **92**(3): p. 351-66.
170. Fan, C.Y., S. Lee, and D.M. Cyr, *Mechanisms for regulation of Hsp70 function by Hsp40.* Cell Stress Chaperones, 2003. **8**(4): p. 309-16.
171. Szabo, A., et al., *The ATP hydrolysis-dependent reaction cycle of the Escherichia coli Hsp70 system DnaK, DnaJ, and GrpE.* Proc Natl Acad Sci U S A, 1994. **91**(22): p. 10345-9.
172. Rosser, M.F., et al., *Chaperone functions of the E3 ubiquitin ligase CHIP.* J Biol Chem, 2007. **282**(31): p. 22267-77.
173. Akerfelt, M., R.I. Morimoto, and L. Sistonen, *Heat shock factors: integrators of cell stress, development and lifespan.* Nat Rev Mol Cell Biol, 2010. **11**(8): p. 545-55.
174. Garrido, C., et al., *Heat shock proteins 27 and 70: anti-apoptotic proteins with tumorigenic properties.* Cell Cycle, 2006. **5**(22): p. 2592-601.
175. Elsner, L., et al., *The endogenous danger signals HSP70 and MICA cooperate in the activation of cytotoxic effector functions of NK cells.* J Cell Mol Med, 2010. **14**(4): p. 992-1002.
176. Ciocca, D.R. and S.K. Calderwood, *Heat shock proteins in cancer: diagnostic, prognostic, predictive, and treatment implications.* Cell Stress Chaperones, 2005. **10**(2): p. 86-103.
177. Jaattela, M., *Over-expression of hsp70 confers tumorigenicity to mouse fibrosarcoma cells.* Int J Cancer, 1995. **60**(5): p. 689-93.
178. Pratt, W.B., *The role of heat shock proteins in regulating the function, folding, and trafficking of the glucocorticoid receptor.* J Biol Chem, 1993. **268**(29): p. 21455-8.
179. Prodromou, C., et al., *Regulation of Hsp90 ATPase activity by tetratricopeptide repeat (TPR)-domain co-chaperones.* EMBO J, 1999. **18**(3): p. 754-62.

180. Panaretou, B., et al., *Activation of the ATPase activity of hsp90 by the stress-regulated cochaperone aha1.* Mol Cell, 2002. **10**(6): p. 1307-18.
181. Schwartzberg, P.L., *The many faces of Src: multiple functions of a prototypical tyrosine kinase.* Oncogene, 1998. **17**(11 Reviews): p. 1463-8.
182. Miyata, Y. and E. Nishida, *Distantly related cousins of MAP kinase: biochemical properties and possible physiological functions.* Biochem Biophys Res Commun, 1999. **266**(2): p. 291-5.
183. Malumbres, M. and M. Barbacid, *Mammalian cyclin-dependent kinases.* Trends Biochem Sci, 2005. **30**(11): p. 630-41.
184. Lin, Y., T.R. Hupp, and C. Stevens, *Death-associated protein kinase (DAPK) and signal transduction: additional roles beyond cell death.* FEBS J, 2010. **277**(1): p. 48-57.
185. Holt, S.E., et al., *Functional requirement of p23 and Hsp90 in telomerase complexes.* Genes Dev, 1999. **13**(7): p. 817-26.
186. Sarkar, S., et al., *Oxidative inhibition of Hsp90 disrupts the super-chaperone complex and attenuates pancreatic adenocarcinoma in vitro and in vivo.* Int J Cancer, 2013. **132**(3): p. 695-706.
187. Xu, W. and L. Neckers, *Targeting the molecular chaperone heat shock protein 90 provides a multifaceted effect on diverse cell signaling pathways of cancer cells.* Clin Cancer Res, 2007. **13**(6): p. 1625-9.
188. Chaudhury, S., T.R. Welch, and B.S. Blagg, *Hsp90 as a target for drug development.* ChemMedChem, 2006. **1**(12): p. 1331-40.
189. Morimoto, R.I., *Regulation of the heat shock transcriptional response: cross talk between a family of heat shock factors, molecular chaperones, and negative regulators.* Genes Dev, 1998. **12**(24): p. 3788-96.
190. Ananthan, J., A.L. Goldberg, and R. Voellmy, *Abnormal proteins serve as eukaryotic stress signals and trigger the activation of heat shock genes.* Science, 1986. **232**(4749): p. 522-4.
191. Xie, Y., et al., *Heat shock factor 1 represses transcription of the IL-1beta gene through physical interaction with the nuclear factor of interleukin 6.* J Biol Chem, 2002. **277**(14): p. 11802-10.
192. Koizumi, S., et al., *Cadmium-responsive element of the human heme oxygenase-1 gene mediates heat shock factor 1-dependent transcriptional activation.* J Biol Chem, 2007. **282**(12): p. 8715-23.
193. Franceschelli, S., et al., *Bag3 gene expression is regulated by heat shock factor 1.* J Cell Physiol, 2008. **215**(3): p. 575-7.
194. Michel, D., et al., *Stress-induced transcription of the clusterin/apoJ gene.* Biochem J, 1997. **328 (Pt 1)**: p. 45-50.
195. Fu, Q., et al., *Involvement of heat shock factor 1 in statin-induced transcriptional upregulation of endothelial thrombomodulin.* Circ Res, 2008. **103**(4): p. 369-77.
196. Zhao, R., X. Ma, and G.X. Shen, *Transcriptional regulation of plasminogen activator inhibitor-1 in vascular endothelial cells induced by oxidized very low density lipoproteins.* Mol Cell Biochem, 2008. **317**(1-2): p. 197-204.
197. Mendillo, M.L., et al., *HSF1 drives a transcriptional program distinct from heat shock to support highly malignant human cancers.* Cell, 2012. **150**(3): p. 549-62.
198. Zhao, Y.H., et al., *Upregulation of lactate dehydrogenase A by ErbB2 through heat shock factor 1 promotes breast cancer cell glycolysis and growth.* Oncogene, 2009. **28**(42): p. 3689-701.
199. Stanhill, A., et al., *Ha-ras(val12) induces HSP70b transcription via the HSE/HSF1 system, but HSP70b expression is suppressed in Ha-ras(val12)-transformed cells.* Oncogene, 2006. **25**(10): p. 1485-95.
200. Gagliano, N., F. Grizzi, and G. Annoni, *Mechanisms of aging and liver functions.* Dig Dis, 2007. **25**(2): p. 118-23.

201. Sherman, M.Y. and A.L. Goldberg, *Cellular defenses against unfolded proteins: a cell biologist thinks about neurodegenerative diseases.* Neuron, 2001. **29**(1): p. 15-32.
202. Kayani, A.C., J.P. Morton, and A. McArdle, *The exercise-induced stress response in skeletal muscle: failure during aging.* Appl Physiol Nutr Metab, 2008. **33**(5): p. 1033-41.
203. Morley, J.F. and R.I. Morimoto, *Regulation of longevity in Caenorhabditis elegans by heat shock factor and molecular chaperones.* Mol Biol Cell, 2004. **15**(2): p. 657-64.
204. Steele, A.D., et al., *Heat shock factor 1 regulates lifespan as distinct from disease onset in prion disease.* Proc Natl Acad Sci U S A, 2008. **105**(36): p. 13626-31.
205. Vasilaki, A., M.J. Jackson, and A. McArdle, *Attenuated HSP70 response in skeletal muscle of aged rats following contractile activity.* Muscle Nerve, 2002. **25**(6): p. 902-5.
206. Vasilaki, A., et al., *Adaptive responses of mouse skeletal muscle to contractile activity: The effect of age.* Mech Ageing Dev, 2006. **127**(11): p. 830-9.
207. Dai, C., et al., *Heat shock factor 1 is a powerful multifaceted modifier of carcinogenesis.* Cell, 2007. **130**(6): p. 1005-18.
208. Whitesell, L. and S.L. Lindquist, *HSP90 and the chaperoning of cancer.* Nat Rev Cancer, 2005. **5**(10): p. 761-72.
209. Volloch, V.Z. and M.Y. Sherman, *Oncogenic potential of Hsp72.* Oncogene, 1999. **18**(24): p. 3648-51.
210. Guo, F., et al., *Mechanistic role of heat shock protein 70 in Bcr-Abl-mediated resistance to apoptosis in human acute leukemia cells.* Blood, 2005. **105**(3): p. 1246-55.
211. Teng, Y., et al., *HSP90 and HSP70 proteins are essential for stabilization and activation of WASF3 metastasis-promoting protein.* J Biol Chem, 2012. **287**(13): p. 10051-9.
212. Fang, F., R. Chang, and L. Yang, *Heat shock factor 1 promotes invasion and metastasis of hepatocellular carcinoma in vitro and in vivo.* Cancer, 2012. **118**(7): p. 1782-94.
213. Boroughs, L.K., et al., *A unique role for heat shock protein 70 and its binding partner tissue transglutaminase in cancer cell migration.* J Biol Chem, 2011. **286**(43): p. 37094-107.
214. Nakamura, Y., et al., *Heat shock factor 1 is required for migration and invasion of human melanoma in vitro and in vivo.* Cancer Lett, 2014. **354**(2): p. 329-35.
215. Hoang, A.T., et al., *A novel association between the human heat shock transcription factor 1 (HSF1) and prostate adenocarcinoma.* Am J Pathol, 2000. **156**(3): p. 857-64.
216. Tang, D., et al., *Expression of heat shock proteins and heat shock protein messenger ribonucleic acid in human prostate carcinoma in vitro and in tumors in vivo.* Cell Stress Chaperones, 2005. **10**(1): p. 46-58.
217. Syrigos, K.N., et al., *Clinical significance of heat shock protein-70 expression in bladder cancer.* Urology, 2003. **61**(3): p. 677-80.
218. Jin, X., D. Moskophidis, and N.F. Mivechi, *Heat shock transcription factor 1 is a key determinant of HCC development by regulating hepatic steatosis and metabolic syndrome.* Cell Metab, 2011. **14**(1): p. 91-103.
219. Min, J.N., et al., *Selective suppression of lymphomas by functional loss of Hsf1 in a p53-deficient mouse model for spontaneous tumors.* Oncogene, 2007. **26**(35): p. 5086-97.
220. Dai, C., et al., *Loss of tumor suppressor NF1 activates HSF1 to promote carcinogenesis.* J Clin Invest, 2012. **122**(10): p. 3742-54.
221. Meng, L., V.L. Gabai, and M.Y. Sherman, *Heat-shock transcription factor HSF1 has a critical role in human epidermal growth factor receptor-2-induced cellular transformation and tumorigenesis.* Oncogene, 2010. **29**(37): p. 5204-13.
222. Wang, B., et al., *Heat shock factor 1 induces cancer stem cell phenotype in breast cancer cell lines.* Breast Cancer Res Treat, 2015. **153**(1): p. 57-66.

223. Chen, Y.F., et al., *Nucleoside analog inhibits microRNA-214 through targeting heat-shock factor 1 in human epithelial ovarian cancer.* Cancer Sci, 2013. **104**(12): p. 1683-9.
224. Siegel, R., D. Naishadham, and A. Jemal, *Cancer statistics, 2013.* Ca-a Cancer Journal for Clinicians, 2013. **63**(1): p. 11-30.
225. Cannistra, S.A., *Cancer of the ovary.* N Engl J Med, 2004. **351**(24): p. 2519-29.
226. Massague, J., *TGFbeta in Cancer.* Cell, 2008. **134**(2): p. 215-30.
227. Zavadil, J. and E.P. Bottinger, *TGF-beta and epithelial-to-mesenchymal transitions.* Oncogene, 2005. **24**(37): p. 5764-74.
228. Moustakas, A. and C.H. Heldin, *Signaling networks guiding epithelial-mesenchymal transitions during embryogenesis and cancer progression.* Cancer Sci, 2007. **98**(10): p. 1512-20.
229. Kunz-Schughart, L.A., M. Kreutz, and R. Knuechel, *Multicellular spheroids: a three-dimensional in vitro culture system to study tumour biology.* International Journal of Experimental Pathology, 1998. **79**(1): p. 1-23.
230. Casey, R.C., et al., *Beta 1-integrins regulate the formation and adhesion of ovarian carcinoma multicellular spheroids.* Am J Pathol, 2001. **159**(6): p. 2071-80.
231. Zhang, S., et al., *Identification and characterization of ovarian cancer-initiating cells from primary human tumors.* Cancer Research, 2008. **68**(11): p. 4311-4320.
232. Korch, C., et al., *DNA profiling analysis of endometrial and ovarian cell lines reveals misidentification, redundancy and contamination.* Gynecol Oncol, 2012. **127**(1): p. 241-8.
233. Nikitin, A., et al., *Pathway studio--the analysis and navigation of molecular networks.* Bioinformatics, 2003. **19**(16): p. 2155-7.
234. Langlois, V.S. and C.J. Martyniuk, *Genome wide analysis of Silurana (Xenopus) tropicalis development reveals dynamic expression using network enrichment analysis.* Mech Dev, 2013. **130**(4-5): p. 304-22.
235. Kelm, J.M., et al., *Method for generation of homogeneous multicellular tumor spheroids applicable to a wide variety of cell types.* Biotechnol Bioeng, 2003. **83**(2): p. 173-80.
236. Penning, T.M., *The aldo-keto reductases (AKRs): Overview.* Chem Biol Interact, 2015. **234**: p. 236-46.
237. Deng, H.B., et al., *Increased expression of dihydrodiol dehydrogenase induces resistance to cisplatin in human ovarian carcinoma cells.* J Biol Chem, 2002. **277**(17): p. 15035-43.
238. Wahlberg, P., et al., *Expression and localization of the serine proteases high-temperature requirement factor A1, serine protease 23, and serine protease 35 in the mouse ovary.* Endocrinology, 2008. **149**(10): p. 5070-7.
239. Lu, P., et al., *Extracellular matrix degradation and remodeling in development and disease.* Cold Spring Harb Perspect Biol, 2011. **3**(12).
240. Leone, V., et al., *The cl2/dro1/ccdc80 null mice develop thyroid and ovarian neoplasias.* Cancer Lett, 2015. **357**(2): p. 535-41.
241. Ferraro, A., et al., *Tumor suppressor role of the CL2/DRO1/CCDC80 gene in thyroid carcinogenesis.* J Clin Endocrinol Metab, 2013. **98**(7): p. 2834-43.
242. Proud, C.G., *mTOR-mediated regulation of translation factors by amino acids.* Biochem Biophys Res Commun, 2004. **313**(2): p. 429-36.
243. Xu, K., P. Liu, and W. Wei, *mTOR signaling in tumorigenesis.* Biochim Biophys Acta, 2014. **1846**(2): p. 638-54.
244. Cheung, A., et al., *Targeting folate receptor alpha for cancer treatment.* Oncotarget, 2016.
245. Harjes, U., J. Kalucka, and P. Carmeliet, *Targeting fatty acid metabolism in cancer and endothelial cells.* Crit Rev Oncol Hematol, 2016. **97**: p. 15-21.
246. dos Santos, C.R., et al., *LDL-cholesterol signaling induces breast cancer proliferation and invasion.* Lipids Health Dis, 2014. **13**: p. 16.

247. Dolcet, X., et al., *NF-kB in development and progression of human cancer.* Virchows Arch, 2005. **446**(5): p. 475-82.
248. Zimmerman, R. and P. Cerutti, *Active oxygen acts as a promoter of transformation in mouse embryo C3H/10T1/2/C18 fibroblasts.* Proc Natl Acad Sci U S A, 1984. **81**(7): p. 2085-7.
249. Beckman, K.B. and B.N. Ames, *Oxidative decay of DNA.* J Biol Chem, 1997. **272**(32): p. 19633-6.
250. Barrera, G., *Oxidative stress and lipid peroxidation products in cancer progression and therapy.* ISRN Oncol, 2012. **2012**: p. 137289.
251. Nguyen, T., P. Nioi, and C.B. Pickett, *The Nrf2-antioxidant response element signaling pathway and its activation by oxidative stress.* J Biol Chem, 2009. **284**(20): p. 13291-5.
252. Wiemer, E.A., *Stressed tumor cell, chemosensitized cancer.* Nat Med, 2011. **17**(12): p. 1552-4.
253. Protti, M.P., et al., *Constitutive expression of the heat shock protein 72 kDa in human melanoma cells.* Cancer Lett, 1994. **85**(2): p. 211-6.
254. Maehara, Y., et al., *Overexpression of the heat shock protein HSP70 family and p53 protein and prognosis for patients with gastric cancer.* Oncology, 2000. **58**(2): p. 144-51.
255. Hatfield, M.P. and S. Lovas, *Role of Hsp70 in cancer growth and survival.* Protein Pept Lett, 2012. **19**(6): p. 616-24.
256. Ciocca, D.R., et al., *Heat shock protein hsp70 in patients with axillary lymph node-negative breast cancer: prognostic implications.* J Natl Cancer Inst, 1993. **85**(7): p. 570-4.
257. Chant, I.D., P.E. Rose, and A.G. Morris, *Analysis of heat-shock protein expression in myeloid leukaemia cells by flow cytometry.* Br J Haematol, 1995. **90**(1): p. 163-8.
258. Jameel, A., et al., *Clinical and biological significance of HSP89 alpha in human breast cancer.* Int J Cancer, 1992. **50**(3): p. 409-15.
259. Nanbu, K., et al., *Prognostic significance of heat shock proteins HSP70 and HSP90 in endometrial carcinomas.* Cancer Detect Prev, 1998. **22**(6): p. 549-55.
260. Trieb, K., et al., *Antibodies to heat shock protein 90 in osteosarcoma patients correlate with response to neoadjuvant chemotherapy.* Br J Cancer, 2000. **82**(1): p. 85-7.
261. Pavan, S., et al., *HSP27 is required for invasion and metastasis triggered by hepatocyte growth factor.* Int J Cancer, 2014. **134**(6): p. 1289-99.
262. Gagou, M.E., et al., *Human PIF1 helicase supports DNA replication and cell growth under oncogenic-stress.* Oncotarget, 2014. **5**(22): p. 11381-98.
263. Grassi, M.L., et al., *Proteomic analysis of ovarian cancer cells during epithelial-mesenchymal transition (EMT) induced by epidermal growth factor (EGF) reveals mechanisms of cell cycle control.* J Proteomics, 2016.
264. Wang, K., D. Li, and L. Sun, *High levels of EGFR expression in tumor stroma are associated with aggressive clinical features in epithelial ovarian cancer.* Onco Targets Ther, 2016. **9**: p. 377-86.
265. Milde-Langosch, K., *The Fos family of transcription factors and their role in tumourigenesis.* Eur J Cancer, 2005. **41**(16): p. 2449-61.
266. Koensgen, D., et al., *Polymorphism of the IL-8 gene and the risk of ovarian cancer.* Cytokine, 2015. **71**(2): p. 334-8.
267. Wang, Y., et al., *Interleukin-8 secretion by ovarian cancer cells increases anchorage-independent growth, proliferation, angiogenic potential, adhesion and invasion.* Cytokine, 2012. **59**(1): p. 145-55.
268. Shahzad, M.M., et al., *Stress effects on FosB- and interleukin-8 (IL8)-driven ovarian cancer growth and metastasis.* J Biol Chem, 2010. **285**(46): p. 35462-70.
269. Olive, P.L. and R.E. Durand, *Drug and radiation resistance in spheroids: cell contact and kinetics.* Cancer Metastasis Rev, 1994. **13**(2): p. 121-38.
270. Akhavan-Niaki, H. and A.A. Samadani, *DNA methylation and cancer development: molecular mechanism.* Cell Biochem Biophys, 2013. **67**(2): p. 501-13.

271. Torres, M.P., et al., *Immunopathogenesis of ovarian cancer.* Minerva Med, 2009. **100**(5): p. 385-400.
272. Jemal, A., et al., *Cancer statistics, 2002.* CA Cancer J Clin, 2002. **52**(1): p. 23-47.
273. Cannistra, S.A., *Is there a "best" choice of second-line agent in the treatment of recurrent, potentially platinum-sensitive ovarian cancer?* J Clin Oncol, 2002. **20**(5): p. 1158-60.
274. Kelland, L., *The resurgence of platinum-based cancer chemotherapy.* Nat Rev Cancer, 2007. **7**(8): p. 573-84.
275. Westerheide, S.D. and R.I. Morimoto, *Heat shock response modulators as therapeutic tools for diseases of protein conformation.* The Journal of biological chemistry, 2005. **280**(39): p. 33097-100.
276. Hartl, F.U., *Molecular chaperones in cellular protein folding.* Nature, 1996. **381**(6583): p. 571-9.
277. Moreno-Bueno, G., et al., *The morphological and molecular features of the epithelial-to-mesenchymal transition.* Nat Protoc, 2009. **4**(11): p. 1591-613.
278. Xu, J., S. Lamouille, and R. Derynck, *TGF-beta-induced epithelial to mesenchymal transition.* Cell Res, 2009. **19**(2): p. 156-72.
279. Cerami, E., et al., *The cBio cancer genomics portal: an open platform for exploring multidimensional cancer genomics data.* Cancer Discov, 2012. **2**(5): p. 401-4.
280. Gao, J., et al., *Integrative analysis of complex cancer genomics and clinical profiles using the cBioPortal.* Sci Signal, 2013. **6**(269): p. pl1.
281. Olson, A., et al., *RNAi Codex: a portal/database for short-hairpin RNA (shRNA) gene-silencing constructs.* Nucleic Acids Res, 2006. **34**(Database issue): p. D153-7.
282. Geback, T., et al., *TScratch: a novel and simple software tool for automated analysis of monolayer wound healing assays.* Biotechniques, 2009. **46**(4): p. 265-74.
283. Timmins, N.E. and L.K. Nielsen, *Generation of multicellular tumor spheroids by the hanging-drop method.* Methods in molecular medicine, 2007. **140**: p. 141-51.
284. Holmberg, C.I., et al., *Multisite phosphorylation provides sophisticated regulation of transcription factors.* Trends Biochem Sci, 2002. **27**(12): p. 619-27.
285. O'Callaghan-Sunol, C. and M.Y. Sherman, *Heat shock transcription factor (HSF1) plays a critical role in cell migration via maintaining MAP kinase signaling.* Cell Cycle, 2006. **5**(13): p. 1431-1437.
286. Li, Y., et al., *MicroRNA-135b, a HSF1 target, promotes tumor invasion and metastasis by regulating RECK and EVI5 in hepatocellular carcinoma.* Oncotarget, 2015. **6**(4): p. 2421-33.
287. Schilling, D., et al., *Sensitizing tumor cells to radiation by targeting the heat shock response.* Cancer Lett, 2015. **360**(2): p. 294-301.
288. Toma-Jonik, A., et al., *Active heat shock transcription factor 1 supports migration of the melanoma cells via vinculin down-regulation.* Cell Signal, 2015. **27**(2): p. 394-401.
289. Carpenter, R.L., et al., *Akt phosphorylates and activates HSF-1 independent of heat shock, leading to Slug overexpression and epithelial-mesenchymal transition (EMT) of HER2-overexpressing breast cancer cells.* Oncogene, 2014.
290. Xi, C., et al., *Heat shock factor Hsf1 cooperates with ErbB2 (Her2/Neu) protein to promote mammary tumorigenesis and metastasis.* J Biol Chem, 2012. **287**(42): p. 35646-57.
291. Kroeger, P.E. and R.I. Morimoto, *Selection of new HSF1 and HSF2 DNA-binding sites reveals difference in trimer cooperativity.* Mol Cell Biol, 1994. **14**(11): p. 7592-603.
292. Neshat, M.S., et al., *Enhanced sensitivity of PTEN-deficient tumors to inhibition of FRAP/mTOR.* Proc Natl Acad Sci U S A, 2001. **98**(18): p. 10314-9.
293. Markert, S., et al., *Alpha-folate receptor expression in epithelial ovarian carcinoma and non-neoplastic ovarian tissue.* Anticancer Res, 2008. **28**(6A): p. 3567-72.
294. Walters, C.L., et al., *Folate and folate receptor alpha antagonists mechanism of action in ovarian cancer.* Gynecol Oncol, 2013. **131**(2): p. 493-8.

295. Ayhan, A., et al., *Ascites and epithelial ovarian cancers: a reappraisal with respect to different aspects.* Int J Gynecol Cancer, 2007. **17**(1): p. 68-75.
296. Pratt, W.B., et al., *Role of hsp90 and the hsp90-binding immunophilins in signalling protein movement.* Cell Signal, 2004. **16**(8): p. 857-72.
297. Neckers, L. and S.P. Ivy, *Heat shock protein 90.* Curr Opin Oncol, 2003. **15**(6): p. 419-24.
298. Wei, Y.Q., et al., *Inhibition of proliferation and induction of apoptosis by abrogation of heat-shock protein (HSP) 70 expression in tumor cells.* Cancer Immunol Immunother, 1995. **40**(2): p. 73-8.
299. Jaattela, M., et al., *Hsp70 exerts its anti-apoptotic function downstream of caspase-3-like proteases.* EMBO J, 1998. **17**(21): p. 6124-34.
300. Banerji, U., *Heat shock protein 90 as a drug target: some like it hot.* Clin Cancer Res, 2009. **15**(1): p. 9-14.
301. Li, Y., et al., *New developments in Hsp90 inhibitors as anti-cancer therapeutics: mechanisms, clinical perspective and more potential.* Drug Resist Updat, 2009. **12**(1-2): p. 17-27.
302. Whitesell, L., et al., *Inhibition of heat shock protein HSP90-pp60v-src heteroprotein complex formation by benzoquinone ansamycins: essential role for stress proteins in oncogenic transformation.* Proc Natl Acad Sci U S A, 1994. **91**(18): p. 8324-8.
303. Neckers, L. and P. Workman, *Hsp90 Molecular Chaperone Inhibitors: Are We There Yet?* Clinical Cancer Research, 2012. **18**(1): p. 64-76.
304. Workman, P., *Combinatorial attack on multistep oncogenesis by inhibiting the Hsp90 molecular chaperone.* Cancer Lett, 2004. **206**(2): p. 149-57.
305. Solit, D.B. and G. Chiosis, *Development and application of Hsp90 inhibitors.* Drug Discov Today, 2008. **13**(1-2): p. 38-43.
306. Ying, W., et al., *Ganetespib, a unique triazolone-containing Hsp90 inhibitor, exhibits potent antitumor activity and a superior safety profile for cancer therapy.* Mol Cancer Ther, 2012. **11**(2): p. 475-84.
307. Goldman, J.W., et al., *A phase I dose-escalation study of the Hsp90 inhibitor STA-9090 administered once weekly in patients with solid tumors.* Journal of Clinical Oncology, 2010. **28**(15).
308. Lancet, J.E., et al., *A Phase I/II Trial of the Potent Hsp90 Inhibitor STA-9090 Administered Once Weekly In Patients with Advanced Hematologic Malignancies.* Blood, 2010. **116**(21): p. 1349-1350.
309. Wong, K., et al., *An open-label phase II study of the Hsp90 inhibitor ganetespib (STA-9090) as monotherapy in patients with advanced non-small cell lung cancer (NSCLC).* Journal of Clinical Oncology, 2011. **29**(15).
310. Demetri, G.D., et al., *An open-label phase II study of the Hsp90 inhibitor ganetespib (STA-9090) in patients (pts) with metastatic and/or unresectable GIST.* Journal of Clinical Oncology, 2011. **29**(15).
311. Modi, S., et al., *HSP90 Inhibition Is Effective in Breast Cancer: A Phase II Trial of Tanespimycin (17-AAG) Plus Trastuzumab in Patients with HER2-Positive Metastatic Breast Cancer Progressing on Trastuzumab.* Clinical Cancer Research, 2011. **17**(15): p. 5132-5139.
312. Liu, H., et al., *Network analysis identifies an HSP90-central hub susceptible in ovarian cancer.* Clin Cancer Res, 2013. **19**(18): p. 5053-67.
313. Westerheide, S.D., et al., *Celastrols as inducers of the heat shock response and cytoprotection.* Journal of Biological Chemistry, 2004. **279**(53): p. 56053-56060.
314. Zhang, T., et al., *Characterization of celastrol to inhibit hsp90 and cdc37 interaction.* J Biol Chem, 2009. **284**(51): p. 35381-9.

315. Kiaei, M., et al., *Celastrol Blocks Neuronal Cell Death and Extends Life in Transgenic Mouse Model of Amyotrophic Lateral Sclerosis.* Neurodegenerative Diseases, 2005. **2**(5): p. 246-254.
316. Faust, K., et al., *Neuroprotective effects of compounds with antioxidant and anti-inflammatory properties in a Drosophila model of Parkinson's disease.* Bmc Neuroscience, 2009. **10**.
317. Li, H., et al., *miR-224 is critical for celastrol-induced inhibition of migration and invasion of hepatocellular carcinoma cells.* Cell Physiol Biochem, 2013. **32**(2): p. 448-58.
318. Chakravarthy, R., et al., *Role of the eIF4E binding protein 4E-BP1 in regulation of the sensitivity of human pancreatic cancer cells to TRAIL and celastrol-induced apoptosis.* Biol Cell, 2013. **105**(9): p. 414-29.
319. Ge, P., et al., *Celastrol causes apoptosis and cell cycle arrest in rat glioma cells.* Neurol Res, 2010. **32**(1): p. 94-100.
320. Peng, B., et al., *Peptide deformylase inhibitor actinonin reduces celastrol's HSP70 induction while synergizing proliferation inhibition in tumor cells.* Bmc Cancer, 2014. **14**.
321. Xu, Y., et al., *Antitumor activity of actinonin in vitro and in vivo.* Clin Cancer Res, 1998. **4**(1): p. 171-6.
322. Wang, Y. and S.R. McAlpine, *N-terminal and C-terminal modulation of Hsp90 produce dissimilar phenotypes.* Chem Commun (Camb), 2015. **51**(8): p. 1410-3.
323. Wang, Y. and S.R. McAlpine, *Combining an Hsp70 inhibitor with either an N- or C-terminal Hsp90 inhibitor produces mechanistically distinct phenotypes.* Org Biomol Chem, 2015. **13**(12): p. 3691-8.
324. Wang, Y. and S.R. McAlpine, *Regulating the cytoprotective response in cancer cells using simultaneous inhibition of Hsp90 and Hsp70.* Org Biomol Chem, 2015. **13**(7): p. 2108-16.
325. Matthews, S.B., et al., *Characterization of a novel novobiocin analogue as a putative C-terminal inhibitor of heat shock protein 90 in prostate cancer cells.* Prostate, 2010. **70**(1): p. 27-36.
326. Eskew, J.D., et al., *Development and characterization of a novel C-terminal inhibitor of Hsp90 in androgen dependent and independent prostate cancer cells.* BMC Cancer, 2011. **11**: p. 468.
327. Armstrong, H.K., et al., *A Novel Class of Hsp90 C-Terminal Modulators Have Pre-Clinical Efficacy in Prostate Tumor Cells Without Induction of a Heat Shock Response.* Prostate, 2016. **76**(16): p. 1546-1559.
328. Zhang, B., Z. Duan, and Y. Zhao, *Mouse models with human immunity and their application in biomedical research.* J Cell Mol Med, 2009. **13**(6): p. 1043-58.
329. Weroha, S.J., et al., *Tumorgrafts as in vivo surrogates for women with ovarian cancer.* Clin Cancer Res, 2014. **20**(5): p. 1288-97.
330. Dobbin, Z.C., et al., *Using heterogeneity of the patient-derived xenograft model to identify the chemoresistant population in ovarian cancer.* Oncotarget, 2014. **5**(18): p. 8750-64.
331. Press, J.Z., et al., *Xenografts of primary human gynecological tumors grown under the renal capsule of NOD/SCID mice show genetic stability during serial transplantation and respond to cytotoxic chemotherapy.* Gynecol Oncol, 2008. **110**(2): p. 256-64.
332. Bankert, R.B., et al., *Humanized mouse model of ovarian cancer recapitulates patient solid tumor progression, ascites formation, and metastasis.* PLoS One, 2011. **6**(9): p. e24420.
333. Williams, S.A., et al., *Patient-derived xenografts, the cancer stem cell paradigm, and cancer pathobiology in the 21st century.* Lab Invest, 2013. **93**(9): p. 970-82.

APPENDICES

Appendix A: Protocols

Counting and Passaging Cells

1. Warm complete media and Trypsin in 37°C water bath for 30 minutes and prepare hood
2. Tilt plate and aspirate off media without touching the bottom of the plate
3. Add 1X PBS[1] to plate and rock gently
4. Aspirate off 1X PBS
5. Add trypsin[2] to plate, rock gently, and place into 37°C incubator for 5 minutes
6. After 5 minutes, check cells under microscope to ensure they have completely rounded and are no longer adhered to the plate
7. If cells are still adhered to the plate, place back in the incubator for 2 minutes
8. Add media[3] to plate to inactivate trypsin
9. Pipette up and down to break up cell clusters
10. Add 50 µL of cells and 50 µL of trypan blue dye to a 1.5 mL microcentrifuge tube
11. Pipette 10 µL of cell mixture to a hemocytometer slide
12. Under the microscope, count 2 boxes of 4x4 squares (Fig. A1)
    a. If total of two boxes is 103, then cell count is 1.03 x 10^6 cells/mL
13. Calculate the appropriate dilution to reach the desired cell concentration
    a. Usually dilute to 75,000 cells per mL
    b. I.E. (5 mL cells / total number cells counted * 75,000 cells)
14. Pipette the applicable cell and media volumes into the desired plate size

Table A1. Solution Volumes for Passaging

Solution	35mm Plate	60mm Plate
PBS[1]	5mL	10mL
Trypsin[2]	500µL	1000µL
Media[3]	5mL	10mL

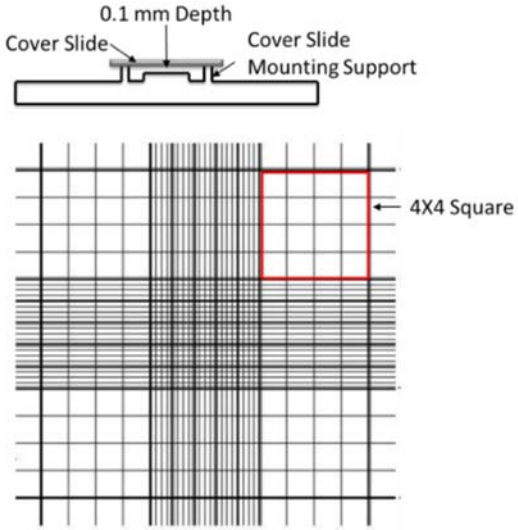

Figure A1. Cell Counting with Hemacytometer

Collecting Cells

1. Warm complete media and Trypsin in 37°C water bath for 30 minutes and prepare hood
2. Tilt plate and aspirate off media without touching the bottom of the plate
3. Add 1X PBS[1] to plate and rock gently
4. Aspirate off 1X PBS
5. Add trypsin[2] to plate, rock gently, and place into 37°C incubator for 5 minutes
6. After 5 minutes, check cells under microscope to ensure they have completely rounded and are no longer adhered to the plate
7. If cells are still adhered to the plate, place back in the incubator for 2 minutes
8. Add media[3] to plate to inactivate trypsin
9. Pipette up and down to break up cell clusters
10. Collect all identical sample sets into a single conical
11. Spin down conical at 1200 rpm for 2 minutes
12. Aspirate off media, leaving the cell pellet remaining
13. Resuspend cell pellet in 500 µL of 1X PBS
14. Transfer cell solution to a new 1.5 mL microcentrifuge tube
15. Centrifuge for 5 minutes at 1200 rpm
16. Apirate off 1X PBS and use immediately or freeze at -80°C for future use

Creating spheroids treated with TGFβ

1. Warm complete media and Trypsin in 37ºC water bath for 30 minutes and prepare hood
2. Wash cells in 60 mm plate with 10 mL 1X PBS and aspirate off
3. Add 1000 µL trypsin and place in 37ºC incubator for 5 minutes
4. Suspend un-adhered cells in 5mL complete media
5. Place in 15 mL conical
6. Spin down at 1000 RPM for 2 minutes
7. Aspirate off media and leave the cell pellet
8. Resuspend in 4 mL complete media
9. Count cells with typan blue via the hemacytometer as described above
10. Dilute cells to concentration of $1x10^6$ cells per mL place in boat
11. Take TGFβ from -80ºC
12. Add 20µl of TGFβ in 4mL media (5µl per mL) directly to cells in boat
13. Prepare untreated 100 mm petri dishes by adding 5 mL 1X PBS to bottom
14. Set multichannel pipette to 20µl
15. Push down pipette to second stop, pull up completely, dispense only 20µl (first stop)
16. Gently rock boat periodically for settlement
17. Flipping right side up, place the lid onto the bottom of the plate
18. Incubate at 37ºC for 72 hours to allow for aggregation

Collecting Spheroids

1. Keep cells on ice during collection
2. Utilizing a 10 mL pipette, tilt plate lid, add 5 mL of chilled 1X PBS to the top cell drop, and allow the subsequent drops to collect at the bottom of the lid
3. Repeat for each row of cell drops
4. Pipette spheroids from the plate into a 15 mL conical
5. Allow spheroids to settle at the bottom of the tube
6. Avoiding the collected spheroids, pipette approximately 4mL of the 1X PBS from conical and repeat procedure for remaining plates
7. Spin down conical at 1000 RPM for 5 minutes
8. Aspirate off 1X PBS without disturbing cell pellet
9. Add 1000 µL 1X PBS to transfer to a 1.5 mL microcentrifuge tube
10. Centrifuge at 1000 RPM for 5 minutes
11. Aspirate 1X PBS, leaving a cell pellet
12. Use immediately or store in -80ºC for further experimentation

RNA extraction and sample processing for Affymetrix 3'IVT Expression System

1. Extract RNA from sample cell pellets according to Qiagen's RNeasy Mini Kit
2. Verify RNA integrity with The Agilent 2100 Bioanalyzer
3. Convert RNA to cDNA and amplify/label with biotin using Affymetrix 3'IVT Expression System
4. Complete the following steps according to Affymetrix technical manual:
    a. Hybridization with the biotin-labeled RNA
    b. Staining
    c. Scanning of chips
5. Normalize data with Affymetrix Expression Console v1.3.1
6. Utilize Pathway Studio 9.0 and ResNEt 10.0 for sub-network enrichment analysis of cell processes

Reverse transcription reaction

1. Make mastermix in 1.5 mL microcentrifuge tube

Table A2. Reagent Volumes for Reverse Transcription Mastermix

Reagent	1 rxn	5.5 rxn	10.5 rxn
10X RT Buffer	2.0	11.0	21.0
25X dNTPs	0.8	4.4	8.4
10X RT Random Primers	2.0	11.0	21.0
RT Enzyme	1.0	5.5	10.5
dH2O	4.2	23.1	44.1
Total	**10 µL**	**55 µL**	**105 µL**

2. Vortex and short spin
3. Transfer 10 µL of mastermix to 0.1 mL tubes
4. Add 10 µL of RNA solution to the 0.1 mL tubes
    a. If necessary, dilute RNA with dH_2O so it does not exceed 2 µg
5. Vortex and short spin
6. Run in thermocycler machine with the following conditions

Table A3. Temperature Conditions for Reverse Transcription Reaction

Temperature	Time (min)
25°C	10
37°C	120
85°C	5

Real-Time Quantitative PCR with SYBR Green

1. Set computer cycle parameters

Table A4. Temperature Conditions for RT-qPCR

Temperature	Time (seconds)	
95°C	45	
95°C	3	X 35-45 cycles
55-60°C	30	

2. Made a working stock of 50 ng/µL template cDNA
3. Add 1 µL of template DNA to wells in vertical triplicate sets
4. Create master mix in a 1.5 mL microcentrifuge tube

Table A5. Reagent Volumes for RT-qPCR Mastermix

Reagent	1 rxn (1 well)	3.3 rxn (3 wells)
SYBR green + ROX	10.0	33.0
Forward Primer	0.2	0.66
Reverse Primer	0.2	0.66
dIH$_2$O	8.6	29.38
Total	**20 mL**	**66 mL**

5. Vortex and short spin
6. Transfer 19 µL of master mix to subsequent wells
7. Cover and seal plate with adhesive and short spin
8. Place plate in RT-qPCR machine and start run
9. After run is complete, analyze relative gene expression via the $2^{-\Delta\Delta Ct}$ method with GAPDH serving as an endogenous control for normalization as well as normalization to the untreated control cell samples

PrestoBlue Cell Viability

1. Load 96 well plate wells with 90 µL of cell solution
2. Add compound in serial dilutions and incubate at 37°C for prescribed time
3. Pipette 10 µL PrestoBlue to each well
4. Incubate plate 37°C for 20 minutes - 2 hours
5. Measure by fluorescence at 570 nm excitation and 600 nm emission using a microplate reader (BioTek)
6. Normalize sample well average to control average
7. Plot data points and standard error appropriately

Western Blot Analysis

SDS-PAGE Gels

1. Prepare BioRad gel apparatus by setting up the casts
2. Make up the desired percentage separating gel in a conical and immediately pour it into ¾ of the cast
3. Pipette 1 mL of hydrated butanol over the separating gel solution

Table A6. Reagent Volumes for Separating Gel

Separating Gel			
Reagent	**8%**	**10%**	**12%**
dH_2O	5.3 mL	4.8 mL	4.3 mL
1.5 M Tris (pH 8.8)	2.5 mL	2.5 mL	2.5 mL
40% Acrylamide	2.0 mL	2.5 mL	3.0 mL
10% SDS	100 µL	100 µL	100 µL
10% APS	100 µL	100 µL	100 µL
TEMED*	4 µL	4 µL	4 µL

*Add TEMED component last

4. Allow separating gel to set for 30 minutes
5. Decant off hydrated butanol and rinse with dH_2O
6. Make up the stacking gel, immediately pour it into the remaining ¼ cast, and insert the desired comb

Table A7. Reagent Volumes for Stacking Gel

Stacking Gel	
Reagent	**4%**
dH_2O	7.3 mL
1.5 M Tris (pH 8.8)	1.25 mL
40% Acrylamide	1.25 mL
10% SDS	100 µL
10% APS	100 µL
TEMED*	10 µL

*Add TEMED component last

7. Allow stacking gel to set for 30 minutes
8. Remove comb, rinse wells with dH_2O, place into electrophoresis chamber, and cover with running buffer

Sample Preparation

1. Add laemmli buffer with beta-mercaptoethanol to normalized samples
2. Denature the proteins by incubating at 95°C for 5 minutes
3. Vortex, short spin, and load each sample as desired into the gel
4. Add laemmli buffer to any unused wells
5. Run the gel at 180V until the dye front just runs off the gel

Blotting

1. Remove gel from apparatus
2. Carefully detach the stacking layer from the separating layer
3. Activate PVDF membrane in 100% methanol for 1 minute
4. Assemble the blot in a large tray of transfer buffer accordingly:

Figure A2. Western Blotting "Sandwich" for Transfer to Membrane

5. Invert the blot assembly and place on the semi-dry transfer machine
6. Run one gel at 300 mA for one hour and two gels for 90 minutes
7. Briefly stain with 0.1% Ponceau solution and then rinse with dH_2O to visualize protein bands and confirm equal loading

8. Add 1-2 drops of NaOH to 5 mL of TBST and incubate the membrane for 30 seconds in this solution to dissipate Ponceau staining

Antibody Staining and Detection

1. Block membrane by rotating at RT in TBST with 5% non-fat dry milk for 30 minutes
2. Rinse in TBST at RT for 30 seconds
3. Incubate the membrane in primary antibody diluted in TBST with 1% non-fat dry milk rotating overnight at 4^{o}C
4. Wash the membrane in TBST for 15 minutes rotating at RT and repeat a total of three times
5. Incubate the membrane in secondary antibody diluted in TBST with 5% non-fat dry milk rotating for 1½ to 2 hours at RT
6. Turn on western blot exposure machine to allow it to warm up for a minimum of 25 minutes
7. Wash the membrane in TBST for 5 minutes rotating at RT and repeat a total of three times
8. Place the membrane on a transparency sheet taped into a cassette
9. Pipette 1 mL of ECL solution (prepared as per box instructions) onto each membrane
10. Cover membrane to reduce light exposure and let incubate for 5 minutes at RT
11. Add another transparency sheet on top of the membrane and tape it down to the cassette
12. In a dark room, expose the membrane to film and run through exposure machine
13. Label the film accordingly and turn off the machine when complete

Western Blot Antibodies

Table A8. Primary Antibodies for Western Blot Analysis

Primary Antibodies					
Antibody	**Manufacturer**	**Cat #**	**Dilution**	**Species**	**Location**
Actin	Santa Cruz	SC-1616-R	1:5000	Rabbit	4ºC
Fibronectin	Thermo Scientific	MS-165-P0	1:1000	Mouse	-20ºC
HSF1 mono	Assay Design	SPA-950	1:750	Rat	-20ºC
HSF1 pS326	Abcam	EP1713Y	1:500	Rabbit	-20ºC
HSP70	Stress Marq	SMC-100B	1:1000	Mouse	-20ºC
HSP90	Cell Signaling	8165	1:1000	Rabbit	-20ºC

Table A9. Secondary Antibodies for Western Blot Analysis

Secondary Antibodies				
Species	**Manufacturer**	**Cat #**	**Dilution**	**Location**
Rabbit	Millipore	PA45011V	1:2500	-20ºC
Mouse	Millipore	PA43009V	1:2500	-20ºC
Rat	Jackson Immuno	112-035-062	1:10,000	4ºC

Doxycycline-Inducible TRIPZ shRNA HSF1 Knockdown Cell Creation

Day 1: Packaging Cells Preparation

1. Split cells so they are 50% - 70% confluency on the day of transfection

Day 2: Packaging Cells Transfection

1. Dilute 1 µg each of retroviral construct, pCGP, and pVSVG envelope plasmid with cell media (without any additives) for a total volume of 300 µL per reaction
2. Vortex and short spin
3. Add 50 µL per reaction of Polyfect Transfection Reaction (Qiagen) to the DNA solution
4. Vortex, short spin, and incubate at RT for 10 minutes
5. Aspirate media from cell plates
6. Wash in 5 mL of 1X PBS and aspirate off
7. Add 9 mL of complete media to cells

8. Add 1 mL per reaction of complete media to the DNA solution after incubation period
9. Pipette up and down and transfer 1350 µL of solution to each plate of cells
10. Gently rock each plate
11. Incubate at 37ºC for 24 hours

Day 3: Replace Media and Target Cell Preparation

1. Replace transfection media with fresh complete media
2. Incubate at 37ºC for 24 hours
3. Plate future transfected cells in 60 mm plate

Day 4: Collect Virus and Infect Target Cells

1. Warm complete media and 37ºC water bath for 30 minutes and prepare hood
2. Collect virus media from packaging cells into a conical and replace with fresh complete media
3. Incubate packaging cells at 37ºC for 24 hours
4. Filter virus media through a 0.45 micron PVDF filter
5. Add equal volume of complete media to filtered virus media
6. Add 8 µg/mL of hexadimethrinebromide to virus media
7. Pipette 4 mL of virus media solution per plate to target cells
8. Incubate target cells at 37ºC

Day 5: Collect Second Round of Virus

1. Collect virus media from packaging cells into a conical and discard cells
2. Filter virus media through a 0.45 micron PVDF filter
3. Add equal volume of complete media to filtered virus media
4. Freeze at -80ºC for use in day 6
5. Replace virus media on target cells with fresh media and passage if confluent

Day 6: Re-Infect Target Cells

1. Thaw virus media from day 5 and add 8 µg/mL of hexadimethrinebromide
2. Pipette 4 mL of virus media solution per plate to target cells
3. Incubate target cells at 37ºC

Day 7: Replace Target Cell Media

1. Replace virus media on target cells with fresh media and passage if confluent

Day 8+: Selection

1. Select for infected cells by adding puromycin to media (SKOV3=0.5 µg/mL, HEY=1.0 µg/mL)
2. After 5 days of selection, cells which have been successfully infected should begin proliferating
3. After selection, continue treatment of 0.2 µg/mL puromycin for maintenance

Wound healing assay

1. Plate 3 x 10^5 cells per well in a 6-well plate
2. Treat with 1 µg/mL of doxycycline for HSF1 KD inducible cells or leave untreated
3. Incubate for 48 hours at 37^{o}C
4. Create 2 vertical and 2 horizontal lines in the confluent cells with a 2 µL pipette tip
5. Wash cells with 1X PBS
6. Add 5 mL media without additives
7. Photograph the cells immediately and then again after 12 hours with an EVOS inverted microscope (Advanced Microscopy Group)
8. Calculate would closure with TScratch software

Cell migration assay

1. Treat cells with 1.0 µg/mL of doxycycline for HSF1 KD inducible cells or leave untreated
2. Incubate at 37^{o}C for 48 hours
3. Remove media, wash with 1X PBS, and replace with media containing no additives
4. Incubate at 37^{o}C for 24 hours
5. Wash with 1X PBS, add trypsin to un-adhere the cells, and resuspend in additive-free media
6. Add 2.5 x 10^4 cells to the upper portion of the Boyden chamber
7. Pipette 400 µL of complete media to the lower chamber
8. Incubate at 37^{o}C for 16 hours
9. After incubation, remove cells on the upper chamber surface with a cotton swab
10. Fix and stain cells on the lower chamber surface with 1% (w/v) crystal violet in methanol
11. Count cells in 10 random fields of view from each well

Appendix B: Gene set enrichment analysis. Provided are the total number of entities within a network, expanded and measured entities in the pathway, enrichment scores, median fold change of the network, and the p-value. Also provided is the Gene Set Category.

Name	*Total Entities*	*Expanded Entities*	*Measured Entities*	*Enrich. Score*	*Normal. ES*	*Median change*	*p-value*	*Gene Set Category*
Actin Cytoskeleton Regulation	51	551	528	0.31765	1.26305	1.01748	0.01078	Ariadne Cell Signaling Pathways
AGER -> NF-kB signaling	14	34	33	0.52429	1.46053	1.06437	0.0293	Ariadne Receptor Signaling Pathways
Axon Guidance	58	1051	983	0.27633	1.14787	-1.01045	0.04988	Ariadne Cell Signaling Pathways
Biosynthesis of CoA and holo-ACP	16	21	10	-0.6627	-1.4878	-1.19956	0.05	Ariadne Metabolic Pathways
Branched chain amino acids metabolism	99	123	50	-0.6871	-2.23849	-1.35191	0	Ariadne Metabolic Pathways
CCR2/5 -> STAT signaling	20	20	16	0.69406	1.58304	1.00347	0.01581	Ariadne Receptor Signaling Pathways
CCR5 -> TP53 signaling	17	17	13	0.69792	1.63466	-1.0087	0.01931	Ariadne Receptor Signaling Pathways
Cell cycle	140	585	483	0.30307	1.21387	1.05336	0.03704	Ariadne Cell Process Pathways
CHRAC Chromating Remodeling	16	289	214	0.39429	1.46877	1.07923	0.0061	Ariadne Cell Process Pathways
CSF2R -> NF-kB signaling	6	14	14	0.67175	1.58485	1.18509	0.02222	Ariadne Receptor Signaling Pathways
DDR1 -> NF-kB signaling	14	22	21	0.57985	1.4977	1.17283	0.0303	Ariadne Receptor Signaling Pathways
DNA Replication	29	134	119	0.39631	1.37964	1.08298	0.03333	Ariadne Cell Process Pathways
EphrinR -> STAT signaling	15	15	15	0.62648	1.48748	1.15269	0.04724	Ariadne Receptor Signaling Pathways
Fatty acid oxidation	73	99	39	-0.552	-1.64026	-1.1708	0	Ariadne Metabolic Pathways
FibronectinR -> AP-1/ELK-SRF/SREBF signaling	55	105	98	0.4226	1.43344	1.05885	0.03051	Ariadne Receptor Signaling Pathways

FibronectinR -> NF-kB signaling	22	58	55	0.49258	1.51462	1.08298	0.03484	Ariadne Receptor Signaling Pathways
Folate biosynthesis	63	66	20	-0.6041	-1.60545	-1.30586	0	Ariadne Metabolic Pathways
Glycogen metabolism	37	55	34	-0.5597	-1.68753	-1.12117	0.00413	Ariadne Metabolic Pathways
Glycosylphosphatidylinositol(GPI)-anchor biosynthesis	32	195	50	-0.5068	-1.64655	-1.13092	0	Ariadne Metabolic Pathways
Gonadotrope Cell Activation	71	728	688	0.32639	1.32513	-1.03526	0	Ariadne Cell Signaling Pathways
Hedgehog Pathway	17	626	581	0.33211	1.32792	1.05702	0.00272	Ariadne Cell Signaling Pathways
Histone Acethylation	33	329	262	0.36642	1.38583	1.05702	0.01176	Ariadne Cell Process Pathways
Histone and DNA Methylation	37	352	273	0.36652	1.39196	1.05885	0	Ariadne Cell Process Pathways
Histones Sumoylation	25	252	201	0.40564	1.48278	1.09051	0	Ariadne Cell Process Pathways
Histones Ubiquitylation	23	334	267	0.44031	1.67112	1.12506	0	Ariadne Cell Process Pathways
IGF1R -> ELK-SRF/HIF1A/MYC/SREBF signaling	23	46	43	0.52628	1.51745	1.26138	0.02555	Ariadne Receptor Signaling Pathways
IL6R -> CEBP/ELK-SRF signaling	18	24	24	0.64418	1.66813	1.36841	0	Ariadne Receptor Signaling Pathways
INO80 Chromating Remodeling	25	449	365	0.32253	1.25759	1.05702	0.02571	Ariadne Cell Process Pathways
Insulin Action	50	912	840	-0.2518	-1.12304	-1.0299	0.02885	Ariadne Cell Signaling Pathways
LeptinR -> ELK-SRF signaling	16	22	22	0.61225	1.55556	1.36841	0.01852	Ariadne Receptor Signaling Pathways
Lysine metabolsm	84	139	58	-0.4593	-1.50721	-1.18304	0.01869	Ariadne Metabolic Pathways
MacrophageR -> CEBPB/NF-kB signaling	21	43	42	0.49483	1.46306	1.06992	0.04348	Ariadne Receptor Signaling Pathways
Malonate, propanoate and beta-alanine metabolism	99	121	53	-0.4545	-1.46122	-1.08862	0.0177	Ariadne Metabolic Pathways

Mast Cell Activation	64	558	514	0.36922	1.48169	-1.01045	0	Ariadne Cell Signaling Pathways
Metabolism of glucocorticoids and mineralcorticoids	75	85	18	0.77862	1.96404	1.04972	0	Ariadne Metabolic Pathways
Metabolism of glycerophospholipids and ether lipids	152	492	223	-0.3425	-1.36331	-1.06437	0	Ariadne Metabolic Pathways
Mevalonate pathway	40	44	18	-0.5792	-1.48262	-1.16675	0.04641	Ariadne Metabolic Pathways
mRNA Transcription and Processing	49	391	313	0.35818	1.3867	1.07549	0.00292	Ariadne Cell Process Pathways
N-Glycan biosynthesis	76	215	82	-0.4706	-1.63392	-1.10191	0	Ariadne Metabolic Pathways
Nicotinate and nicotinamide metabolism	54	146	35	-0.5403	-1.59015	-1.15669	0.01852	Ariadne Metabolic Pathways
NK Cell Activation	59	539	495	0.35242	1.39815	1.00696	0	Ariadne Cell Signaling Pathways
Notch Pathway	40	1487	1375	0.27811	1.16303	-1.00521	0.02564	Ariadne Cell Signaling Pathways
NURD Chromating Remodeling	31	307	222	0.38026	1.39857	1.06253	0.00292	Ariadne Cell Process Pathways
NURF Chromating Remodeling	17	288	207	0.39264	1.45065	1.06253	0.00904	Ariadne Cell Process Pathways
PECAM -> SP1 signaling	12	18	18	0.69123	1.67127	1.36841	0.01792	Ariadne Receptor Signaling Pathways
Phenylalanine and Tyrosine metabolism	130	161	56	-0.4499	-1.46545	-1.08862	0.02315	Ariadne Metabolic Pathways
PTAFR -> NF-kB signaling	22	63	57	0.47289	1.41304	1.12896	0.03915	Ariadne Receptor Signaling Pathways
PTPRC -> BCL6 signaling	21	27	24	0.6188	1.59146	1.17691	0.01111	Ariadne Receptor Signaling Pathways
ROS metabolism	43	72	35	0.61282	1.71224	-1.00347	0.00699	Ariadne Metabolic Pathways
Skeletal Myogenesis Control	70	589	555	0.29613	1.19784	-1.03886	0.02997	Ariadne Cell Signaling Pathways
Sphingolipid metabolism	86	322	119	-0.4111	-1.53622	-1.06622	0	Ariadne Metabolic Pathways
SRCAP Chromating Remodeling	20	284	213	0.3977	1.44951	1.07923	0.00904	Ariadne Cell

								Process Pathways
SWI/SNF BRG1/BAF Chromating Remodeling	25	284	210	0.39355	1.46011	1.07549	0.00304	Ariadne Cell Process Pathways
SWI/SNF BRG1/PBAF Chromating Remodeling	26	285	211	0.39264	1.45068	1.06253	0.00617	Ariadne Cell Process Pathways
T Cell Activation	80	957	794	0.32951	1.34745	1.00347	0	Ariadne Cell Signaling Pathways
ThrombopoietinR -> SP1 signaling	12	18	18	0.63547	1.49265	1.35191	0.01538	Ariadne Receptor Signaling Pathways
TLR4/5/7/9 -> NF-kB signaling	19	27	23	0.56954	1.47303	1.07363	0.03008	Ariadne Receptor Signaling Pathways
TNFR -> AP-1/ATF/TP53 signaling	40	40	38	0.57226	1.64605	1.16473	0.00346	Ariadne Receptor Signaling Pathways
TNFR -> CREB/ELK-SRF signaling	42	45	43	0.53299	1.59125	1.16473	0.01695	Ariadne Receptor Signaling Pathways
TNFR -> NF-kB signaling	32	40	38	0.61455	1.76894	1.12896	0.0034	Ariadne Receptor Signaling Pathways
TNFRSF1A -> AP-1/ATF/TP53 signaling	30	36	34	0.63831	1.77934	1.27456	0	Ariadne Receptor Signaling Pathways
TNFRSF1A -> CREB/ELK-SRF signaling	32	41	39	0.60603	1.75651	1.29012	0.00353	Ariadne Receptor Signaling Pathways
TNFRSF6 -> HSF1 signaling	15	15	15	0.67724	1.59139	1.25266	0.00781	Ariadne Receptor Signaling Pathways
Translation Control	86	1012	922	0.27908	1.15021	-1.02633	0.03874	Ariadne Cell Signaling Pathways
Tryptophan metabolism	112	326	135	-0.465	-1.72372	-1.10957	0	Ariadne Metabolic Pathways
Ubiquitin-dependent Protein Degradation	15	125	100	0.5559	1.84663	1.32869	0	Ariadne Cell Process Pathways
VasopressinR1 -> STAT signaling	16	50	45	-0.4917	-1.50595	-1.09809	0.02791	Ariadne Receptor Signaling Pathways
VEGFR -> NFATC signaling	26	37	31	0.60393	1.72553	1.12896	0.00733	Ariadne Receptor Signaling Pathways
Vitamin B5 (pantothenate) metabolism	24	29	9	0.77523	1.64224	1.06069	0.0155	Ariadne Metabolic Pathways

Appendix C: Complete list of sub-networks that are related to the response to stress, the DNA methylation pathway and the histone acetylation pathway.

Name	Type	Description	Connectivity	Probe Value	Local Connectivity	Indegree	Outdegree
chromosome condensation	Cell Process		330	-2.4751	2	2	0
chromatin remodeling	Cell Process		1017	8.2821	3	3	0
EP300	Protein	E1A binding protein p300	1503	1.1627	5	1	4
KAT2B	Protein	K(lysine) acetyltransferase 2B	406	1.3732	4	1	3
transcription initiation	Cell Process		278		2	2	0
SIRT1	Protein	sirtuin 1	844	2.3254	6	1	5
MECP2	Protein	methyl CpG binding protein 2 (Rett syndrome)	343	1.4845	2	0	2
NCOA1	Protein	nuclear receptor coactivator 1	414	-1.2592	5	0	5
BRCA1	Protein	breast cancer 1, early onset	858	-1.1507	3	0	3
NCOA3	Protein	nuclear receptor coactivator 3	468	8.4708	3	0	3
CREBBP	Protein	CREB binding protein	813	2.254	3	0	3
histone H3	Functional Class		1267	1.0943	8	7	1
histone deacetylase	Functional Class		2000	-3.1766	9	5	4
histone acetyltransferase	Functional Class		754	-2.1886	4	0	4
HDAC2	Protein	histone deacetylase 2	461	2.0314	1	0	1
KAT5	Protein	K(lysine) acetyltransferase 5	290	-1.3059	2	0	2
HDAC1	Protein	histone deacetylase 1	890	1.6818	5	0	5
histone H4	Functional Class		506	1.0122	5	5	0
protein nucleus import	Cell Process		42	1.7441	1	1	0
NuRD complex	Complex		125	2.2153	2	0	2
histone H2B	Functional Class		190	8.2821	1	1	0
NCOR2	Protein	nuclear receptor corepressor 2	376	-1.1728	2	0	2
NCOR1	Protein	nuclear receptor co-repressor 1	423	-1.2746	2	0	2
RBBP4	Protein	retinoblastoma binding protein 4	128	1.3566	1	0	1
SIN3A	Protein	SIN3 homolog A, transcription regulator (yeast)	156	1.4439	6	0	6
KAT2A	Protein	K(lysine) acetyltransferase 2A	287	-1.9725	1	0	1
SAP30	Protein	Sin3A-associated protein, 30kDa	231	3.0367	1	0	1

histone H2A	Functional Class		172	2.1697	3	3	0
KPNA2	Protein	karyopherin alpha 2 (RAG cohort 1, importin alpha 1)	343		2	1	1
RBBP7	Protein	retinoblastoma binding protein 7	80	1.0886	2	0	2
SAP18	Protein	Sin3A-associated protein, 18kDa	19	2.7274	2	0	2
trichostatin A	Small Molecule		1		1	0	1
sodium butyrate	Small Molecule		1		1	0	1